POTENT AND POTENTIALLY NON-CARDIOTOXIC ANTHRACYCLINES: THEIR SYNTHESIS, BIOLOGICAL EVALUATION, AND COMPARISON OF HYDROZONE-MEDIATED REDUCTIONS

by

Jerrett Holdaway

A thesis submitted in partial fulfillment

of the requirements for the degree of

Master of Science in Chemistry

Boise State University

May 2018

BOISE STATE UNIVERSITY GRADUATE COLLEGE

DEFENSE COMMITTEE AND FINAL READING APPROVALS

of the thesis submitted by

Jerrett Holdaway

Thesis Title: Potent and Potentially Non-Cardiotoxic Anthracyclines; Their Synthesis, Biological Evaluation, and Comparison of Hydrozone-Mediated Reductions

Date of Final Oral Examination: 1 December 2017

The following individuals read and discussed the thesis submitted by student Jerrett Holdaway, and they evaluated his presentation and response to questions during the final oral examination. They found that the student passed the final oral examination.

Don Warner, Ph.D.	Chair, Supervisory Committee
Kenneth A. Cornell, Ph.D.	Member, Supervisory Committee
Kristen A. Mitchell, Ph.D.	Member, Supervisory Committee

The final reading approval of the thesis was granted by Don Warner, Ph.D., Chair of the Supervisory Committee. The thesis was approved by the Graduate College.

DEDICATION

I would like to dedicate this project to my family and friends who have been by my side during this challenging and rewarding chapter of my life at Boise State University. I would also like to give thanks to all of those who have helped me grow both professionally and as a person.

ACKNOWLEDGEMENTS

I would like to acknowledge Dr. Don Warner for allowing me to have the tremendous opportunity of working on this project and for his countless efforts to help me grow as a scientist. As well, much thanks goes to Dr. Ken Cornell for providing guidance and support throughout my graduate education. Furthermore, I would like to give appreciation to Dr. Kristen Mitchell for being a part of my committee. Finally, this project would not have been successful without the efforts of Phil Moon, LJ McKenzie, and Tyler Smith in performing the *in vitro* experiments, Dr. Joe Dumais, Dr. Xinzhu Pu, and Matthew Turner for their help during characterization, and Pete Barnes for his help synthesizing these compounds.

The work in this thesis was supported by the Institutional Development Award (IDeA) from the National Institute of General Medical Sciences of the National Institutes of Health Grant #P20GM103408 and #P20GM109095, GEM Pharmaceuticals LLC, and the State of Idaho IGEM Grant, and the Boise State University Office of Research. I would also like to thank and acknowledge the support from both the Department of Chemistry and Biochemistry and the Biomolecular Research Center at Boise State University for providing me with the means to support my education through granting me teaching assistantships and summer fellowships.

ABSTRACT

After nearly half a century since medical approval, the anthracycline doxorubicin (DOX) remains one of the most potent and clinically useful anticancer agents. In spite of its long history, however, the cytotoxic mechanisms of DOX have been debated and remain controversial. Several well-supported mechanisms will be discussed, such as the potential to intercalate DNA and induce apoptosis through topoisomerase poisoning, free radical formation, and DNA cross-linking. While DOX has substantial medical importance, it is plagued by a life-threatening dose-dependent cardiotoxic side effect associated with several structural groups. A number of modifications to DOX have been accomplished to attempt to remove treatment-induced cardiotoxicity, including the reduction of the C-13 carbonyl to a methylene and conversion of the quinone moiety to a less reactive iminoquinone. This modified form, termed 5-imino-13-deoxydoxorubicin (DIDOX), has displayed no cardiotoxic side effects in any clinical setting. However, these structural changes have reduced the potency of the drug more than four-fold.

In this work, six different analogs of DIDOX were synthesized and evaluated for *in vitro* cytotoxicity against an array of cancer cell lines. The six analogs were designed to incorporate reactive moieties attached to the 3'-amine of the daunasamine sugar. Of the six synthesized, four were at least as cytotoxic as DOX, and several were up to 100-fold more potent. Preliminary results also suggest that modifications to the 3'-amine attenuate the multidrug resistance observed during anthracycline treatment. In addition to the synthesis and preliminary evaluation of new anthracycline analogs, this work explored methods for

improving the synthesis of DIDOX. Specifically, the reduction of DOX's carbonyl to produce C-13-deoxydoxorubicin (DeoxyDOX) was explored using six different sulfonylhydrazones, and the relative production of the reduced form was compared. Four of the new hydrazones exhibited the potential to improve the overall amount of DeoxyDOX generated, compared to the currently used methods. In summary, the work described presents both the findings for the synthesis of potent and non-cardiotoxic derivatives of doxorubicin that show promise for overcoming multi-drug resistance and potential improvements toward enhancing the overall yield of DIDOX and related analogs.

TABLE OF CONTENTS

LIST OF TABLES

LIST OF FIGURES AND SCHEMES

LIST OF ABBREVIATIONS

ABC	ATP-binding cassette
AML	Acute myelogenous leukemia
BDMAT	bis(N,N-dimethylacetamide) hydrogen tribromide
BSH	Benzenesulfonyl Hydrazide
DeoxyDOX	13-Deoxydoxorubicin
DEX	Dexrazoxane
DIDOX	5-Imino-13-deoxydoxorubicin
DNR	Daunorubicin
DOX	Doxorubicin
DOXol	Doxorubicinol
eNOS	Endothelial nitric oxide synthase
EPI	Epirubicin
EWS	Electron-withdrawing sulfonyl
FSH	4-fluorobenzenesulfonohydrazide
GSH	Reduced Glutathione
GST	Glutathione S-transferase
IDA	Idarubicin
LA	Lewis acid
LVEF	Left ventricular ejection fraction
MDR	Multidrug resistance
NSH	4-Nitrobenzenesulfonohydrazide

PDOX	2-Pyrrolinodoxorubicin
PEG	Polyethylene glycol
PGP	P-glycoprotein
PPTS	Pyridinium p-toluenesolfonate
PSH	Pyridine 3-sulfonylhydrazide
RA	Relative abundance
ROS	Reactive oxygen species
SG	Sulfonyl group
SR	Sarcoplasmic reticulum
TFAA	Trifluoroacetic anhydride
TOPOII	Topoisomerase II
TFSH	4-(Trifluoromethyl) benzenesulfonohydrazide
TSH	Tosylhydrazide

CHAPTER ONE: CYTOTOXICITY, CARDIOTOXICITY, AND CANCER RESISTANCE: MECHANISMS OF DOXORUBICIN

1.1 Cancer

As population and median age increase, so does the number of individuals who have been directly affected by cancer (Miller, 2016). Cancer can be characterized as a disease linked with accelerated cell cycles, genomic alterations, chemotaxis, and invasive growth, ultimately leading to death if left untreated. As such, cancer has been—and continues to be—a growing issue amongst developed nations. It is the second leading cause of death in the United States, with 1.7 million new diagnoses and roughly 600,000 deaths during 2016 (Siegel, 2016). However, the five-year survival rate for many cancers—such as breast cancer, leukemia, and all combined childhood cancers—has improved significantly over the last several decades (DeSantis, 2014). Reasons for better prognoses are largely the result of improved chemotherapy drugs, surgical techniques, radiation targeting, and increased diagnosis during earlier stages. However, a significant difficulty with the use of chemotherapeutics stems from the existence of a vast array of different tumor subtypes, such as well-differentiated, dedifferentiated, round cell, and pleomorphic. This is problematic because sensitivity to various therapeutic agents greatly depends on the subtype (Jones, 2005). For example, tumor response is generally better for patients diagnosed with round cell liposarcomas compared to those who have well-differentiated or dedifferentiated liposarcomas.

1.2 Doxorubicin as a Treatment

One drug currently available to effectively treat cancer is doxorubicin (DOX), which is classified as a broad-spectrum, anthracycline, antitumor antibiotic. DOX has been in widespread use for more than 50 years as one of the most effective chemotherapeutics ever developed (Weiss, 1992). Its mechanisms (**section 1.4**) involve DNA intercalation, enzymatic inhibition, free radical generation, DNA alkylation, and cross-link formation. While DOX is an effective treatment for a wide range of solid and hematologic malignancies, it is plagued by dose-dependent cardiotoxic side effects, eventually leading to congestive heart failure (Lefrak, 1973; Cusack, 1993). These cardiotoxic effects (**section 1.5**) can occur acutely or may develop years after treatments have ceased (Lipshultz, 1991). Unfortunately, this cardiotoxicity diminishes the duration that DOX can be safely administered, and a maximum cumulative dose of 450 mg/m^2 has been established (Gottdiener, 1981; Swain, 2003). There are two structural characteristics of DOX that have been associated with cardiotoxicity: the quinone moiety and the C-13 carbonyl (Olson, 1988; Boucek, 1997). A separate complication with DOX is the onset of drug resistance, which is a leading basis for the failure of recurrent breast cancer treatment (Boa, 2011). As a result, attempts have been made to overcome these complications through changes in delivery mechanism, co-treatment with dexrazoxane, as well as synthetic modifications to the structure of the anthracycline (**sections 1.6 & 1.7.4**).

1.3 Anthracycline Structural Features and Semi-Synthetic Analogs

For decades, anthracyclines have been a mainstay chemotherapeutic. The first anthracycline, Daunorubicin (DNR), was discovered in the early 1960's after being isolated as a natural product from several different wild strains of *Streptomyces* (Minotti, Menna,

2004). DOX was later isolated in 1969 after mutating a strain of the DNR-producing *Streptomyces peucetius*. DOX and DNR have similar structures, both consisting of tetracyclic aglycone rings as well as a sugar moiety (**Figure 1.1**). The aglycone is made up of a quinone and an adjacent hydroquinone, a methoxy moiety, and a carbonyl-containing side chain. Attached to the tetracyclic aglycone is a 3-amino-2,3,6-trideoxy-L-fucosyl sugar substituent—called daunosamine—that binds via a glycosidic bond. An important substituent of the daunosamine is the 3'-amine—the importance of which will be discussed later. The difference between these two drugs involves a variation in the termination of the carbonyl side chain: DOX with a primary alcohol and DNR with a methyl group at the C-14 position.

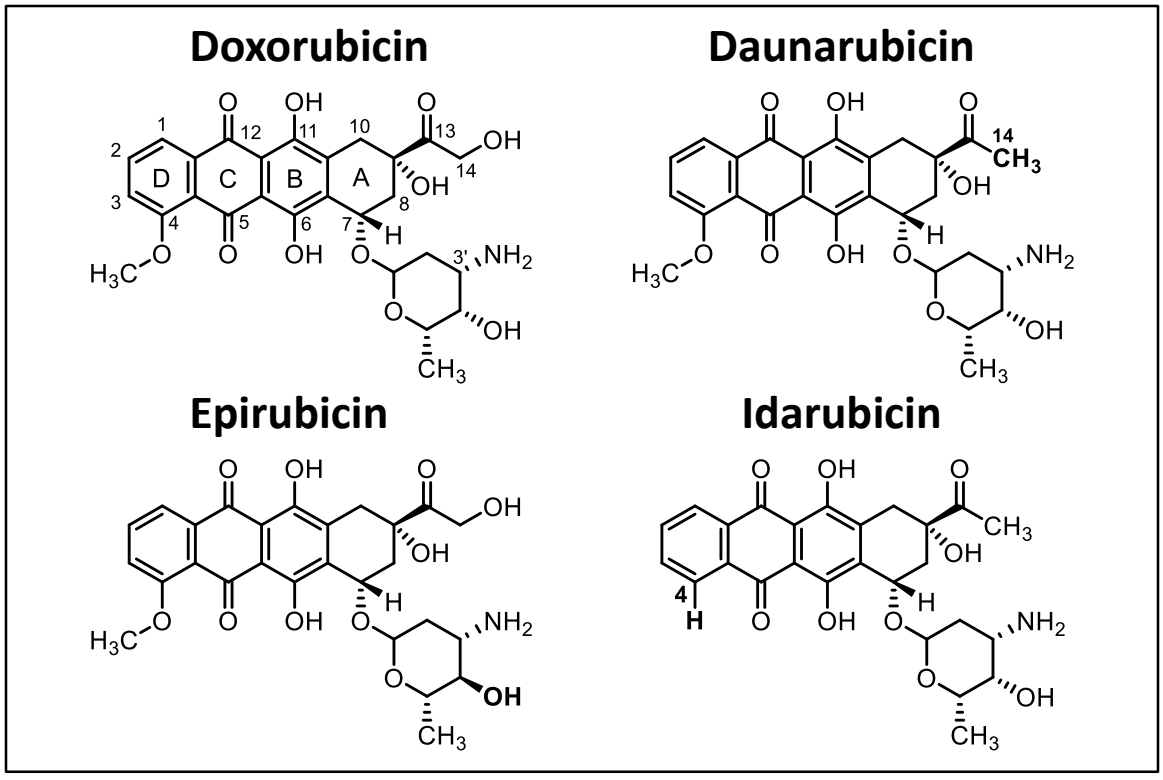

Figure 1.1 Structure of four anthracycline anticancer antibiotics. Daunorubicin is lacking the C-14 terminal alcohol and its analog idarubicin has had the C-4 methoxy excised. Epirubicin is identical to DOX with the exception of the epimerization of the daunosamine alcohol.

While the structures and mechanisms of action of DOX and DNR are very similar, the minor difference in the carbonyl side chain alters their activity considerably. Historically, DOX has been used in the treatment of breast cancer, childhood solid tumors, soft tissue sarcomas, and lymphomas, whereas DNR has been used to treat lymphoblastic and myeloblastic leukemias (Bernard, 1973; Danesi, 2002; Gruber, 2004; Harashima, 1999; Preisler, 1984; Verweij, 2000).

Although DOX and DNR have medicinal importance, their clinical use has been limited because of multidirectional cytotoxicity, with cardiotoxicity being the most detrimental. The search for a better anthracycline has only produced a few clinically useful analogs, as shown above in **Figure 1.1**. These include the semi-synthetic DOX analog epirubicin (EPI) and the DNR analog idarubicin (IDA) (Holdener, 1985; Lopez, 1984; Daghestani, 1985; Ganzina, 1986).

EPI is a derivative of DOX and is formed by epimerization of the daunosamine hydroxyl from an axial to equatorial position (Zabudkin, 2014, Patent No. 8,802,830). Interestingly, this DOX analog is generated from a multistep transformation of DNR. Initially, the 3'-amine of DNR is protected using trifluoroacetic anhydride followed by oxidation of the daunosamine hydroxyl to a carbonyl (**Figure 1.2**). This allows for $NaBH_4$ reduction from the axial direction to produce the epimerized hydroxyl, which is now in the equatorial position. After deprotection, the carbonyl side chain is brominated, using bis(N,N-dimethylacetamide) hydrogen tribromide (BDMAT), and then hydroxylated to generate EPI with an overall yield of 26%. This simple, yet important, structural change has allowed for a higher and more effective dose, which is now commonly utilized in

neoadjuvant and adjuvant therapies, such as during treatment for node-positive breast cancer (Buzdar, 2005; French, 2001).

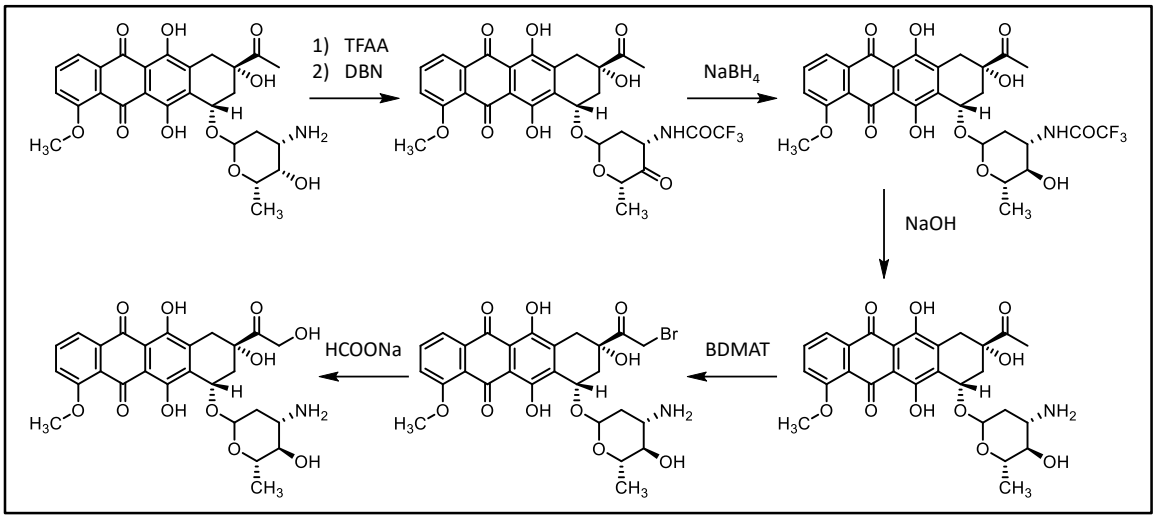

Figure 1.2 Epimerization of DOX and synthesis of EPI. The amine of DNR is protected using trifluoroacetic anhydride (TFAA), and then the daunosamine hydroxyl is oxidized to a carbonyl. Reduction of the carbonyl from the axial direction with $NaBH_4$ generates a hydroxyl that is now in the equatorial position. Following amine deprotection, monobromination of the carbonyl side chain is accomplished using bis(N,N-dimethylacetamide) hydrogen tribromide (BDMAT) and then EPI is generated after hydroxylation of C-14.

While EPI is an epimerized derivative of DOX, IDA structurally mimics DNR in that the methoxy moiety has been removed from the tetracyclic rings (**Figure 1.3**) (Zabudkin, 2014, Patent No. 8,846,882). This has been accomplished by first protecting the 3'-amine before demethylation of the methoxy group. The newly formed phenol is transformed into a triflate, and a palladium catalyst is employed to complete the reduction. IDA is obtained, after amine deprotection, in up to 44% overall yield. This seemingly minor change has allowed IDA to outperform DNR in the treatment of acute myelogenous leukemia (AML) (Berman, 1991; Vogler, 1992). For instance, during a phase 3 trial, complete remission of AML was seen in 71% of patients treated with IDA and only 58% when treated with DNR.

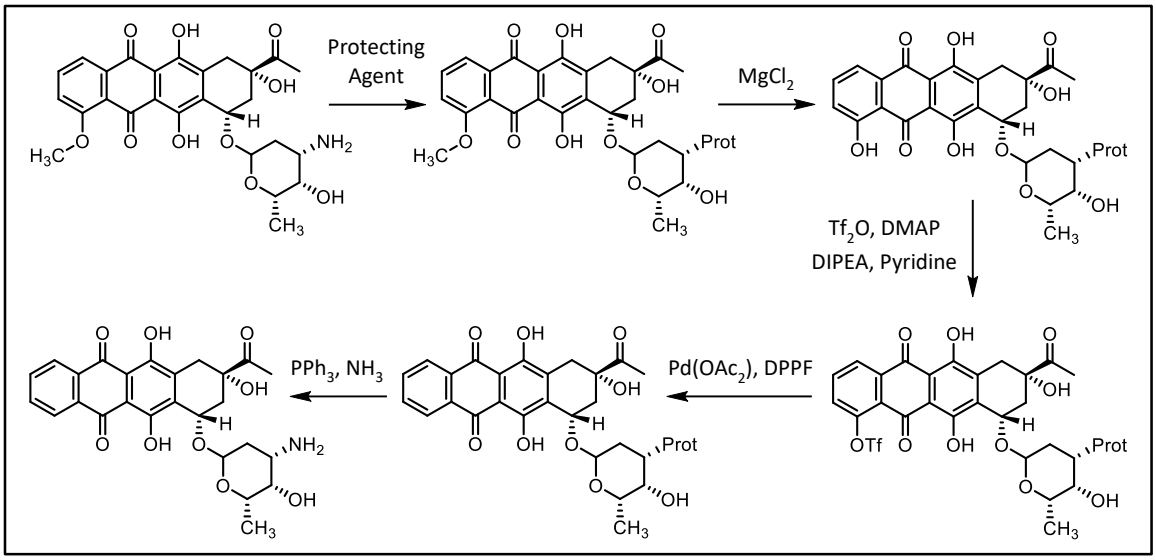

Figure 1.3 Demethoxylation of DNR to synthesize IDA. First, the amine is protected, typically with trifluoroacetic anhydride, and then the methoxy group is demethylated. The resulting phenol is converted into a triflate that is removed via palladium catalyzed reduction. Finally, the amine is deprotected to obtain IDA.

1.4 Mechanisms of Action

Although nearly half a century of research has gone into trying to understand the cytotoxic mechanisms employed by DOX, the means by which it acts against cancer remains under debate (Minotti, 2004). Of the many mechanisms that have been proposed, only those thought to be most responsible for the anticancer activity will be discussed here. These include DNA intercalation and enzyme inhibition, production of free radical facilitated damage, and the formation of cross-links inhibiting cellular proliferation. Interestingly, each of these mechanisms results in irreversible DNA damage, albeit using vastly different pathways.

1.4.1 Intercalation and Topoisomerase II Inhibition

One of the most accepted mechanisms of DOX-induced cytotoxicity involves the inhibition of the enzyme topoisomerase II (TOPOII). In mammalian cells, TOPOII catalyzes a variety of DNA isomerization reactions, such as catenation, decatenation, and

relaxation of superhelical twists (Berger, 1996) through the sequence of events depicted in **Figure 1.4**. First, TOPOII binds to the G-segment of DNA, leading to a conformational change in the enzyme. Next, the T-segment and ATP bind to TOPOII triggering another conformational change and temporary scission of the G-segment. Next, the T-segment is passed through the split strands and released from the complex. Finally, TOPOII reseals and releases both the G-segment and ADP to regenerate the starting enzyme.

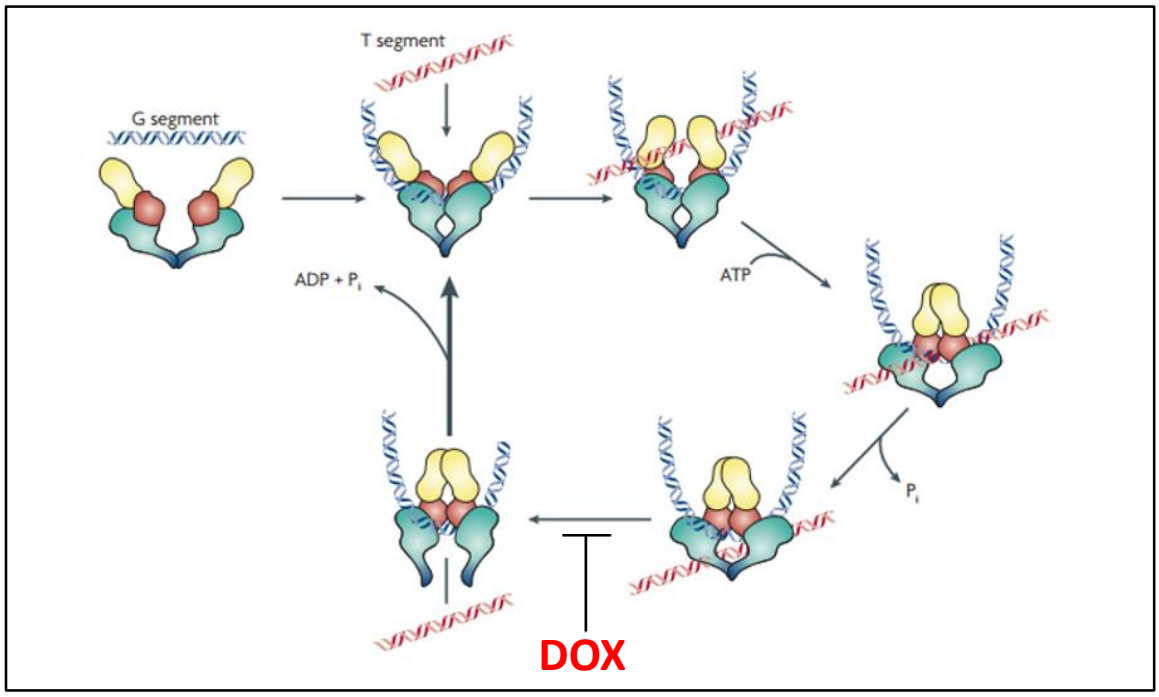

Figure 1.4 TOPOII-mediated DNA cleavage. TOPOII initially binds to the G-segment of DNA and then brings in the T-segment. It then uses ATP to open the G-segment and passes the T-segment through. The cleaved strands become re-fused and the T-segment is released from the complex, followed by the release of the G-segment or additional unwinding. This process repeats to unwind DNA. DOX inhibits this process by inducing covalently bound TOPOII-DNA complexes with the G-segment of DNA. (figure modified from Nitiss, 2009).

DOX stabilization of the TOPOII-DNA complex after strand scission is one of the mechanisms proposed to be responsible for its cytotoxic activity. Stabilizing this complex inhibits the enzyme from rebinding the G-segments and leads to irreversible strand breaks (Tewey, 1984). DOX facilitates the formation of these complexes by providing a unique

structural change in the DNA that allows a tyrosine in TOPOII to act as a nucleophile and bind to a DNA base pair (Gao, 2014; Mueller-Planitz, 2007). The ability of DOX to facilitate TOPOII binding relies on its ability to intercalate in between DNA strands (**Figure 1.5**) (Capranico, 1990). The tetracyclic structure is crucial for intercalation, as x-ray crystallography has determined that ring D occupies the intercalation site and that rings B and C form hydrophobic interactions with adjacent base pairs. The daunosamine moiety and ring A reside in the minor groove and provide stability for the formation of the DOX-TOPOII-DNA complex through hydrogen bonding (Frederick, 1990; Wang, 1987). Damage associated with TOPOII-DNA complexes induces growth arrest followed by programmed cell death (Harris, 2001).

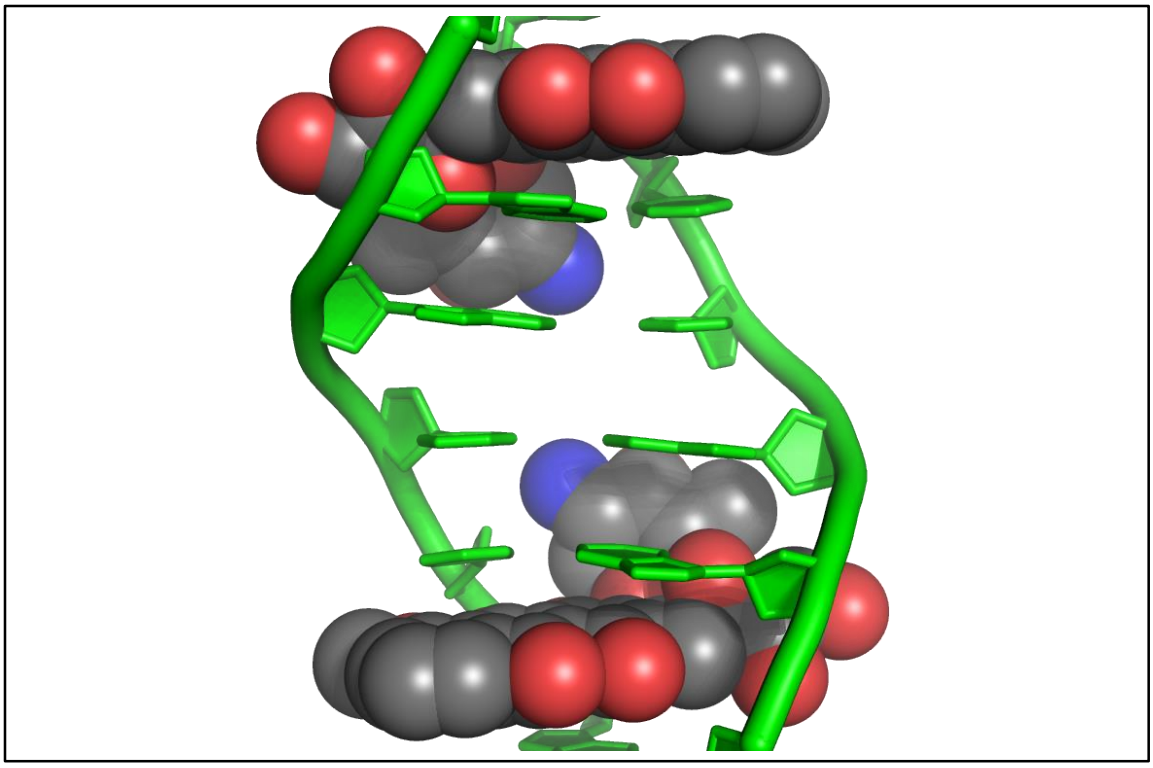

Figure 1.5 DOX-DNA intercalation. The terminal ring of DOX's tetracyclic moiety sits in between the double strands of DNA and the remaining rings stabilize this intercalation. The daunosamine sugar rests in the minor grove of DNA and hydrogen bonds to adjacent base pairs. (figure modified from Frederick, 1990)

1.4.2 Free Radical-Mediated Apoptosis

An intrinsic property of DOX is its ability to catalyze the generation of intracellular reactive oxygen species (ROS). The mechanism of ROS production occurs catalytically as a result of the structurally encompassed quinone moiety present in DOX. The quinone is capable of undergoing a single-electron shuttling mechanism (i.e. redox cycling) mediated through NADPH, iron-quinone complexes, and nitric oxide synthase mechanisms (Bachur, 1979; Bachur, 1977; Cummings, 1992; Rajagopalan, 1988; Vásquez-Vivar, 1997). Initiation of the NADPH redox cycling cascade occurs when NADPH reduces a flavoprotein, such as flavin adenine dinucleotide, by transfer of a lone hydride (**Figure 1.6**) (Shen, 1999). A successive single-electron transfer from the reduced flavoprotein to the quinone of DOX then forms a reactive semi-quinone that readily transfers its electron to molecular oxygen, generating superoxide radicals.

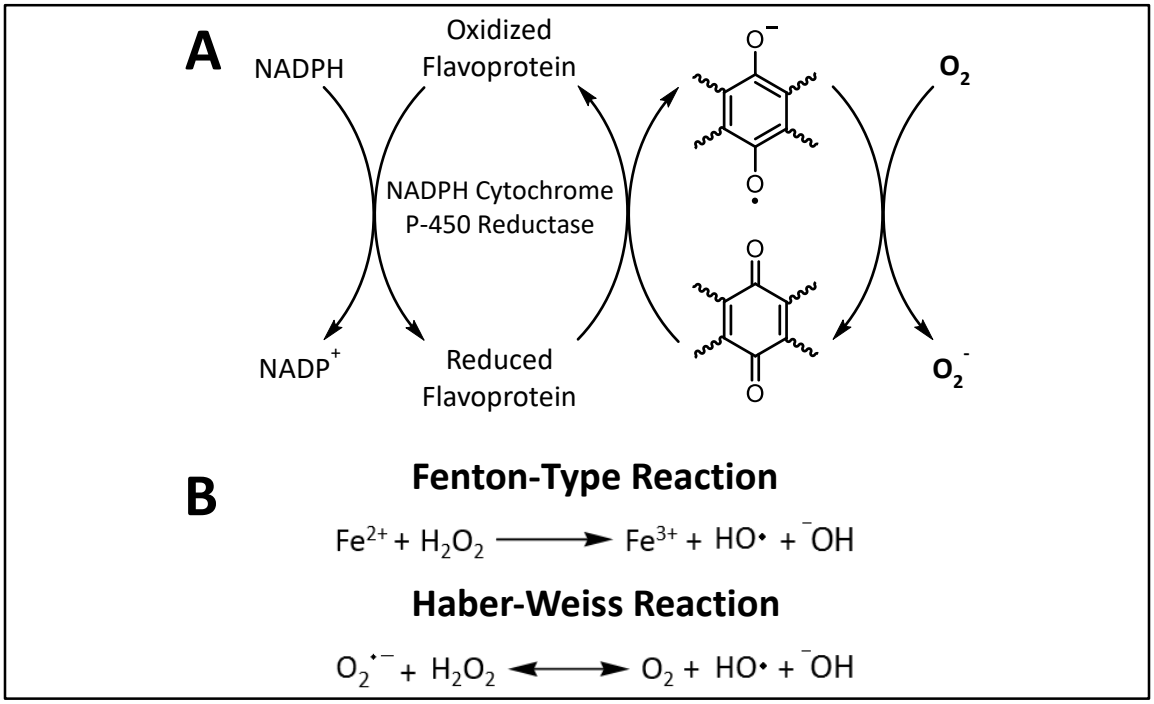

Figure 1.6 DOX production of reactive oxygen species. (A) Quinone redox cycling catalytically produces superoxides that may directly lead to cellular damage or indirectly through formation of peroxides. **(B)** Peroxides react with free iron or superoxides to form highly reactive hydroxyl radicals.

As shown by **Figure 1.6**, these superoxide radicals can follow a Haber-Weiss style mechanism to create more damaging hydroxyl radicals. Other mechanisms have been suggested for iron-catalyzed ROS production, such as a Fenton-type reaction where Fe^{2+} is oxidized to Fe^{3+} by donating an electron to a peroxide species that is produced during redox cycling. These reactive hydroxyl products cause DNA base pair damage through oxidation, resulting in the dysfunction of DNA synthesis (Doroshow, 1986).

1.4.3 DNA Alkylation and Virtual Cross-Linking

Another mechanism of DOX cytotoxicity involves the ability to form covalent DNA adducts using quinone-radical produced formaldehyde. After DOX diffuses into the nucleus of a cell, formaldehyde-mediated dimerization occurs, followed by hydrolysis to create a reactive Schiff base (**Figure 1.7**) (Cutts, 2003; Swift, 2006; Taatjes, 1998; Taatjes, 1999; Zeman, 1998). In order to support the proposed mechanism, a synthetic dimer was first isolated by treating DOX with excess formaldehyde, then hydrolyzed in a phosphate buffer. Next, DNA was treated with this hydrolyzed-dimer and exhibited similar DNA-drug adducts as with free, unmodified DOX.

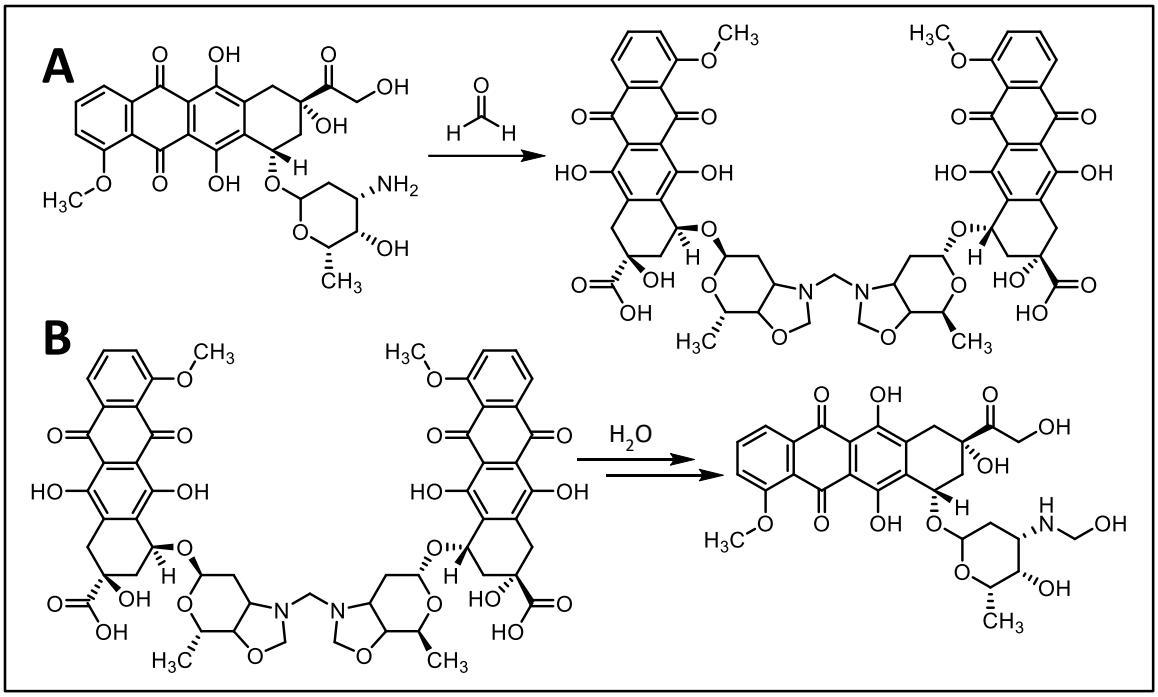

Figure 1.7 Formaldehyde-mediated dimerization. (A) The reaction of two DOX molecules with formaldehyde leads to the formation of a dimer with two methylene groups and a binding oxazolidine at the 3'-nitrogen of the daunosamine sugar. **(B)** Hydrolysis of the dimer generates two DOX molecules containing an unstable hemiaminal, which goes on to form a Schiff base.

While normally observed in low quantities, redox cycling-mediated oxidation results in a spike of cellular formaldehyde. For example, peroxides formed during redox cycling undergo a Baeyer-Villiger type oxidation with DOX at the C-13 position (**Figure 1.8**). This ester intermediate was able to be isolated by treating DOX with dithiothreitol and hydrogen peroxide (Taatjes, 1997). Mass spectrometry results suggest that the hydroxymethyl of the ester was able to leave as reactive formaldehyde by producing a carboxylic acid in place of the carbonyl side chain of DOX. Other carbon sources, such as spermine, can also undergo ROS-mediated oxidation to release formaldehyde.

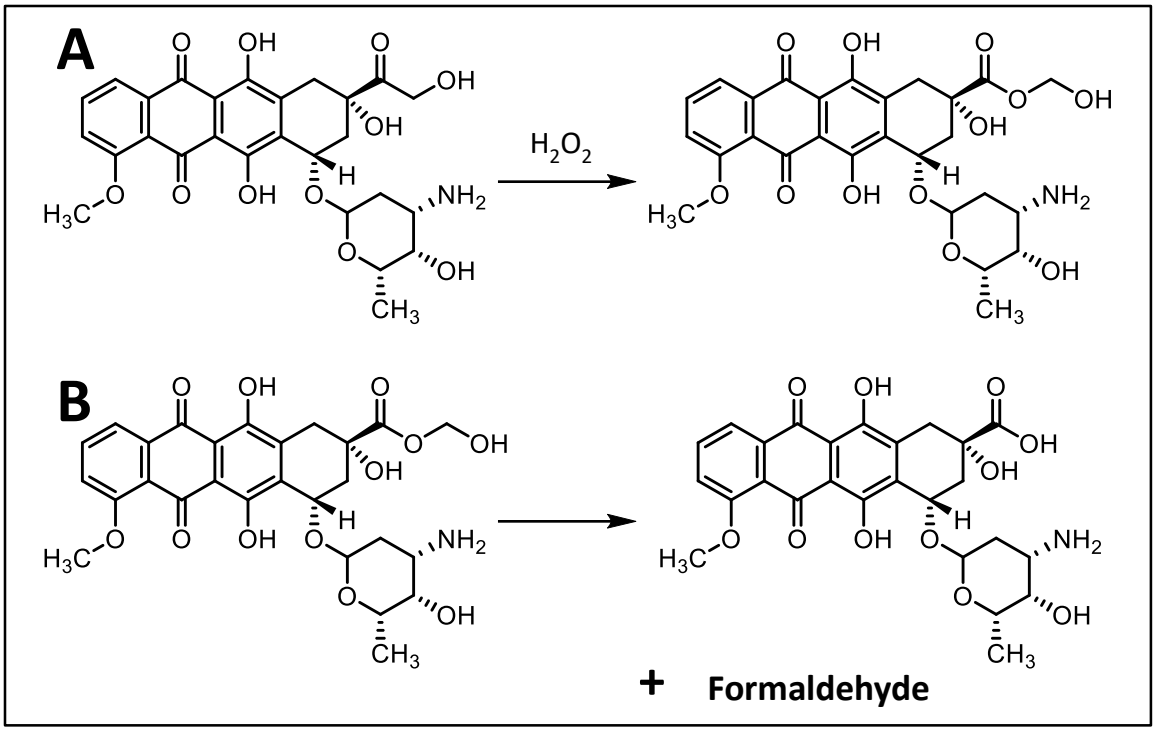

Figure 1.8 Formation of formaldehyde from DOX oxidation. (A) Baeyer-Villiger oxidation of DOX with hydrogen peroxide forms an ester intermediate. **(B)** The oxidized intermediate then decomposes to produce formaldehyde and a carboxylic acid.

During intercalation, a combination of hydrogen bonding and the newly formed Schiff base produce a virtual interstrand cross-link (**Figure 1.9**). The cross-linking initiates when a guanine 2-amino group in the minor groove of DNA covalently attaches to the daunosamine sugar as a monoadduct. After covalent modification, hydrogen bonding of DOX's C-9 alcohol to an opposing guanine base binds the DNA tightly together, forming what is known as a virtual cross-link. While true interstrand cross-links covalently attach to both DNA strands, the hydrogen bonding and monoadduct of the virtual cross-link produces analogous functionality (Barthel, 2016). Such cross-linking considerably slows DNA strand exchange and inhibits cellular proliferation.

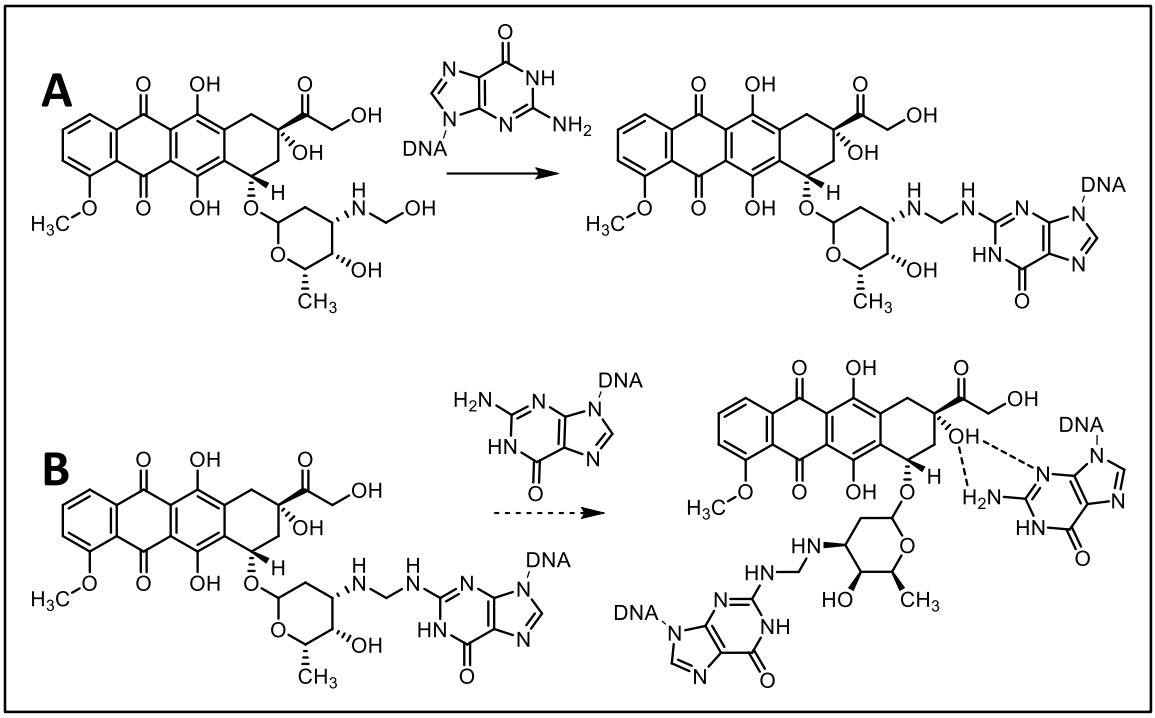

Figure 1.9 Formation of virtual cross-links. (A) Guanine acts as a nucleophile and binds to the Schiff base present on DOX. **(B**) After covalent attachment to one guanine, the virtual cross-link forms through hydrogen bonding of an opposing guanine.

1.5 Mechanisms of Cardiotoxicity

While DOX is an effective anticancer agent, its use is restricted by the onset of cardiotoxicity, of which the mechanisms have been extensively studied (Olson, 1988; Kumar, 2001). One mode of DOX-induced cardiotoxicity includes the formation of an alcohol-containing metabolite that accumulates within cardiac tissue, which results in ion-pump disruption and decreased cardiac contractility. Along with the DOX metabolite, the quinone moiety has been implicated in generating cardiotoxic side effects—via the formation of ROS—along with the ability of DOX to inhibit important antioxidant enzymes located in cardiac tissue.

1.5.1 Doxorubicin's Cardiotoxic Alcohol Metabolite

After treatment, roughly 50% of DOX becomes metabolized before being excreted. Unfortunately, the main alcohol metabolite, doxorubicinol (DOXol), has a large role in

DOX associated cardiotoxicity (**Figure 1.10**) (Kassner, 2008; Schaupp, 2015). Formed via enzymatic two-electron reduction of the C-13 carbonyl, accomplished by the enzyme carbonyl reductase, DOXol acts as a potent inhibitor of various membrane-associate ion pumps. These include calcium pumps in cardiac sarcoplasmic reticulum (SR), sodium/potassium pumps of cardiac sarcolemma, and F_0F_1 proton pumps of cardiac mitochondria (Robert Jr, 1987). This leads to considerable disruption as ion pumps are vital for muscle relaxation and cell signaling. Appreciable inhibition of SR calcium pumps occurs at relatively low concentrations of DOXol (IC_{50} <5μg/mL), whereas, DOX exhibits no measurable inhibition until concentrations exceed 100-fold that of DOXol (Olson, 1988).

As well as inhibiting ion pumps, DOXol has a higher propensity than DOX to accumulate within cardiac tissue, where the severity of cardiomyopathy is directly correlated to increasing concentration (Dodd, 1993; Stewart, 1992). DOXol accumulation into cardiac tissue has been established to occur in a time-dependent manner, determined using rabbit cardiac tissue. Specifically, DOXol demonstrated consistent decreases in myocardial contractility, cardiac relaxation, and an increase in muscle stiffness over time (Mushlin, 1993). The continual accumulation of DOXol results in chronic cardiotoxicity and eventually leads to life-threatening congestive heart failure.

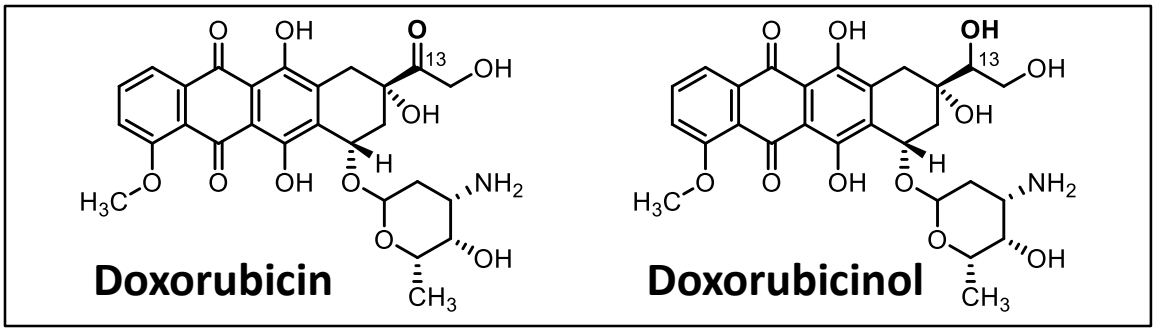

Figure 1.10 Formation of doxorubicin's cardiotoxic alcohol metabolite. The formation of DOX's cardiotoxic alcohol metabolite, DOXol, is produced by enzymatic carbonyl reductase-mediated reduction of the C-13 carbonyl. This metabolite readily accumulates in cardiac tissue and disrupts normal function.

1.5.2 Quinone Redox Cycling-Mediated Cardiotoxicity

Cardiac myocytes have been shown to be more susceptible than other cells to oxidative damage (Burton, 1984). In the presence of ROS, such as hydroxyl radicals, cardiac cell length shortens and ultimately leads to irreversible hypercontraction, followed by cytolysis. As a result of this sensitivity, the quinone moiety of DOX has been linked to cardiotoxicity due to catalyzing the production of ROS (Kumar, 2001). This becomes especially problematic considering the ability of DOX to accumulate and collect in cardiac tissue, as mentioned earlier. Another source of cardiac sensitivity stems from low levels of cardiac catalase activity to protect against hydrogen peroxide. This forces cardiac tissue to rely on glutathione peroxidase and superoxide dismutase for free radical scavenging. However, DOX inhibits these two critically important enzymes, leaving the cardiac tissue vulnerable to oxidative damage (Sawyer, 1999; Siveski-Iliskovic, 1995; Doroshow, 1980;). Notably, changes in enzymatic antioxidant capacity and increases in cardiac oxidative stress occur as early as the first dose of DOX (Li, 2002).

1.5.3 Nitric Oxide Synthase-Dependent ROS Formation

Reduction of the quinone moiety has been proposed to follow several different mechanisms. One proposal involves the binding of DOX to the reductase domain of endothelial nitric oxide synthase (eNOS) followed by subsequent reduction (Vásquez-Vivar, 1997). The K_m value of eNOS for DOX is 50 times lower than that of other reductase enzymes, such as cytochrome P450 reductase, which suggests that eNOS is likely responsible for the majority of reductions at low DOX concentrations. Furthermore, DOX-eNOS binding results in an increased production of superoxide and successive ROS species, which subsequently react with nitric oxide to form an even stronger oxidizing agent: peroxynitrite (Weinstein, 2000; Beckman, 1996). Within cardiac tissue, the formation of peroxynitrite is especially problematic as nitric oxide is maintained at high concentration due to its involvement in the regulation of contractility, endothelial integrity and platelet aggregation (Loscalzo, 1995). The formation of this potent oxidant significantly increases protein nitration and leads to acute cardiac disfunction (Kooy, 1997).

1.5.4 Iron Regulatory Protein Inhibition

Deviation from proper cellular iron homeostasis is a contributing factor for both chronic and acute cardiotoxicity (Minotti, 1999; Minotti, 2001; Myers, 1998). Disruption of iron regulation during treatment occurs when the drug's metabolite, DOXol, delocalizes iron from iron regulatory protein-1 as well as DOX-mediated ROS that disables iron regulatory protein-2. For example, rats exposed to clinically equivalent plasma concentrations of DOX (7.5-10 μM) exhibit inactivation of iron regulatory protein-2 (Minotti, Recalcati, 2004). The inhibition of these regulatory proteins prevents cardiac cells

from recognizing changes in iron availability, consequently disrupting proper homeostasis. This can be detrimental because moderately reactive peroxides and superoxides formed during treatment will react with free iron, via a Fenton-type reaction, to produce highly reactive hydroxyl radicals.

1.6 Overcoming Cardiotoxicity

Years of research have been dedicated to eliminating the cardiotoxic side effects of DOX. The following discussion describes the most promising and clinically relevant approaches that have demonstrated a reduction in cardiotoxicity, such as the encapsulation of DOX in a pegylated liposome, which reduces its free concentration and uptake into myocytes. Another approach uses co-administration with the ROS scavenging drug, dexrazoxane, to limit quinone-cardiac damage. Additionally, synthetic modifications of the anthracycline structure, as seen in EPI and IDA will be discussed. Finally, while these earlier methods have attenuated cardiotoxicity, only direct synthetic modifications to DOX's quinone and C-13 carbonyl have led to a completely non-cardiotoxic anthracycline.

1.6.1 Pegylated Liposomal Doxorubicin

One attempt to curb DOX-induced cardiomyopathy has been to encapsulate the drug within 100 nm diameter liposomes coated with polyethylene glycol (PEG) bound to the outer surface, which has been marketed as DOXil (**Figure 1.11**) (Batist, 2001; O'brien, 2004; Wibroe, 2016). The encapsulatoin protects against metabolic degradation and excretion by reducing the plasma concentration of free DOX compared to that of non-encapsulated therapies, allowing for a longer circulation time (Gabizon, 1994). These effects are the result of the hydrophilic PEG surface, which have been shown to reduce opsonization and reticuloendothelial uptake (Allen, 1991).

Although not completely understood, there is evidence suggesting that DOXil preferentially accumulates and releases DOX within tumor tissue, likely due to leaky vasculature and elevated ammonia concentrations (Chauhan, 2012). After 48 hours of incubation in either plasma or buffer, less than 5% of DOX diffuses from DOXil, whereas more than 35% is released when 5 mM ammonia, a biologically relevant concentration, is present (Silverman, 2015). The limited potential to form free DOX and preferred uptake into cancerous tissue helps prevent cardiac drug-accumulation and subsequent cardiotoxicity. For example, in a clinical study where 42 patients were administered doses exceeding that of 500 mg/m^2 DOXil and monitored for changes in left ventricular ejection fraction (LVEF), it was found that only five of these patients had a drop of 10% or more LVEF post-treatment (Safra, 2000). This demonstrated that treatment of encapsulated DOX, rather than free DOX, provides some level of cardiac protection.

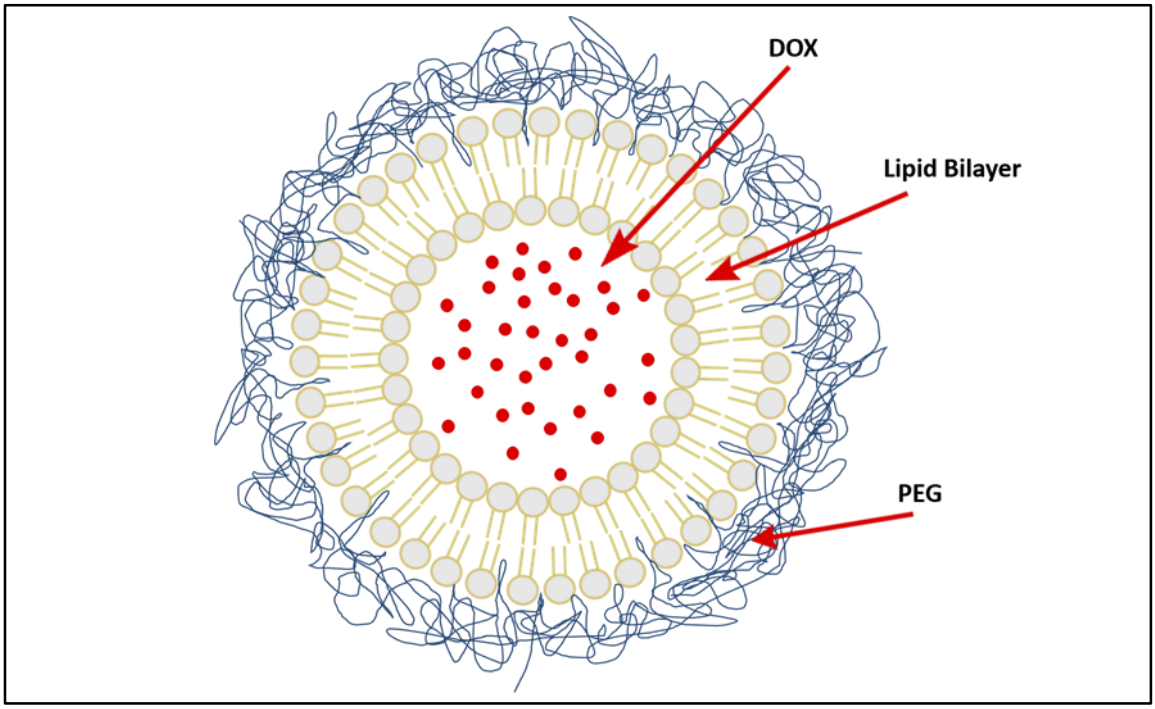

Figure 1.11 Pegylated liposome of DOXil. DOX (red dots) is encapsulated in a lipid bilayer coated with PEG. The lipid bilayer prevents DOX release outside tumor site and the PEG shell inhibits immune or metabolic removal of the complex.

1.6.2 Dexrazoxane Co-Treatment

Co-administration of DOX with ROS scavengers has been another approach used to mitigate DOX-induced cardiotoxicity (Lipshultz, 2010). One ROS scavenger, dexrazoxane (DEX, **Figure 1.12**), used in this manner for more than 20 years, reduces ROS generation by inhibiting the formation of iron-quinone complexes (Hasinoff, 1998). In order to prevent these complexes, DEX must first undergo enzymatic hydrolysis, mediated by dihydroorotase, to open both rings. Once in the ring-opened form, it detaches iron from the quinone and chelates intracellular iron, which prevents complex formation (Junjing, 2010; Šimůnek, 2008). Furthermore, DEX scavenges for hydroxyl and superoxide radicals in its parent, ring-closed form (Galetta, 2010). The effectiveness of this approach was demonstrated by comparing atrial contractility of rats administered DEX prior to chronic anthracycline treatment (Cusack, 2006). From this study, DEX treated rats had roughly 3 times greater atrial contractility (27 g/s) compared to those not given the ROS scavenger (10 g/s) and had similar contractility to a control group (33 g/s). As a result, co-administration of DEX attenuated the risk of cardiotoxicity without impairing DOX cytotoxicity.

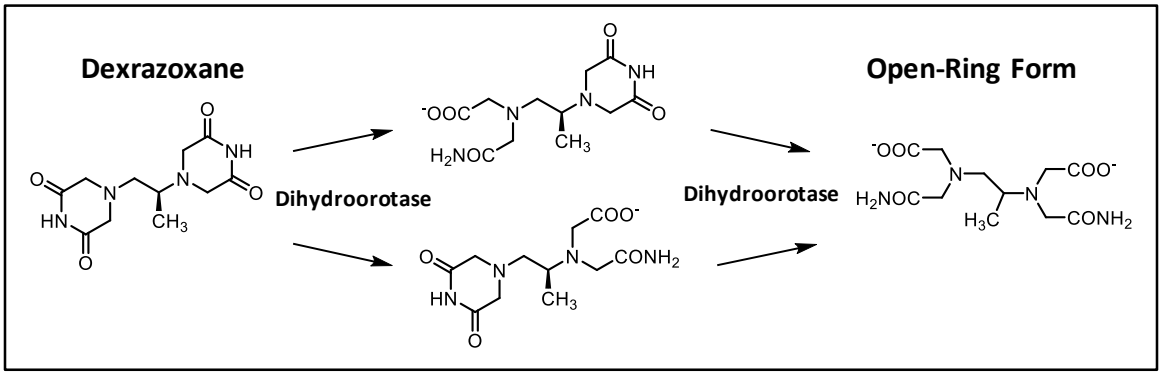

Figure 1.12 Activation of dexrazoxane for iron-chelation. Opening both rings on dexrazoxane requires dihydroorotase-mediated hydrolysis. Once in the open form, DEX can inhibit quinone-iron complexes by chelation of intracellular iron, thus preventing ROS formation.

1.6.3 Epirubicin and Idarubicin Analogs

In an effort to overcome the cardiotoxic nature of anthracyclines, the structurally modified analog EPI was developed (**Figure 1.13**). It was found that EPI produced similar antitumor activity as DOX, while being less cardiotoxic (Torti, 1986; Weiss, 1992). In fact, it was found that roughly 180 mg/m^2 more EPI was required before similar cardiotoxic injuries occurred. The single epimerization of the daunosamine hydroxyl decreases cardiotoxicity due to an increased occurrence of glucuronidation: the attachment of glucuronic acid via a glycosidic bond to the daunosamine hydroxyl group. The amplified glucuronidation helps facilitate the excretion of EPI and as a result shortens the elimination phase, generating superior plasma clearance than DOX.

An additional anthracycline analog, IDA (**Figure 1.13**), has also been studied for its potential to be less cardiotoxic (Daghestani, 1985; Ganzina, 1986). This analog is similar to DNR with the only difference stemming from the elimination of the C-4 methoxy on the tetracyclic moiety. The removal of this group provides better affinity toward lipids allowing for the possibility of oral administration instead of intravenously. While the *in vivo* studies show that, mass to mass, this analog produces more cardiotoxicity than DNR, overall cardiotoxicity is reduced because patients only require one fifth of IDA for similar anticancer effects.

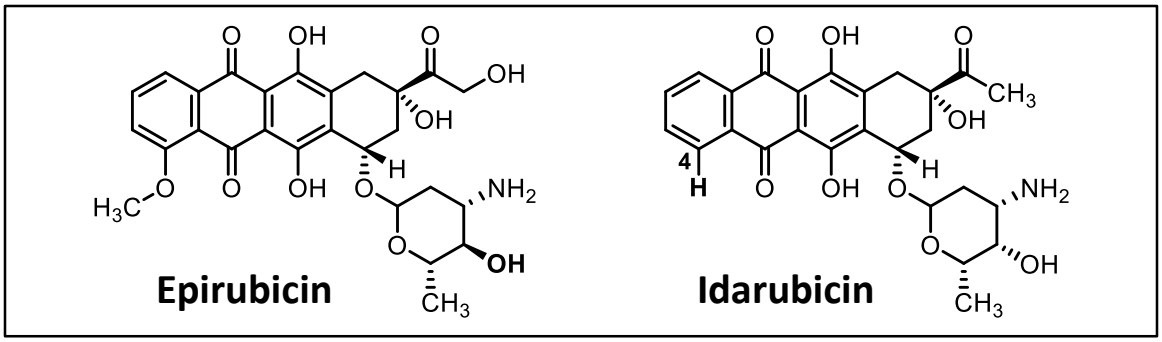

Figure 1.13 Structures of Epirubicin and Idarubicin. Epirubicin is a DOX based analog with a single epimerization of the daunosamine hydroxyl. Idarubicin is a demethoxylated analog of DNR.

1.6.4 Synthetic Modifications of Anthracycline Core to Overcome Cardiotoxicity

Synthetic chemists have sought to alleviate cardiotoxicity by removing the structural moieties responsible for inducing the undesired effects. Since metabolism of the C-13 carbonyl to the corresponding alcohol has been proposed to result in cardiac dysfunction, this was a logical functional group to attempt modifying. One successful modification followed a Wolff-Kishner style reduction of the C-13 carbonyl to a methylene, forming 13-deoxydoxorubicin (DeoxyDOX, **Figure 1.14**) (Smith, 1978). While DeoxyDOX, entered into clinical trials by GEM Pharmaceuticals under the name "GPX-100", does not interact with carbonyl reductase to form DOXol, a phase 2 clinical trial was terminated early because several patients began displaying signs of cardiac disfunction (Holstein, 2015).

The lack of success with DeoxyDOX indicated that the quinone moiety also has an integral role in the onset of cardiotoxicity. As a result, a second-generation analog, 5-imino-13-deoxydoxorubicin (DIDOX), was developed by converting the quinone of DeoxyDOX to a less reactive iminoquinone. The new compound is termed "GPX-150" by GEM Pharmaceuticals (**Figure 1.14**) (Acton, 1981). The combination of these structural modifications prevents the formation of the cardiotoxic alcohol metabolite and ROS from

quinone redox cycling. In experiments using rabbit heart models, no sign of cardiotoxicity was observed during or after DIDOX treatment (Frank, 2016; Olson, 2007; Hohl, 2013). One experiment revealed that left atrial contractility was reduced by roughly half when treated with DOX ($P < 0.001$) compared to those treated with DIDOX.

While DIDOX decreases cardiotoxicity, the structural alterations have imposed a cytotoxic disadvantage: DIDOX is about four-fold less potent than DOX. For instance, in a [^{3}H]-thymidine incorporation assay using human promyelocytic leukemia (HL60) cells, DIDOX exhibited an IC_{50} of 593 nM, whereas that of DOX was 148 nM (Holstein, 2015). A separate shortfall of DIDOX involves the synthesis, where the reduction to obtain DeoxyDOX has a yield as low as five percent. The combination of low yield and suppressed potency makes DIDOX a much more expensive chemotherapeutic to manufacture.

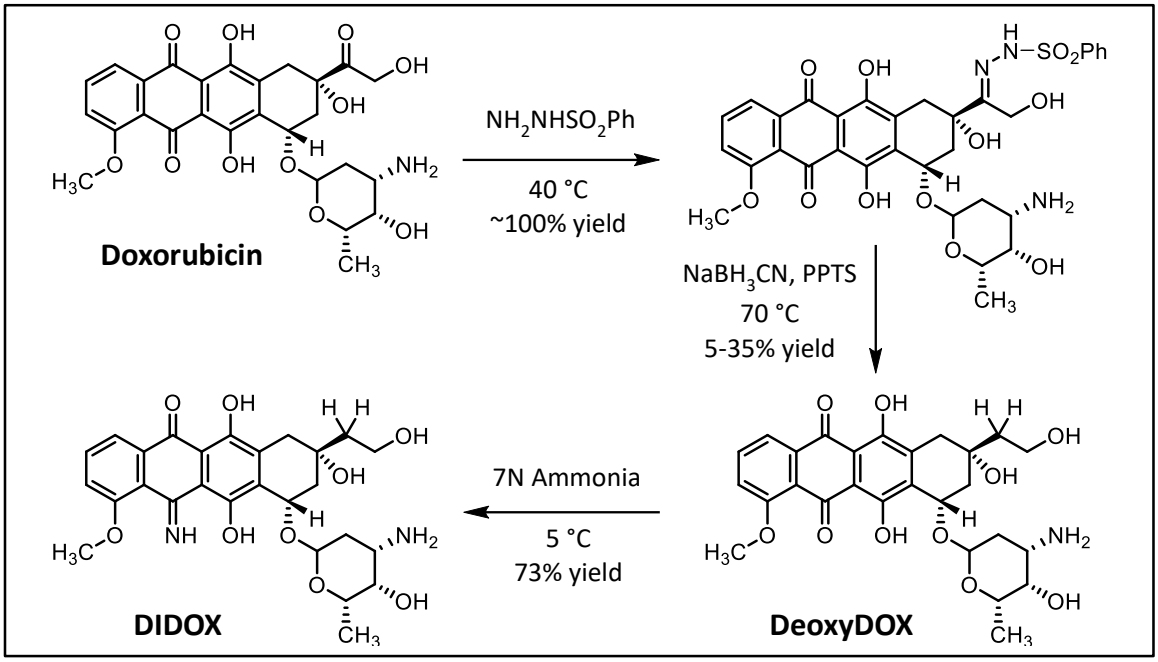

Figure 1.14 Synthesis of DIDOX. The initial step involves an imine condensation at the C-13 carbonyl using benzenesulfonyl hydrazide. DeoxyDOX is then formed after a Wolff-Kishner reduction using sodium cyanoborohydride and pyridinium p-toluenesulfonate. The final step to obtain DIDOX uses concentrated ammonia to convert the quinone to an iminoquinone.

1.7 Cancer Resistance

The development of multidrug resistance (MDR), such as resistance to DOX, has led to the failure of life-saving therapies, notably when attempting to treat recurring breast cancer (Bao, 2011). Characteristic of MDR is the overexpression of P-glycoprotein (PGP) (Frézard, 2001; Loe, 1996). It has been well documented that PGP is involved in molecular efflux and that this efflux capacity is potentially an underlying cause for MDR. Glutathione has also been implicated with assisting drug efflux leading to MDR. Also, alterations to the mechanisms and structure of TOPOII contribute to resistance of anthracycline treatment. These important mechanisms of resistance to DOX will be discussed in the sections that follow.

1.7.1 P-Glycoprotein-Mediated Resistance

The human ATP-binding cassette (ABC) transporter family has drawn interest due to its possible role in MDR. This family contains a variety of structurally related membrane proteins responsible for moving substrates against their concentration gradients, notably across intra- and extracellular membranes (Dean, 2001). Overexpression of one member of the ABC transporter family, PGP, is observed in drug resistant cancer lines and continues to be the focus of intense research (Cordon-Cardo, 1989; Koziolová, 2016). Pharmacokinetic studies determined that PGP is able to recognize a broad spectrum of drugs, such as DOX, and transport them outside the cell (**Figure 1.15**) (Lin, 2003). Remarkably, when previously sensitive cells were transfected with a PGP expression vector, their sensitivity to DOX decreased up to 15-fold (Grant, 1994). Not only does PGP have a preference for molecules containing multiple aromatic rings, efflux occurs roughly three times faster if the molecule contains a basic center able to accept a proton (Priebe,

1993). Both of these structural features are consistent with that of DOX and understandably allow for preferential efflux of this drug. In addition, it has become evident that PGP overexpression occurs in cell lines expressing resistance to drugs such as DOX, which results in reduced intracellular concentrations of DOX and the failing of its anticancer potential (Grant, 1994).

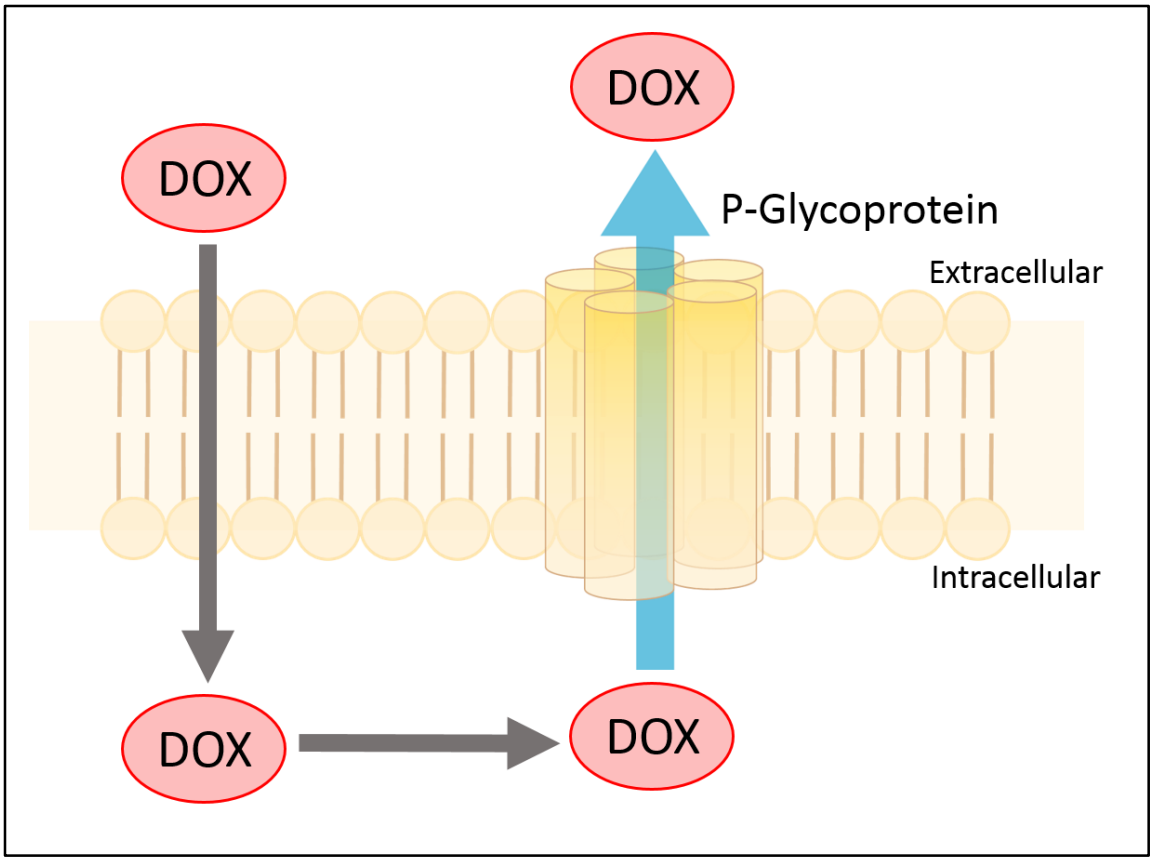

Figure 1.15 P-Glycoprotein efflux. Although DOX passively diffuses across the cell membrane, PGP efficiently recognizes, binds, and transports the drug back into the extracellular space. This efflux protein is up-regulated in MDR cancer cells.

1.7.2 Glutathione MDR

Glutathione S-transferase (GST) is a ubiquitous cytoplasmic enzyme responsible for xenobiotic biotransformation and metabolism. The increased expression of one subclass, GSTπ, is linked to numerous cancer lines resistant to DOX (Goto, 2001). The reduced form of glutathione (GSH) has a function in facilitating the efflux of DOX through

the formation of DOX-GSH adducts, which are recognized by ABC transporters. GSTπ has a role in the formation of these adducts, however, a specific mechanism has yet to be proposed. To demonstrate GSTπ-facilitated resistance, MCF-7 human breast cancer cells were transfected with the GSTπ gene and evaluated for resistance (Moscow, 1989). These cells expressed resistance correlating to the concentration of GSTπ, where lower level provided roughly three-fold resistance and higher levels expressed nearly 4.5-fold resistance. Additionally, GSTπ accumulates inside the nucleus of cells, where it exhibits peroxidase activity to scavenge DOX-induced ROS, limiting DNA lesions and reducing activity.

1.7.3 Topoisomerase II-Mediated Resistance

Several tumors, such as small- and non-small cell lung cancer, develop MDR because of reduced TOPOII activity (Cole, 1991). Evidently, a decreased concentration or activity of this enzyme inhibits the effectiveness of DOX, due to one of its primary mechanisms relying on the interaction and inhibition of TOPOII. For example, a resistant KB/VM-4 cancer line, developed by growing HeLa cells under 31-53 nM Teniposide pressure, expressed only 21% relative TOPOII concentrations. This allowed for an 11-fold increase in resistance to DOX (Matsuo, 1990). While conclusive evidence for one mechanism over the other has yet to be offered, the onset of MDR is likely a combination of those described.

1.7.4 Daunosamine Functionalization to Overcome Multidrug Resistance

As mentioned previously, DOX covalently binds to DNA through an aldehyde intermediate produced from free radical reactions. However, DOX-resistant cells have a high expression of antioxidants and drug efflux proteins that prevent this important

cytotoxic event from occurring (Gariboldi, 2003). Additionally, synthetic modifications of the 3'-amine on DOX have been able to prevent the inhibition of DNA cross-links and PGP drug efflux (Beckman, 1988; Bielack, 1994; Streeter, 1986; Taatjes, 2001).

Modification to the 3'-amine of DOX has included a variety of moieties that contain an intrinsic ability to form covalent DNA adducts without relying on metabolic activation (Wassermann, 1986). One example is the modified drug 2-pyrrolinodoxorubicin (PDOX), synthesized with a five-membered pyrrolino ring on the daunosamine sugar (Stepankova, 2011; Studenovsky, 2011). This pyrrolino moiety acts as a masked aldehyde capable of forming covalent bonds with DNA (**Figure 1.16**) (Nagy, 1996). The formation occurs when the nitrogen from a DNA base pair, such as guanine, acts as a nucleophile to form an aminal adduct with the iminium carbon. After modification, hydrogen bonding occurs with an adjacent guanine base to complete the DNA virtual cross-link (Cullinane, 1993). Such functionalization has been able to overcome MDR and will be discussed in further detail in the next chapter.

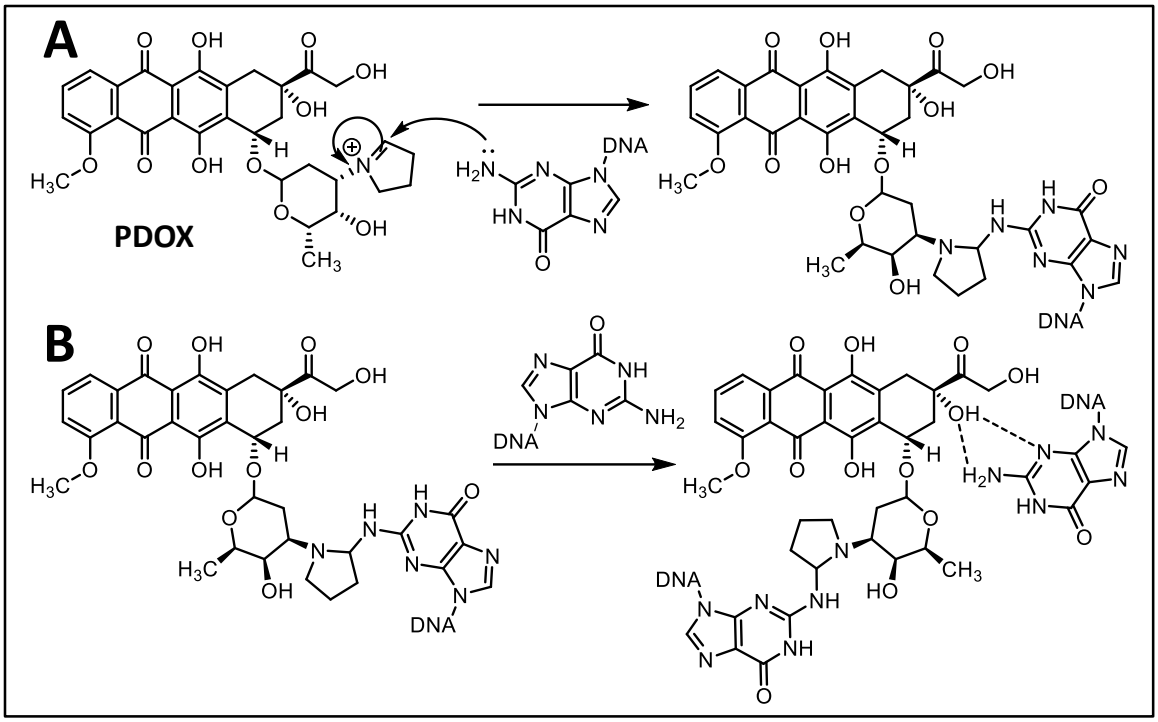

Figure 1.16 PDOX DNA cross-linking. (A) Guanine acts as a nucleophile and reacts with the pyrroline to neutralize the reactive iminium. **(B)** After initial attachment of one guanine, hydrogen bonding with an adjacent guanine completes the virtual cross-link.

1.8 Concluding Remarks

While the cardiotoxic side effects limit use, anthracyclines such as DOX remain important in anticancer therapies. The push toward a better anthracycline has been a focus for decades and continues to be of interest. The successes of several methods and analogs have given hope that one day a clinically useful anthracycline will be available without the alarm of cardiac damage. The work described in this thesis has a directed focus on combining the success of synthetic modifications to remove the potential of cardiotoxicity with that of improving anthracycline efficacy against cancer.

1.9 References

Acton, E. M., & Tong, G. L. (1981). Synthesis and preliminary antitumor evaluation of 5-iminodoxorubicin. *Journal of Medicinal Chemistry*, *24*(6), 669-673.

Allen, T. M., Hansen, C., Martin, F., Redemann, C., & Yau-Young, A. (1991). Liposomes containing synthetic lipid derivatives of poly (ethylene glycol) show prolonged circulation half-lives in vivo. *Biochimica et Biophysica Acta (BBA)-Biomembranes*, *1066*(1), 29-36.

Bachur, N. R., GORDON, S. L., & GEE, M. V. (1977). Anthracycline antibiotic augmentation of microsomal electron transport and free radical formation. *Molecular Pharmacology*, *13*(5), 901-910.

Bachur, N. R., Gordon, S. L., Gee, M. V., & Kon, H. (1979). NADPH cytochrome P-450 reductase activation of quinone anticancer agents to free radicals. *Proceedings of the National Academy of Sciences*, *76*(2), 954-957.

Bao, L., Haque, A., Jackson, K., Hazari, S., Moroz, K., Jetly, R., & Dash, S. (2011). Increased expression of P-glycoprotein is associated with doxorubicin chemoresistance in the metastatic 4T1 breast cancer model. *The American Journal of Pathology*, *178*(2), 838-852.

Barthel, B. L., Mooz, E. L., Wiener, L. E., Koch, G. G., & Koch, T. H. (2016). Correlation of in situ oxazolidine formation with highly synergistic cytotoxicity and DNA cross-linking in cancer cells from combinations of doxorubicin and formaldehyde. *Journal of Medicinal Chemistry*, *59*(5), 2205-2221.

Batist, G., Ramakrishnan, G., Rao, C. S., Chandrasekharan, A., Gutheil, J., Guthrie, T., & Tkaczuk, K. (2001). Reduced cardiotoxicity and preserved antitumor efficacy of liposome-encapsulated doxorubicin and cyclophosphamide compared with conventional doxorubicin and cyclophosphamide in a randomized, multicenter trial of metastatic breast cancer. *Journal of Clinical Oncology*, *19*(5), 1444-1454.

Beckman, R. A., McFall, P. J., Sikic, B. I., & Smith, S. D. (1988). Doxorubicin and the alkylating anthracycline 3′-deamino-3′-(3-cyano-4-morpholinyl) doxorubicin: comparative in vitro potency against leukemia and bone marrow cells. *Journal of the National Cancer Institute*, *80*(5), 361-365.

Beckman, J. S., & Koppenol, W. H. (1996). Nitric oxide, superoxide, and peroxynitrite: the good, the bad, and ugly. *American Journal of Physiology-Cell Physiology*, *271*(5), C1424-C1437.

Berger, J. M., Gamblin, S. J., Harrison, S. C., & Wang, J. C. (1996). Structure and mechanism of DNA topoisomerase II. *Nature*, *379*(6562), 225.

Berman, E., Heller, G., Santorsa, J., McKenzie, S., Gee, T., Kempin, S., & Gabrilove, J. (1991). Results of a randomized trial comparing idarubicin and cytosine arabinoside with daunorubicin and cytosine arabinoside in adult patients with newly diagnosed acute myelogenous leukemia. *Blood*, *77*(8), 1666-1674.

Bernard, J., Weil, M., Boiron, M., Jacquillat, C., Flandrin, G., & Gemon, M. F. (1973). Acute promyelocytic leukemia: results of treatment by daunorubicin. *Blood*, *41*(4), 489-496.

Bielack, S. S., Kallenbach, K., Looft, G., Erttmann, R., & Winkler, K. (1994). Structurally modified anthracyclines retain activity in a cell line with simultaneous typical and atypical multidrug resistance. *Anticancer Research*, *15*(4), 1279-1284.

Boucek, R. J. (1997). Mechanisms for anthracycline-induced cardiomyopathy: clinical and laboratory correlations. *Progress in Pediatric Cardiology*, *8*(2), 59-70.

Burton, K. P., McCord, J. M., & Ghai, G. E. E. T. H. A. (1984). Myocardial alterations due to free-radical generation. *American Journal of Physiology-Heart and Circulatory Physiology*, *246*(6), H776-H783.

Buzdar, A. U., Ibrahim, N. K., Francis, D., Booser, D. J., Thomas, E. S., Theriault, R. L., & Cristofanilli, M. (2005). Significantly higher pathologic complete remission rate after neoadjuvant therapy with trastuzumab, paclitaxel, and epirubicin chemotherapy: results of a randomized trial in human epidermal growth factor receptor 2–positive operable breast cancer. *Journal of Clinical Oncology*, *23*(16), 3676-3685.

Capranico, G., Kohn, K. W., & Pommier, Y. (1990). Local sequence requirements for DNA cleavage by mammalian topoisomerase II in the presence of doxorubicin. *Nucleic Acids Research, 18*(22), 6611-6619.

Chauhan, V. P., Stylianopoulos, T., Martin, J. D., Popović, Z., Chen, O., Kamoun, W. S., & Jain, R. K. (2012). Normalization of tumour blood vessels improves the delivery of nanomedicines in a size-dependent manner. *Nature Nanotechnology*, *7*(6), 383-388.

Cole, S. P., Chanda, E. R., Dicke, F. P., Gerlach, J. H., & Mirski, S. E. (1991). Non-P-glycoprotein-mediated multidrug resistance in a small cell lung cancer cell line: evidence for decreased susceptibility to drug-induced DNA damage and reduced levels of topoisomerase II. *Cancer Research*, *51*(13), 3345-3352.

Cordon-Cardo, C., O'Brien, J. P., Casals, D., Rittman-Grauer, L., Biedler, J. L., Melamed, M. R., & Bertino, J. R. (1989). Multidrug-resistance gene (P-glycoprotein) is expressed by endothelial cells at blood-brain barrier sites. *Proceedings of the National Academy of Sciences*, *86*(2), 695-698.

Cullinane, C., & Phillips, D. R. (1993). Thermal stability of DNA adducts induced by cyanomorpholinoadriamycin in vitro. *Nucleic Acids Research*, *21*(8), 1857-1862.

Cummings, J., Willmott, N., Hoey, B. M., Marley, E. S., & SMyth, J. F. (1992). The consequences of doxorubicin quinone reduction in vivo in tumour tissue. *Biochemical Pharmacology*, *44*(11), 2165-2174.

Cusack, B. J., Mushlin, P. S., Voulelis, L. D., Li, X. D., Boucek, R. J., & Olson, R. D. (1993). Daunorubicin-induced cardiac injury in the rabbit: a role for daunorubicinol?. *Toxicology and Applied Pharmacology*, *118*(2), 177-185.

Cusack, B. J., Gambliel, H., Musser, B., Hadjokas, N., Shadle, S. E., Charlier, H., & Olson, R. D. (2006). Prevention of chronic anthracycline cardiotoxicity in the adult Fischer 344 rat by dexrazoxane and effects on iron metabolism. *Cancer Chemotherapy and Pharmacology*, *58*(4), 517-526.

Cutts, S. M., Swift, L. P., Rephaeli, A., Nudelman, A., & Phillips, D. R. (2003). Sequence specificity of adriamycin-DNA adducts in human tumor cells1. *Molecular Cancer Therapeutics*, *2*(7), 661-670.

Danesi, R., Fogli, S., Gennari, A., Conte, P., & Del Tacca, M. (2002). Pharmacokinetic-pharmacodynamic relationships of the anthracycline anticancer drugs. *Clinical Pharmacokinetics*, *41*(6), 431-444.

Daghestani, A. N., Arlin, Z. A., Leyland-Jones, B., Gee, T. S., Kempin, S. J., Mertelsmann, R., & Clarkson, B. D. (1985). Phase I and II clinical and pharmacological study of 4-demethoxydaunorubicin (idarubicin) in adult patients with acute leukemia. *Cancer Research*, *45*(3), 1408-1412.

Dean, M., Hamon, Y., & Chimini, G. (2001). The human ATP-binding cassette (ABC) transporter superfamily. *Journal of Lipid Research*, *42*(7), 1007-1017.

DeSantis, C. E., Lin, C. C., Mariotto, A. B., Siegel, R. L., Stein, K. D., Kramer, J. L., & Jemal, A. (2014). Cancer treatment and survivorship statistics, 2014. *CA: A Cancer Journal for Clinicians*, *64*(4), 252-271.

Dodd, D. A., Atkinson, J. B., Olson, R. D., Buck, S., Cusack, B. J., Fleischer, S., & Boucek Jr, R. J.

(1993). Doxorubicin cardiomyopathy is associated with a decrease in calcium release channel of the sarcoplasmic reticulum in a chronic rabbit model. *Journal of Clinical Investigation*, *91*(4), 1697.

Doroshow, J. H., Locker, G. Y., & Myers, C. E. (1980). Enzymatic defenses of the mouse heart against reactive oxygen metabolites: alterations produced by doxorubicin. *Journal of Clinical Investigation*, *65*(1), 128.

Doroshow, J. H., & Davies, K. J. (1986). Redox cycling of anthracyclines by cardiac mitochondria. II. Formation of superoxide anion, hydrogen peroxide, and hydroxyl radical. *Journal of Biological Chemistry*, *261*(7), 3068-3074.

Frank, N. E., Cusack, B. J., Talley, T. T., Walsh, G. M., & Olson, R. D. (2016). Comparative effects of doxorubicin and a doxorubicin analog, 13-deoxy, 5-iminodoxorubicin (GPX-150), on human topoisomerase IIβ activity and cardiac function in a chronic rabbit model. *Investigational New Drugs*, *34*(6), 693-700.

Frederick, C. A., Williams, L. D., Ughetto, G., Van der Marel, G. A., Van Boom, J. H., Rich, A., & Wang, A. H. (1990). Structural comparison of anticancer drug-DNA complexes: adriamycin and daunomycin. *Biochemistry*, *29*(10), 2538-2549.

French Adjuvant Study Group. (2001). Benefit of a high-dose epirubicin regimen in adjuvant chemotherapy for node-positive breast cancer patients with poor prognostic factors: 5-year follow-up results of French Adjuvant Study Group 05 randomized trial. *Journal of Clinical Oncology*, *19*(3), 602-611.

Frézard, F., Pereira-Maia, E., Quidu, P., Priebe, W., & Garnier-Suillerot, A. (2001). P-Glycoprotein preferentially effluxes anthracyclines containing free basic versus charged amine. *The FEBS Journal*, *268*(6), 1561-1567.

Gabizon, A., Catane, R., Uziely, B., Kaufman, B., Safra, T., Cohen, R., & Barenholz, Y. (1994). Prolonged circulation time and enhanced accumulation in malignant exudates of doxorubicin encapsulated in polyethylene-glycol coated liposomes. *Cancer Research*, *54*(4), 987-992.

Galetta, F., Franzoni, F., Cervetti, G., Regoli, F., Fallahi, P., Tocchini, L., & Santoro, G. (2010). In vitro and in vivo study on the antioxidant activity of dexrazoxane. *Biomedicine & Pharmacotherapy*, *64*(4), 259-263.

Ganzina, F., Pacciarini, M. A., & Pietro, N. (1986). Idarubicin (4-demethoxydaunorubicin). *Investigational new drugs*, *4*(1), 85-105.

Gao, R., Schellenberg, M. J., Shar-yin, N. H., Abdelmalak, M., Marchand, C., Nitiss, K. C., & Pommier, Y. (2014). Proteolytic degradation of topoisomerase II (Top2) enables the processing of Top2· DNA and Top2· RNA covalent complexes by tyrosyl-DNA-phosphodiesterase 2 (TDP2). *Journal of Biological Chemistry*, *289*(26), 17960-17969.

Gariboldi, M. B., Ravizza, R., Riganti, L., Meschini, S., Calcabrini, A., Marra, M., & Monti, E. (2003). Molecular determinants of intrinsic resistance to doxorubicin in human cancer cell lines. *International Journal of Oncology*, *22*(5), 1057-1064.

Goto, S., Ihara, Y., Urata, Y., Izumi, S., Abe, K., Koji, T., & Kondo, T. (2001). Doxorubicin-induced DNA intercalation and scavenging by nuclear glutathione S-transferase π. *The FASEB Journal*, *15*(14), 2702-2714.

Gottdiener, J. S., Mathisen, D. J., Borer, J. S., Bonow, R. O., Myers, C. E., Barr, L. H., & Rosenberg, S. A. (1981). Doxorubicin cardiotoxicity: assessment of late left ventricular dysfunction by radionuclide cineangiography. *Annals of Internal Medicine*, *94*(4_Part_1), 430-435.

Grant, C. E., Valdimarsson, G., Hipfner, D. R., Almquist, K. C., Cole, S. P., & Deeley, R. G. (1994). Overexpression of multidrug resistance-associated protein (MRP) increases resistance to natural product drugs. *Cancer Research*, *54*(2), 357-361.

Gruber, B. M., Anuszewska, E. L., & Priebe, W. (2004). The effect of new anthracycline derivatives on the induction of apoptotic processes in human neoplastic cells. *Folia Histochemica et Cytobiologica*, *42*(2), 127-130.

Harashima, H., Iida, S., Urakami, Y., Tsuchihashi, M., & Kiwada, H. (1999). Optimization of antitumor effect of liposomally encapsulated doxorubicin based on simulations by pharmacokinetic/pharmacodynamic modeling. *Journal of Controlled Release*, *61*(1), 93-106.

Harris, L. N., Yang, L., Liotcheva, V., Pauli, S., Iglehart, J. D., Colvin, O. M., & Hsieh, T. S. (2001). Induction of topoisomerase II activity after ErbB2 activation is associated with a differential response to breast cancer chemotherapy. *Clinical Cancer Research*, *7*(6), 1497-1504.

Hasinoff, B. B. (1998, August). Chemistry of dexrazoxane and analogues. *Seminars in Oncology* (Vol. 25, No. 4 Suppl 10, pp. 3-9).

Hohl, R. J., Vestal, R. E., Holstein, S. A., Olson, R. D., Parrott, K., & Walsh, G. M. (2013). Phase I dose-escalation clinical trial with 5-imino-13-deoxydoxorubicin in cancer patients.

Holdener, E. E., Hansen, H. H., Høst, H., Bruntsch, U., Cavalli, F., Renard, J., & Rozencweig, M. (1985). Epirubicin in colorectal cancer. *Investigational New Drugs*, *3*(1), 63-66.

Holstein, S. A., Bigelow, J. C., Olson, R. D., Vestal, R. E., Walsh, G. M., & Hohl, R. J. (2015). Phase I and pharmacokinetic study of the novel anthracycline derivative 5-imino-13-deoxydoxorubicin (GPX-150) in patients with advanced solid tumors. *Investigational New Drugs, 33*(3), 594-602.

Jones, R. L., Fisher, C., Al-Muderis, O., & Judson, I. R. (2005). Differential sensitivity of liposarcoma subtypes to chemotherapy. *European Journal of Cancer, 41*(18), 2853-2860.

Junjing, Z., Yan, Z., & Baolu, Z. (2010). Scavenging effects of dexrazoxane on free radicals. *Journal of Clinical Biochemistry and Nutrition, 47*(3), 238-245.

Kassner, N., Huse, K., Martin, H. J., Gödtel-Armbrust, U., Metzger, A., Meineke, I., & Wojnowski, L. (2008). Carbonyl reductase 1 is a predominant doxorubicin reductase in the human liver. *Drug Metabolism and Disposition, 36*(10), 2113-2120.

Kooy, N. W., Lewis, S. J., Royall, J. A., Yao, Z. Y., Kelly, D. R., & Beckman, J. S. (1997). Extensive tyrosine nitration in human myocardial inflammation: evidence for the presence of peroxynitrite. *Critical Care Medicine, 25*(5), 812-819.

Koziolová, E., Janoušková, O., Cuchalová, L., Hvězdová, Z., Hraběta, J., Eckschlager, T., & Šubr, V. (2016). Overcoming multidrug resistance in Dox-resistant neuroblastoma cell lines via treatment with HPMA copolymer conjugates containing anthracyclines and P-gp inhibitors. *Journal of Controlled Release, 233*, 136-146.

Kumar, D., Kirshenbaum, L. A., Li, T., Danelisen, I., & Singal, P. K. (2001). Apoptosis in adriamycin cardiomyopathy and its modulation by probucol. *Antioxidants and Redox Signaling, 3*(1), 135-145.

Lefrak, E. A., Piťha, J., Rosenheim, S., & Gottlieb, J. A. (1973). A clinicopathologic analysis of adriamycin cardiotoxicity. *Cancer, 32*(2), 302-314.

Li, T., Danelisen, I., & Singal, P. K. (2002). Early changes in myocardial antioxidant enzymes in rats treated with adriamycin. *Molecular and Cellular Biochemistry, 232*(1), 19-26.

Lin, J. H., & Yamazaki, M. (2003). Role of P-glycoprotein in pharmacokinetics. *Clinical Pharmacokinetics*, *42*(1), 59-98.

Lipshultz, S. E., Colan, S. D., Gelber, R. D., Perez-Atayde, A. R., Sallan, S. E., & Sanders, S. P. (1991). Late cardiac effects of doxorubicin therapy for acute lymphoblastic leukemia in childhood. *New England Journal of Medicine*, *324*(12), 808-815.

Lipshultz, S. E., Scully, R. E., Lipsitz, S. R., Sallan, S. E., Silverman, L. B., Miller, T. L., & Larsen, E. (2010). Assessment of dexrazoxane as a cardioprotectant in doxorubicin-treated children with high-risk acute lymphoblastic leukaemia: long-term follow-up of a prospective, randomised, multicentre trial. *The Lancet Oncology*, *11*(10), 950-961.

Loe, D. W., Deeley, R. G., & Cole, S. P. C. (1996). Biology of the multidrug resistance-associated protein, MRP. *European Journal of Cancer*, *32*(6), 945-957.

Lopez, M., Perno, C. F., Papaldo, P., Lauro, L., Ganzina, F., & Barduagni, A. (1984). Phase II study of epirubicin in advanced malignant melanoma. *Investigational New Drugs*, *2*(3), 315-317.

Loscalzo, J., & Welch, G. (1995). Nitric oxide and its role in the cardiovascular system. *Progress in Cardiovascular Diseases*, *38*(2), 87-104.

Matsuo, K. I., Kohno, K., Takano, H., Sato, S. I., Kiue, A., & Kuwano, M. (1990). Reduction of drug accumulation and DNA topoisomerase II activity in acquired teniposide-resistant human cancer KB cell lines. *Cancer Research*, *50*(18), 5819-5824.

Miller, K. D., Siegel, R. L., Lin, C. C., Mariotto, A. B., Kramer, J. L., Rowland, J. H., & Jemal, A. (2016). Cancer treatment and survivorship statistics, 2016. *CA: A Cancer Journal for Clinicians*, *66*(4), 271-289.

Minotti, G., Cairo, G., & Monti, E. (1999). Role of iron in anthracycline cardiotoxicity: new tunes for an old song?. *The FASEB Journal*, *13*(2), 199-212.

Minotti, G., Ronchi, R., Salvatorelli, E., Menna, P., & Cairo, G. (2001). Doxorubicin irreversibly inactivates iron regulatory proteins 1 and 2 in cardiomyocytes. *Cancer Research*, *61*(23), 8422-8428.

Minotti, G., Menna, P., Salvatorelli, E., Cairo, G., & Gianni, L. (2004). Anthracyclines: molecular advances and pharmacologic developments in antitumor activity and cardiotoxicity. *Pharmacological Reviews*, *56*(2), 185-229.

Minotti, G., Recalcati, S., Menna, P., Salvatorelli, E., Corna, G., & Cairo, G. (2004). Doxorubicin cardiotoxicity and the control of iron metabolism: quinone-dependent and independent mechanisms. *Methods in Enzymology*, *378*, 340-361.

Moscow, J. A., Townsend, A. J., & Cowan, K. H. (1989). Elevation of pi class glutathione S-transferase activity in human breast cancer cells by transfection of the GST pi gene and its effect on sensitivity to toxins. *Molecular Pharmacology*, *36*(1), 22-28.

Mueller-Planitz, F., & Herschlag, D. (2007). DNA topoisomerase II selects DNA cleavage sites based on reactivity rather than binding affinity. *Nucleic Acids Research*, *35*(11), 3764-3773.

Mushlin, P. S., Cusack, B. J., Boucek, R. J., Andrejuk, T., Li, X., & Olson, R. D. (1993). Time-related increases in cardiac concentrations of doxorubicinol could interact with doxorubicin to depress myocardial contractile function. *British Journal of Pharmacology*, *110*(3), 975-982.

Myers, C. (1998, August). The role of iron in doxorubicin-induced cardiomyopathy. In *Seminars in Oncology* (Vol. 25, No. 4 Suppl 10, pp. 10-14).

Nagy, A., Armatis, P., & Schally, A. V. (1996). High yield conversion of doxorubicin to 2-pyrrolinodoxorubicin, an analog 500-1000 times more potent: structure-activity relationship of daunosamine-modified derivatives of doxorubicin. *Proceedings of the National Academy of Sciences*, *93*(6), 2464-2469.

Nitiss, J. L. (2009). Targeting DNA topoisomerase II in cancer chemotherapy. *Nature Reviews. Cancer*, *9*(5), 338.

O'brien, M. E. R., Wigler, N., Inbar, M. C. B. C. S. G., Rosso, R., Grischke, E., Santoro, A., & Orlandi, F. (2004). Reduced cardiotoxicity and comparable efficacy in a phase III trial of pegylated liposomal doxorubicin HCl (CAELYX™/Doxil®) versus conventional doxorubicin for first-line treatment of metastatic breast cancer. *Annals of Oncology*, *15*(3), 440-449.

Olson, R. D., Mushlin, P. S., Brenner, D. E., Fleischer, S., Cusack, B. J., Chang, B. K., & Boucek, R. J. (1988). Doxorubicin cardiotoxicity may be caused by its metabolite, doxorubicinol. *Proceedings of the National Academy of Sciences*, *85*(10), 3585-3589.

Olson, R. D., Headley, M. B., Hodzic, A., Walsh, G. M., & Wingett, D. G. (2007). In vitro and in vivo immunosuppressive activity of a novel anthracycline, 13-deoxy, 5-iminodoxorubicin. *International Immunopharmacology*, *7*(6), 734-743.

Preisler, H. D., Gessner, T., Azarnia, N., Bolanowska, W., Epstein, J., Early, A. P., & Joyce, R. (1984). Relationship between plasma adriamycin levels and the outcome of remission induction therapy for acute nonlymphocytic leukemia. *Cancer Chemotherapy and Pharmacology*, *12*(2), 125-130.

Priebe, W., Van, N. T., Burke, T. G., & Perez-Soler, R. (1993). Removal of the basic center from doxorubicin partially overcomes multidrug resistance and decreases cardiotoxicity. *Anti-cancer drugs*, *4*(1), 37-48.

Rajagopalan, S., Politi, P. M., Sinha, B. K., & Myers, C. E. (1988). Adriamycin-induced free radical formation in the perfused rat heart: implications for cardiotoxicity. *Cancer Research*, *48*(17), 4766-4769.

Robert Jr, J., Olson, R. D., Brenner, D. E., Ogunbunmi, E. M., Inui, M., & Fleischer, S. (1987). The major metabolite of doxorubicin is a potent inhibitor of membrane-associated ion pumps. *Journal of Biological Chemistry*, *262*(33), 15851-15856.

Safra, T., Muggia, F., Jeffers, S., Tsao-Wei, D. D., Groshen, S., Lyass, O., & Gabizon, A. (2000). Pegylated liposomal doxorubicin (doxil): reduced clinical cardiotoxicity in patients reaching or exceeding cumulative doses of 500 mg/m2. *Annals of Oncology*, *11*(8), 1029-1033.

Sawyer, D. B., Fukazawa, R., Arstall, M. A., & Kelly, R. A. (1999). Daunorubicin-induced apoptosis in rat cardiac myocytes is inhibited by dexrazoxane. *Circulation Research, 84*(3), 257-265.

Schaupp, C. M., White, C. C., Merrill, G. F., & Kavanagh, T. J. (2015). Metabolism of doxorubicin to the cardiotoxic metabolite doxorubicinol is increased in a mouse model of chronic glutathione deficiency: A potential role for carbonyl reductase 3. *Chemico-Biological Interactions, 234*, 154-161.

Shen, A. L., Sem, D. S., & Kasper, C. B. (1999). Mechanistic studies on the reductive half-reaction of NADPH-cytochrome P450 oxidoreductase. *Journal of Biological Chemistry, 274*(9), 5391-5398.

Siegel, R. L., Miller, K. D., & Jemal, A. (2016). Cancer statistics, 2016. *CA: A Cancer Journal for Clinicians, 66*(1), 7-30.

Silverman, L., & Barenholz, Y. (2015). In vitro experiments showing enhanced release of doxorubicin from Doxil® in the presence of ammonia may explain drug release at tumor site. *Nanomedicine: Nanotechnology, Biology and Medicine, 11*(7), 1841-1850.

Siveski-Iliskovic, N., Hill, M., Chow, D. A., & Singal, P. K. (1995). Probucol protects against adriamycin cardiomyopathy without interfering with its antitumor effect. *Circulation, 91*(1), 10-15.

Šimůnek, T., Štěrba, M., Popelova, O., Kaiserova, H., Adamcova, M., Hroch, M., & Geršl, V. (2008). Anthracycline toxicity to cardiomyocytes or cancer cells is differently affected by iron chelation with salicylaldehyde isonicotinoyl hydrazone. *British Journal of Pharmacology, 155*(1), 138-148.

Smith, T. H., Fujiwara, A. N., & Henry, D. W. (January 01, 1978). Adriamycin analogues. 2. Synthesis of 13-deoxyanthracyclines. *Journal of Medicinal Chemistry, 21,* 3, 280-3.

Stepankova, J., Studenovsky, M., Malina, J., Kasparkova, J., Liskova, B., Novakova, O., & Brabec, V. (2011). DNA interactions of 2-pyrrolinodoxorubicin, a distinctively

more potent daunosamine-modified analogue of doxorubicin. *Biochemical Pharmacology*, *82*(3), 227-235.

Stewart, D. J., Grewaal, D. A. R. S. H. A. N., Green, R. M., Mikhael, N., Goel, R. A. K. E. S. H., Montpetit, V. A., & Redmond, M. D. (1992). Concentrations of doxorubicin and its metabolites in human autopsy heart and other tissues. *Anticancer Research*, *13*(6A), 1945-1952.

Streeter, D. G., Johl, J. S., Gordon, G. R., & Peters, J. H. (1986). Uptake and retention of morpholinyl anthracyclines by adriamycin-sensitive and-resistant P388 cells. *Cancer Chemotherapy and Pharmacology*, *16*(3), 247-252.

Studenovsky, M., Ulbrich, K., Ibrahimova, M., & Rihova, B. (2011). Polymer conjugates of the highly potent cytostatic drug 2-pyrrolinodoxorubicin. *European Journal of Pharmaceutical Sciences*, *42*(1), 156-163.

Swain, S. M., Whaley, F. S., & Ewer, M. S. (2003). Congestive heart failure in patients treated with doxorubicin. *Cancer*, *97*(11), 2869-2879.

Swift, L. P., Rephaeli, A., Nudelman, A., Phillips, D. R., & Cutts, S. M. (2006). Doxorubicin-DNA adducts induce a non-topoisomerase II–mediated form of cell death. *Cancer Research*, *66*(9), 4863-4871.

Taatjes, D. J., Gaudiano, G., Resing, K., & Koch, T. H. (1997). Redox pathway leading to the alkylation of DNA by the anthracycline, antitumor drugs adriamycin and daunomycin. *Journal of Medicinal Chemistry*, *40*(8), 1276-1286.

Taatjes, D. J., Fenick, D. J., & Koch, T. H. (1998). Epidoxoform: A hydrolytically more stable anthracycline− formaldehyde conjugate toxic to resistant tumor cells. *Journal of Medicinal Chemistry*, *41*(8), 1306-1314.\

Taatjes, D. J., Fenick, D. J., & Koch, T. H. (1999). Nuclear targeting and nuclear retention of anthracycline− formaldehyde conjugates implicates DNA covalent bonding in the cytotoxic mechanism of anthracyclines. *Chemical Research in Toxicology*, *12*(7), 588-596.

Taatjes, D. J., & Koch, T. H. (2001). Nuclear targeting and retention of anthracycline antitumor drugs in sensitive and resistant tumor cells. *Current Medicinal Chemistry*, *8*(1), 15-29.

Tewey, K. M., Rowe, T. C., Yang, L., Halligan, B. D., & Liu, L. F. (1984). Adriamycin-induced DNA damage mediated by mammalian DNA topoisomerase II. *Science*, *226*(4673), 466-468.

Torti, F. M., Bristow, M. M., Lum, B. L., Carter, S. K., Howes, A. E., Aston, D. A., & Billingham, M. E. (1986). Cardiotoxicity of epirubicin and doxorubicin: assessment by endomyocardial biopsy. *Cancer Research*, *46*(7), 3722-3727.

Vásquez-Vivar, J., Martasek, P., Hogg, N., Masters, B. S. S., Pritchard, K. A., & Kalyanaraman, B. (1997). Endothelial nitric oxide synthase-dependent superoxide generation from adriamycin. *Biochemistry*, *36*(38), 11293-11297.

Verweij, J., Lee, S. M., Ruka, W., Buesa, J., Coleman, R., van Hoessel, R., & Judson, I. R. (2000). Randomized phase II study of docetaxel versus doxorubicin in first-and second-line chemotherapy for locally advanced or metastatic soft tissue sarcomas in adults: a study of the European Organization for Research and Treatment of Cancer Soft Tissue and Bone Sarcoma Group. *Journal of Clinical Oncology*, *18*(10), 2081-2086.

Vogler, W. R., Velez-Garcia, E., Weiner, R. S., Flaum, M. A., Bartolucci, A. A., Omura, G. A., & Banks, P. L. (1992). A phase III trial comparing idarubicin and daunorubicin in combination with cytarabine in acute myelogenous leukemia: a Southeastern Cancer Study Group Study. *Journal of Clinical Oncology, 10*(7), 1103-1111.

Wang, A. H., Ughetto, G., Quigley, G. J., & Rich, A. (1987). Interactions between an anthracycline antibiotic and DNA: molecular structure of daunomycin complexed to d (CpGpTpApCpG) at 1.2-. ANG. resolution. *Biochemistry*, *26*(4), 1152-1163.

Wassermann, K., Zwelling, L. A., Mullins, T. D., Silberman, L. E., Andersson, B. S., Bakic, M., & Newman, R. A. (1986). Effects of 3′-deamino-3′-(3-cyano-4-morpholinyl) doxorubicin and doxorubicin on the survival, DNA integrity, and

nucleolar morphology of human leukemia cells in vitro. *Cancer Research*, *46*(8), 4041-4046.

Weinstein, D. M., Mihm, M. J., & Bauer, J. A. (2000). Cardiac peroxynitrite formation and left ventricular dysfunction following doxorubicin treatment in mice. *Journal of Pharmacology and Experimental Therapeutics*, *294*(1), 396-401.

Weiss, R. B. (1992, December). The anthracyclines: will we ever find a better doxorubicin?. In *Seminars in Oncology* (Vol. 19, No. 6, pp. 670-686).

Wibroe, P. P., Ahmadvand, D., Oghabian, M. A., Yaghmur, A., & Moghimi, S. M. (2016). An integrated assessment of morphology, size, and complement activation of the PEGylated liposomal doxorubicin products Doxil®, Caelyx®, DOXOrubicin, and SinaDoxosome. *Journal of Controlled Release*, *221*, 1-8.

Zabudkin, A. F., Matvienko, V., Itkin, A. M., & Matveev, A. (2014). *U.S. Patent No. 8,802,830*. Washington, DC: U.S. Patent and Trademark Office.

Zabudkin, A., Matvienko, V., & Matvyeyev, A. (2014). *U.S. Patent No. 8,846,882*. Washington, DC: U.S. Patent and Trademark Office.

Zeman, S. M., Phillips, D. R., & Crothers, D. M. (1998). Characterization of covalent adriamycin-DNA adducts. *Proceedings of the National Academy of Sciences*, *95*(20), 11561-11565.

CHAPTER TWO: SYNTHESIS AND BIOLOGICAL EVALUATION OF POTENT AND POTENTIALLY NON-CARDIOTOXIC ANTHRACYCLINE ANALOGS

2.1 Introduction

Anthracycline drugs have been used in anticancer therapies for decades, the most clinically important being doxorubicin (DOX) (Weiss, 1992). DOX has proven to be effective against a broad spectrum of solid and hematologic malignancies and is often used in combination with various other chemotherapeutic agents (Danesi, 2002; Gruber, 2004; Verweij, 2000). Although the exact mechanism of DOX is still highly debated, the means of antiproliferation have been suggested to follow a variety of pathways. One supported mechanism involves the intercalation of DOX between DNA double strands followed by topoisomerase II poisoning, leading to irreversible DNA scissions (Capranico, 1990, Tewey, 1984). Additionally, DOX contains a quinone moiety capable of catalyzing the production of intracellular reactive oxygen species (ROS) through NADPH-mediated single-electron shuttling, iron-quinone complexes, or nitric oxide synthase (Cummings, 1992; Shen, 1999; Vásquez-Vivar, 1997). These reactive species generate DNA base pair damage and initiate lipid peroxidation. Another characteristic mechanism involves DNA alkylation and the formation of virtual cross-links (Cutts, 2003; Taatjes, 1998). When DOX enters the cell, it reacts with formaldehyde to create a Schiff base on the daunosamine moiety, allowing it to covalently bind to DNA followed by hydrogen bonding to adjacent DNA bases.

While the effectiveness of DOX is well accepted, its use is severely limited due to the onset of dose-dependent carditoxicity that leads to the eventual outcome of congestive heart failure (Lefrak, 1973; Cusack, 1993). This cardiotoxicity restricts the extent that DOX can be utilized, as the maximum cumulative dose has been established at 450 mg/m^2 (Swain, 2003) The structural moieties responsible for this side effect have been determined to include both the C-13 carbonyl as well as the quinone (**Figure 2.1**) (Olson, 1988; Boucek, 1997). When the C-13 carbonyl is reduced to an alcohol, mediated by the enzyme carbonyl reductase, it forms the major DOX metabolite doxorubicinol (DOXol) (Kassner, 2008; Robert Jr, 1987). This metabolite accumulates in cardiac tissues where it acts as a potent inhibitor of various membrane-associated ion pumps, such as calcium pumps in cardiac sarcoplasmic reticulum, sodium/potassium pumps of cardiac sarcolemma, and F_0F_1 proton pumps of cardiac mitochondria.

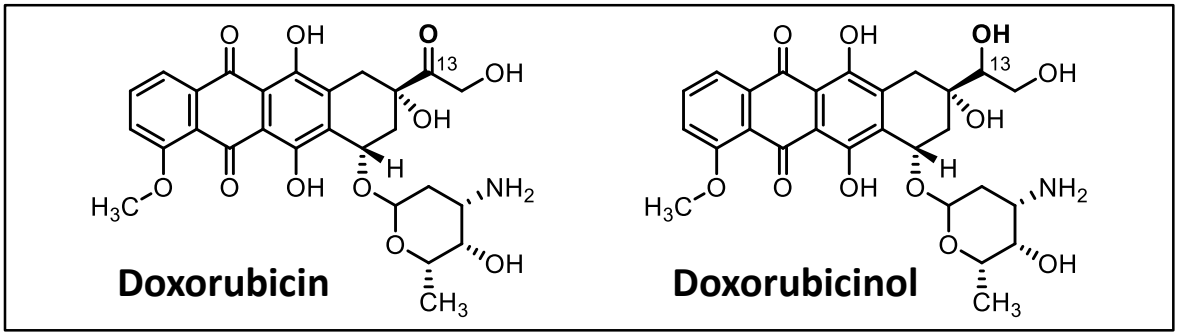

Figure 2.1 DOX and the cardiotoxic metabolite doxorubicinol. Single-electron reduction of the quinone moiety of ring C catalyzes the production of cardiac damaging ROS. The alcohol metabolite, DOXol, is formed by carbonyl reductase-mediated reduction of DOX's C-13 carbonyl, which then accumulates and inhibits ion pumps of cardiac tissue.

While quinone-produced ROS is part of the mechanism of DOX cytotoxicity, cardiac myocytes have a disproportionate susceptibility to this oxidative damage compared to that of other cells (Burton, 1984; Kumar, 2001; Sawyer, 1999; Siveski-Iliskovic, 1995). This stems from cardiac cells expressing low levels of catalase activity in combination with

the inhibitory effect of DOX toward glutathione peroxidase, superoxide dismutase, and other ROS-scavenging enzymes. In order to minimize the cardiotoxic side effects, DOX has been co-administered with dexrazoxane, a ROS scavenger. Additionally, encapsulation with liposomes coated with polyethylene glycol proved helpful to decrease uptake into cardiac tissue, which subsequently reduces cardiotoxicity (Batist, 2001; O'brien, 2004). However, neither of these methods have been able to completely eliminate cardiotoxicity because the two cardiotoxic moieties responsible remain intact.

A separate complication of DOX treatments is the development of multidrug resistance (MDR), the onset of which has made previous life-saving treatments ineffective, as seen when attempting to treat recurring breast cancer (Bao, 2011; Grant, 1994). Such resistance was shown in one study using BALB/c mice, where metastatic tumors of murine mammary carcinoma did not exhibit growth arrest when treated with DOX, as expected with cells displaying MDR. While there is not a complete understanding of MDR, a strong correlation between the overexpression of membrane transporters, such as P-glycoprotein (PGP), and resistance is well documented (Frézard, 2001; Loe, 1996). Not only does PGP recognize and efflux a broad spectrum of drugs, including DOX, but it also has a preference for drugs that contain multiple aromatic rings and a basic nitrogen (Priebe, 1993). Both features are consistent with the structure of DOX and, as such, render efflux particularly favorable for this drug.

Successful synthesis of a non-cardiotoxic DOX analog was achieved in previous work (**Scheme 2.1**) (Frank, 2016; Olson, 2007; Hohl, 2013). This was accomplished through a reduction of the C-13 carbonyl to a methylene followed by the conversion of the highly reactive quinone to a less reactive iminoquinone, forming the final product, 5-imino-

13-deoxydoxorubicin (DIDOX). These modifications prevent the formation of the cardiotoxic DOXol metabolite and inhibit the production of quinone-ROS. Notably, DIDOX has been investigated for signs of cardiotoxicity using rabbit heart models and in clinical trials in humans, and both have revealed no cardiac injury. In-human studies found that DIDOX concentrations as high as 265 mg/m^2 could be administered without any sign of cardiotoxicity, even if the patient had previously been treated with anthracyclines (Holstein, 2015). However, these modifications come with a cytotoxic disadvantage, as DIDOX is, on average, four times less potent than the unadulterated parent compound. For example, [^{3}H]-thymidine incorporation assays reported DIDOX to have an IC_{50} of 593 nM against HL60 cells, whereas DOX had an IC_{50} of 148 nM against the same cell line.

In order to synthesize DIDOX, the C-13 carbonyl of DOX first condenses with benzene sulfonylhydrazide (NH_2NHSO_2Ph) to form a hydrazone-DOX, in very good yield (Smith, 1978). However, the Wolff-Kishner reduction of this hydrazone is incredibly poor, generating the methylene in a yield as low as 5%. While the reducing agent, $NaBH_3CN$, is relatively mild, the high temperature and acidic pyridinium p-toluenesulfonate (PPTS) leads to glycoside hydrolysis, lowering the yield of deoxygenated DOX. Following reduction, the quinone carbonyl is replaced with an imine, in moderate yield, by condensation with concentrated ammonia.

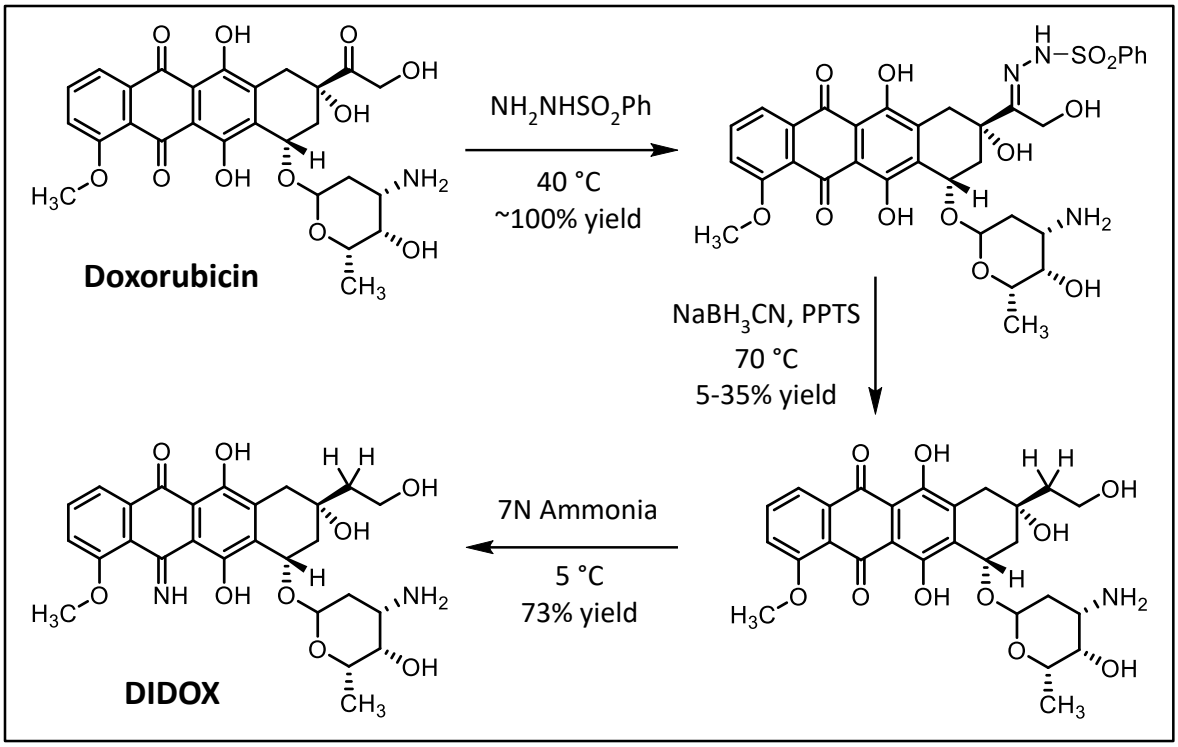

Scheme 2.1 Synthesis of DIDOX. The carbonyl of DOX is reduced to a methylene using a modified Wolff-Kishner reduction. An initial imine condensation occurs using NH_2NHSO_2Ph, which is then reduced using $NaBH_3CN$/PPTS in yields as low as 5%. Afterwords, the quinone is converted to an iminoquinone using 7 N ammonia.

The purpose of this research is to synthesize analogs of DIDOX in order to increase the cytotoxic potency, remove the potential for MDR, and remain non-cardiotoxic. Analysis of literature reports suggests that this can be accomplished by modification of the daunosamine amine to allow for DNA cross-links during intercalation, which has allowed up to a 1000-fold increase in DOX cytotoxicity in certain instances (Acton, 1984; Nagy, 1996). For example, 2-pyrrolinodoxorubicin (PDOX) is synthesized with a five-membered pyrroline ring on the daunosamine sugar to act as a masked aldehyde and is, *in vitro*, more than 500 times more potent against MCF-7 human breast adenocarcionoma than DOX (Nagy, 1996). During intercalation, nitrogen from a DNA base pair acts as a nucleophile to form an aminal adduct with the iminium carbon and then an adjacent base pair hydrogen bonds to the C-9 hydroxyl to form an interstrand virtual cross-link (**Figure 2.2**) (Cullinane,

1993). Alternatively, diacetate-protected analogs, with latent alkylating abilities, have gained interest due to their enhanced stability, as they require enzymatic carboxylate esterase activation before generating a reactive Schiff base (Cherif, 1992).

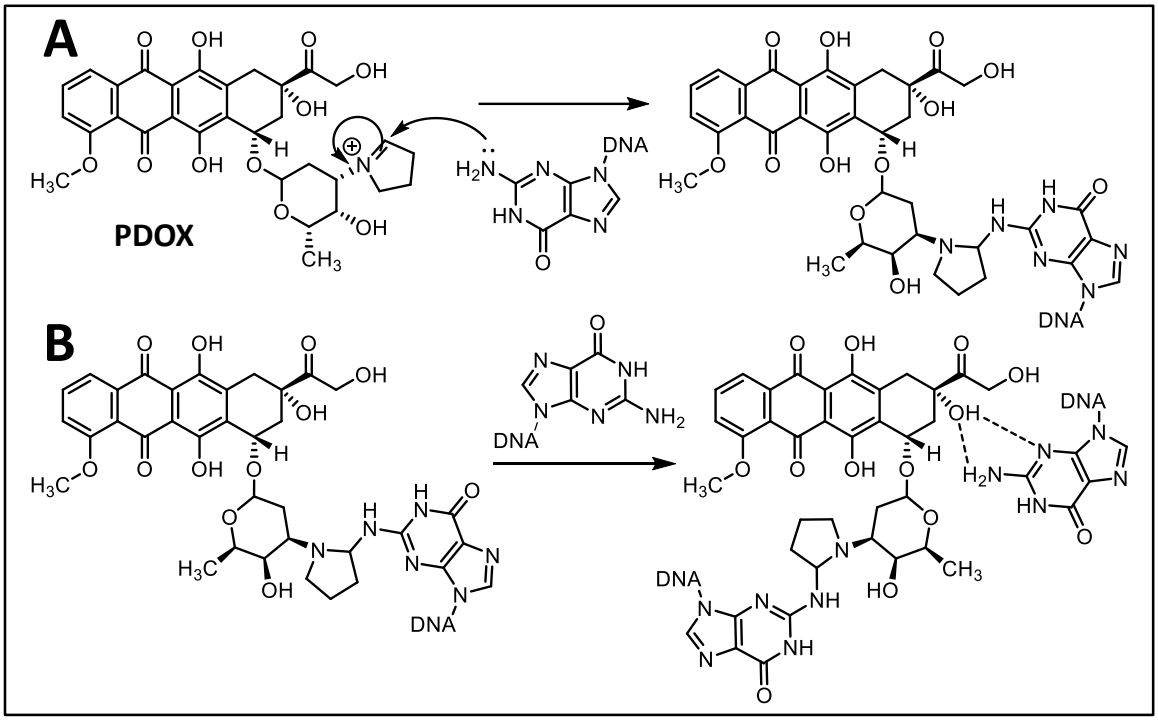

Figure 2.2 PDOX DNA cross-links. (A) During intercalation, a guanine base pair acts as a nucleophile to form an aminal adduct with the iminium carbon. **(B)** Hydrogen bonding with an adjacent base pair then completes the DNA virtual cross-link.

Based upon the reported success of modifying DOX, six analogs of DIDOX were synthesized by attaching alkylating or latent alkylating moieties to the 3'-amine on the daunosamine sugar (**Figure 2.3**). After synthesis of these new drugs, the *in vitro* cytotoxicity was evaluated using a resazurin assay. It was thought that these groups would allow for similar reactivity as seen with comparable DOX analogs, such that covalent attachment to DNA would occur during intercalation to improve potency and reduce MDR related cellular efflux (Streeter, 1986; Studenovsky, 2011).

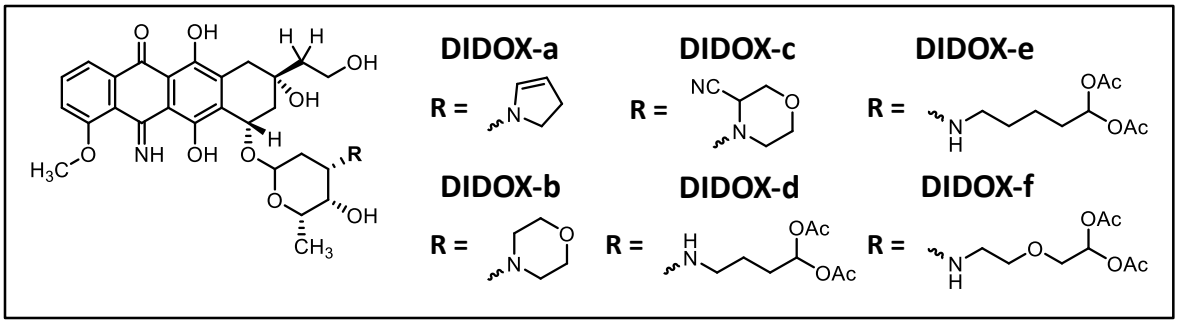

Figure 2.3 DIDOX analogs prepared and evaluated. DIDOX-a, DIDOX-b, and DIDOX-c remove the free basic amine by forming rings. The structure of DIDOX-d, DIDOX-e, and DIDOX-f all have a terminal di-acetate feature, requiring intracellular enzymatic activation before cyclization. All analogs shown are in their free base form.

2.2 Results and Discussion

DIDOX analogs a-f have been structurally characterized and biologically evaluated against seven tumor lines. Four of the six analogs have shown obvious cytotoxic improvements compared with the parent DIDOX and several were equally as potent as DOX. Not only did these analogs improve cytotoxicity, they also retained activity against a MDR cell line, whereas, DIDOX and DOX became significantly less effective.

DIDOX-a and DIDOX-c were synthesized with the innate ability to form DNA cross-links without metabolic activation as they contain a reactive masked aldehyde (Nagy, 1996). This differs from DIDOX-b, which forms these cross-links only after metabolic activation (Lau, 1989). Three of these analogs (DIDOX-d,e,f) were synthesized as diacetate-protected latent aldehydes that, as shown in **Scheme 2.2**, require enzymatic carboxylate esterase activation to first form a geminal diol, which then readily condenses to an aldehyde (Cherif, 1992). Further condensation with the daunosamine amine yields the reactive cyclic moiety, which then forms covalent DNA adducts. Notably, the reactive species of DIDOX-d and DIDOX-f resemble that of DIDOX-a and DIDOX-c, respectively, while DIDOX-e forms a six-membered piperidono ring.

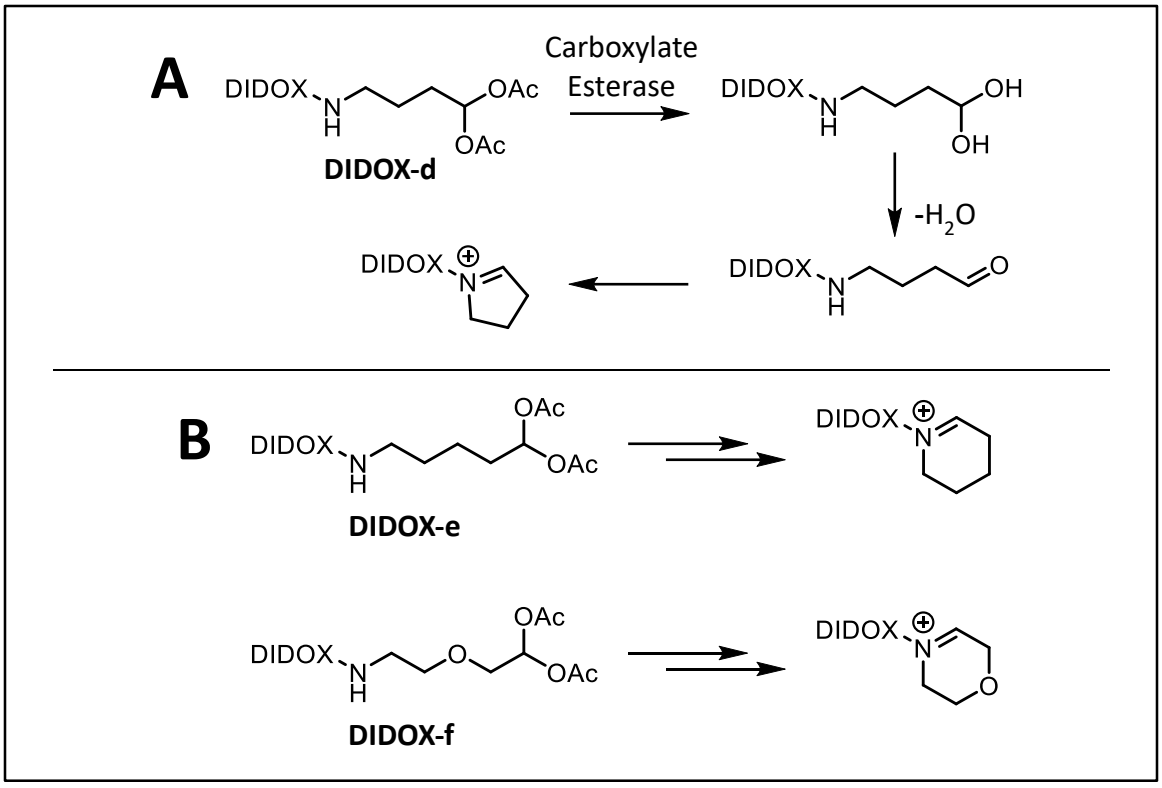

Scheme 2.2 Activation of DIDOX latent aldehyde-analogs by carboxylate esterase. (**A**) DIDOX-d was synthesized with a terminal diacetate, requiring activation to form a reactive iminium. Activation is initiated when carboxylate esterase deprotects the diacetate to form a germinal diol and then dehydration yields an aldehyde species that cyclizes to a reactive pyrrolino iminium through condensation with the daunosamine amine. (**B**) DIDOX-e and DIDOX-f follow analogous activation, with the reactive iminium being part of a piperidono and 1,4-oxizinium moiety, respectively.

2.2.1 DIDOX-a

The synthesis of DIDOX-a used the protocol employed to prepare PDOX, which involves condensing the 3'-amine with 4-iodobutyraldehyde (**1c**) to a Schiff base followed by intramolecular nucleophilic displacement of the iodine (Nagy, 1996). The synthesis of **1c**, prepared as shown in **Scheme 2.3**, first used a Finkelstein reaction to convert 4-chlorobuteraldehyde-1,1-dimethyl acetal (**1a**) to the corresponding iodide. After precipitation of the salts, using hexanes/ether, the pure product was obtained in 88% yield. After substituting halogens, the dimethyl acetal was hydrolyzed in 65% yield to the corresponding aldehyde using aqueous hydrochloric acid. This final iodo-aldehyde, **1c**,

was then used to synthesize DIDOX-a in yields that exceeded 80%. Optimal conditions used 30 equivalents of **1c** and ensured DIDOX was held at low concentrations (ca. 0.06 M). If the reaction was too concentrated, high molecular weight adducts were observed with masses that were consistent with DIDOX dimerization. On the other hand, if the DIDOX was too dilute the reaction would not go to completion. During purification, it was necessary to treat the silica gel with triethylamine prior to loading DIDOX-a to avoid significant decomposition. After purification, DIDOX-a was made into a TFA salt without any significant loss of purity or yield.

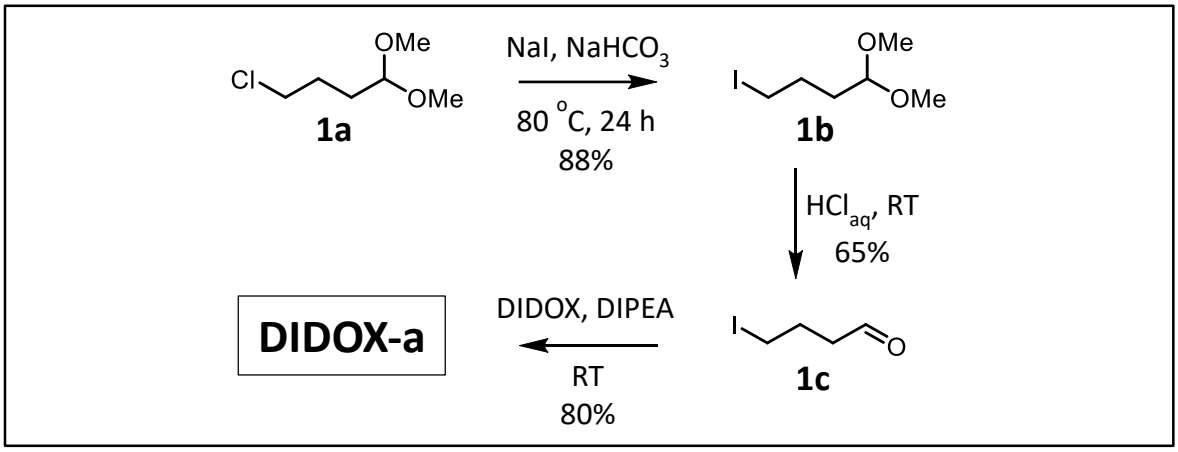

Scheme 2.3 Synthesis of DIDOX-a. 1b was obtained using NaI to substitute the chlorine of **1a** with an iodine. Next, the dimethyl acetal becomes deprotected to an aldehyde using aqueous HCl, which is then condensed with the 3'-amine of DIDOX to produce DIDOX-a.

2.2.2 DIDOX-b

The synthesis to obtain DIDOX-b followed an established route derived from previous literature procedures (**Scheme 2.4**) (Takahashi, 1982). First, both chlorines on **2a** were substituted for iodine, in 77% yield, and then DIDOX was treated with 20 equivalents of **2b** in DMF and DIPEA. The high concentration of diiodide was used to accelerate the first S_N2 substitution (e.g. slow intermolecular followed by quick intramolecular S_N2), to allow for a complete reaction in a reasonable amount of time. After stirring in the dark for

two days and purified on silica, the morpholino DIDOX-b was obtained in 94% yield as a free base, which was later converted to a TFA salt with no loss of yield or purity.

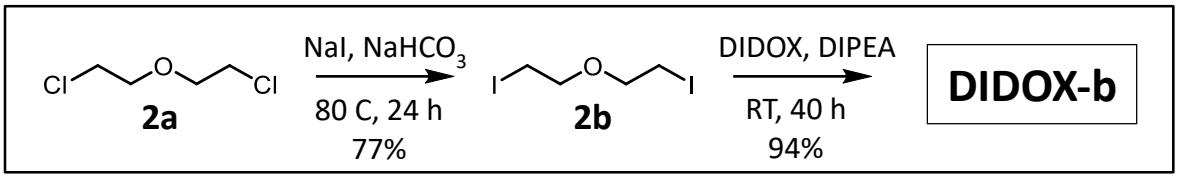

Scheme 2.4 Synthesis of DIDOX-b. Initially, substitution of both chlorines on **2a** for iodine occurred using NaI. Next, DIDOX-b was produced after the daunosamine 3'-amine displaced both iodines by intermolecular then intramolecular S_N2.

2.2.3 DIDOX-c

The synthesis of the cyanomorpholino group found in DIDOX-c required careful consideration since the analogous DOX variant produced the desired product in only 14% yield (Acton, 1981). Indeed, this compound was a by-product generated upon a $NaBH_3CN$ reductive amination step en route to morpholino-DOX (**Scheme 2.5**). As shown, cyanide from the reducing agent adds to the iminium carbon following the first condensation–but before reduction–or after the second condensation. It was reported that the yield of this reaction could not be improved, even when doping with additional cyanide from alternate sources, such as NaCN.

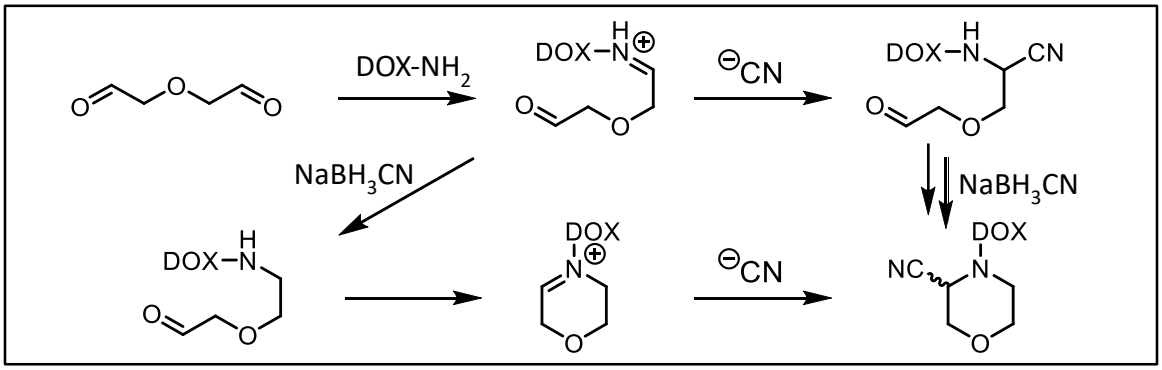

Scheme 2.5 Cyanomorpholino through reductive alkylation. To begin, DOX will first condense with 2,2'-oxybis[acetaldehyde]. Next, a cyanide will either react with the iminium following a second condensation/reduction to form a cyanomorpholino or the iminium is reduced first and a second condensation occurs before the nitrile forms.

The first attempt to improve cyanomorpholino formation followed the synthetic approach outlined in **Scheme 2.6.** This route was devised by modifying the work of Tehrani, et al 2003. In their work, a relatively complex iminium salt was treated with KCN to produce an α-cyano tertiary amine in high yields. Applying this toward DIDOX-c required synthesizing 2-(2-Iodoethoxy)acetaldehyde (**3c**), which was accomplished in two steps from commercially available **3a.** The first step substituted the chlorine for an iodine, which proceeded without any problems and gave a good yield of 92%. The next step, Dess-Martin oxidation, was less efficient and the product was obtained in only a moderate 61% yield. Alkylation of DIDOX with **3c**, followed by treatment with trifluoroacetic acid produced a reactive 1,4-oxizinium-DIDOX intermediate, as determined by LC-MS. Isolation of this intermediate was unsuccessful since it rapidly decomposes during silica gel purification. However, it was believed that purification would be successful after forming the more stable cyanomorpholino by simply adding cyanide to the crude iminium intermediate, in the form of either NaCN or $BnMe_3NCN$. Unfortunately, neither cyanide salt produced the desired product, and altering solvent (MeOH/EtOAc, DMF, DCM, and ACN), reaction time, and reaction temperature yielded no evidence of successful cyanomorpholino-DIDOX formation. In the end, this approach was not able to deliver the desired result and other methods were investigated.

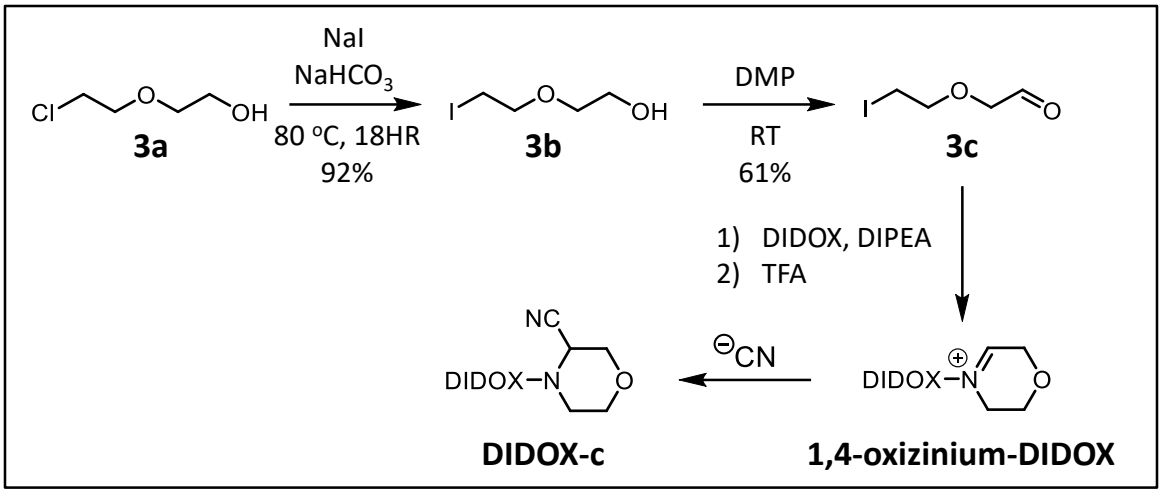

Scheme 2.6 Initial DIDOX-c synthetic attempt. Sodium iodide is used to replace the **3a** chlorine and then **3b** is oxidized using Dess-Martin periodinane. Cyclization of **3c** onto DIDOX occured by condensation of the aldehyde and 3'-amine, followed by intramolecular S_n2 substitution to displace the iodine. Subsequent treatment with TFA forms a charged 1,4-oxizinium intermediate, which when treated with cyanide, produces the desired cyanomorpholino.

The previous success and mild reaction conditions used during the formation of DIDOX-b provided inspiration for a reagent that ultimately proved effective in creating DIDOX-c (**Scheme 2.7**). This new reagent, **3f**, was synthesized to mimic the structure of the diiodide that was previously utilized, however, **3f** would already contain the nitrile required for preparation of the cyanomorpholino moiety. Thus, after two sequential substitution reactions, the nitrile remains as part of the ring. To obtain **3f**, previously synthesized **3c** was converted, in 81% yield, to the cyanohydrin, **3d**, using aqueous NaCN and acetic acid. The hydroxyl group was then formed into a mesylate leaving group, **3e**, in 99% yield. Initially, attempts were made to alkylate DIDOX using **3e** in hopes of producing the cyanomorpholino product, but after many failed attempts it proved necessary to substitute the mesylate for an iodine. This was achieved by heating the mesylate **3e** and NaI at 80 °C for 18 hours to obtain the product, **3f**, in 89% yield. Strangely, the analogous halogen substitutions to form **3b** and **3f** required two separate steps in order to obtain a

final product in high yield. Initially, **3e** had a chlorine in place of the iodine and both mesylate and chlorine substitutions were attempted as a single step, however, a significant amount of starting material remained, even after 48 hours with more than 4 equivalents of NaI. Following alkylation of DIDOX with **3f**, DIDOX-c was isolated as the main reaction product in an exciting yield of 61% and 92% purity, which is more than four times greater than previously published methods used to prepare the analogous cyanomorpholino-DOX. Lastly, DIDOX-c was made into a TFA salt without significant loss of yield or purity.

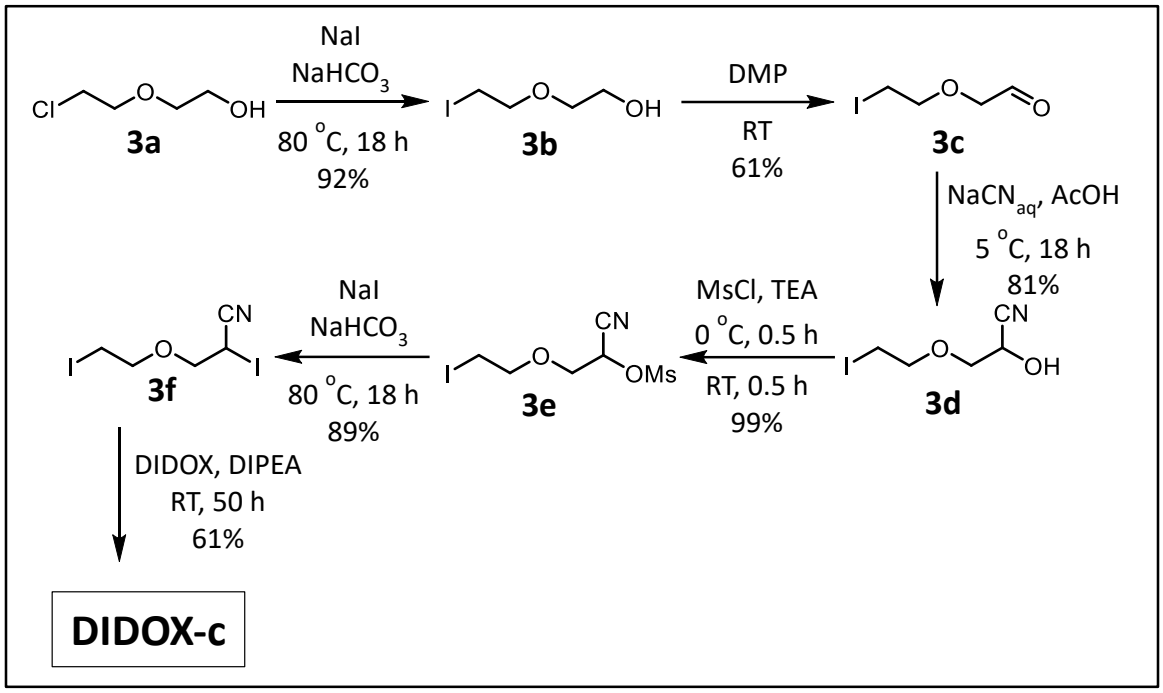

Scheme 2.7 Synthesis of DIDOX-c. The previously synthesized aldehyde, **3c**, was transformed into a cyanohydrin using aqueous sodium cyanide and then the hydroxyl was made into a mesylate leaving group. Sodium iodide was used again to replace the mesylate. Finally, **3f** is used to synthesize DIDOX-c by double nucleophilic substitution.

2.2.4 DIDOX-d and DIDOX-e

DIDOX-d and DIDOX-e were designed to be latent aldehydes comparable to the DOX analogs developed by Cherif et al. and Farquhar et al. The analogs, with their previously described latent aldehydes, were synthesized using the route depicted in **Scheme 2.8**. The chemistry to obtain each of the appropriate reagents, **4d** and **5d,** followed

the same scheme and were produced with adequate yields. The first reaction involved Dess-Martin oxidation of either 4-penten-1-ol or 5-hepten-1-ol, both of which are commercially available. The newly formed aldehydes were treated with acetic anhydride and catalytic $InCl_3$ (0.05 equivalents) to produce the di-acetates **4c** and **5c** in yields of 89% and 43%, respectively, over two steps. Lastly, olefin oxidative cleavage was then performed successfully to obtain **4d** and **5d** using sodium periodate and catalytic $RuCl_3$ (0.035 equivalents) in greater than 40% yield (Yang, 2001).

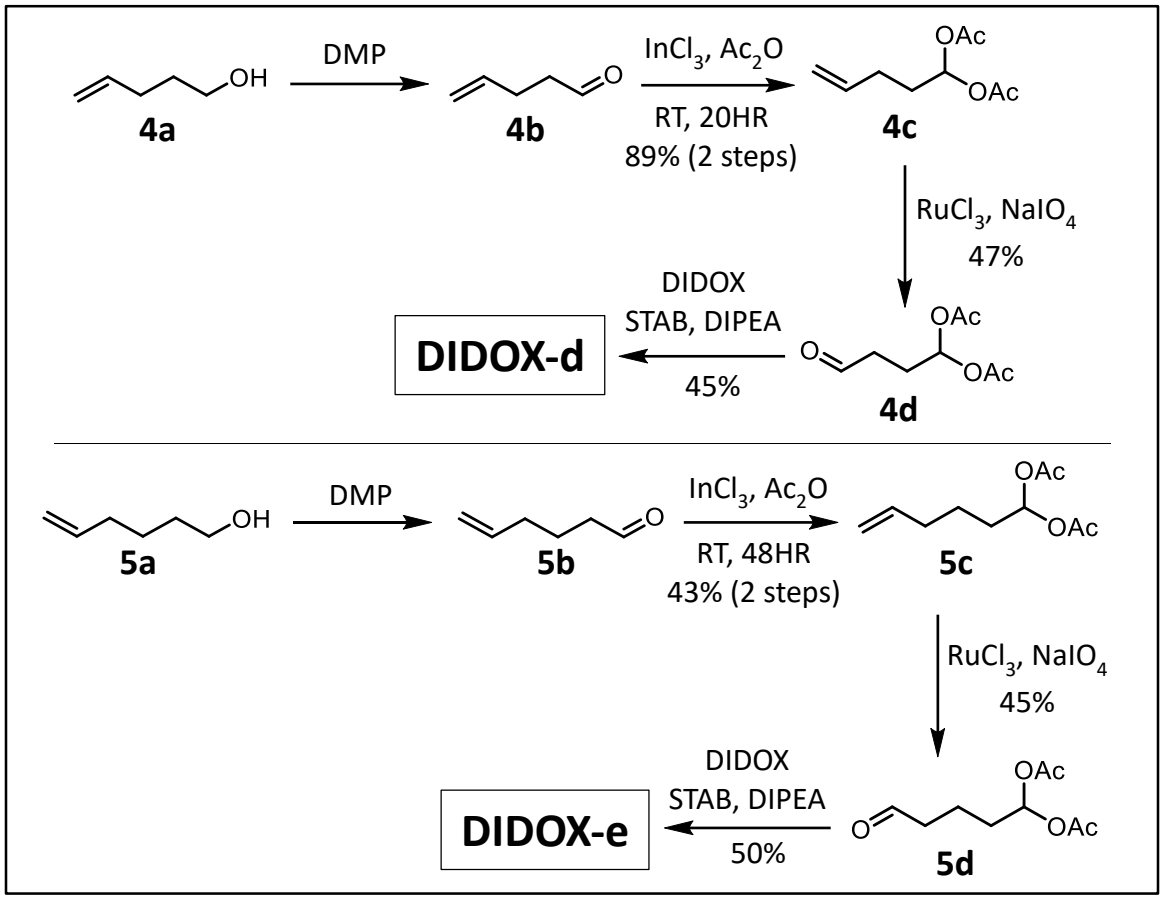

Scheme 2.8 Synthesis of DIDOX-d and DIDOX-e. The synthetic steps to reach **4d** and **5d** are identical and only starting materials, **4a** and **5a**, differ in the length of one methylene. The alcohol is oxidized using Dess-Martin to produce an aldehyde. It is then reacted with acetic anhydride to yield di-acetates **4c** and **5c**. The final aldehydes generated upon oxidative cleavage of the terminal olefin were used to produce DIDOX-d or DIDOX-e in 45% and 50% yield, respectively.

Once **4d** and **5d** were prepared, a reductive activation sequence, proven successful with DOX, was employed. Specifically, DIDOX was treated with 5 equivalents of either aldehyde, **4d** or **5d**, and the reducing agent $NaBH_3CN$ in a 2:1 ACN/H_2O mixture at room temperature for 60 minutes. While these conditions provided success with DOX, no isolatable DIDOX products were generated.

The desired products were eventually synthesized by using a larger excess of **4d** or **5d** (8 equivalents) and altering the solvent to hexafluoroisopropanol (Govindan, 2014). Also, the reducing agent had to be changed to $NaHB(OAc)_3$, because $NaBH_3CN$ was incompatible with this new protonated solvent. The reaction was allowed to proceed for 10 minutes before being directly applied to silica gel for purification. When using DOX as a model system, these conditions generated the desired products in yields approaching 90%. However, when applied to the iminoquinone-containing DIDOX, the products were obtained in yields closer to 50%, after formation of the TFA salt. This result suggests that further optimization is warranted, by variation in solvent, temperature, reducing agent, reaction time, etc.

2.2.5 DIDOX-f

After successful completion of the pro-drugs DIDOX-d and DIDOX-e, attention was shifted to a pro-drug analog of DIDOX-c. The initial attempt to form this DIDOX analog followed the route depicted in **Scheme 2.9**, which was reported to be successful with DOX (Farquhar, 1998). However, when applied to DIDOX, no isolatable product could be obtained. Upon monitoring the reaction via LC-MS, two main products with nearly identical elution times were observed in the chromatogram. Based on the mass to charge ratio, one appeared to be the desired product, whereas, the other had a mass of

731.35 amu and, unfortunately, could not be structurally determined. All attempts at silica gel purification, using numerous solvent systems, were unsuccessful at providing a purified product.

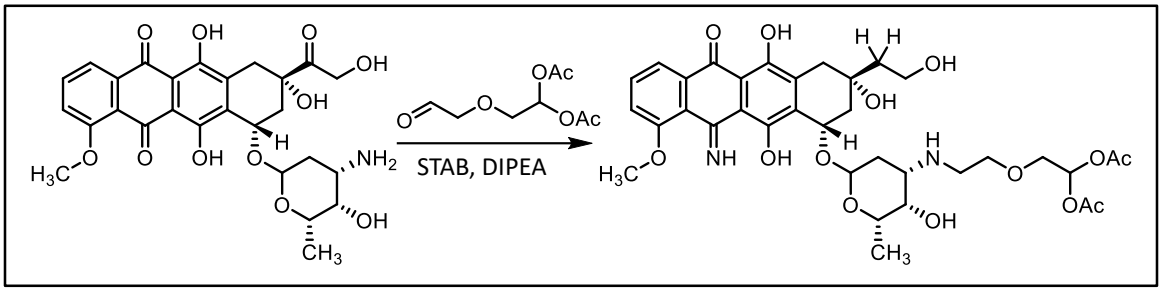

Scheme 2.9 PromorpholinoDOX by reductive alkylation. Formation of product occurred by condensation of DOX and [(2,2-diacetoxyethyl)oxy]-acetaldehyde ether followed by STAB reduction.

A second approach to prepare DIDOX-f used 2-(2-iodoethoxy)ethylidene diacetate (**6d, Scheme 2.10**) and was marginally successful. The synthesis of **6d** involved conversion of the previously prepared **3c** to the diacetate **6d,** which was then combined with DIDOX to afford the desired product. As with the other pro-drug analogs, the $InCl_3/Ac_2O$ approach for preparing the diacetate was attempted, but was abandoned after NMR data showed no sign of product formation. However, switching to a stronger Lewis acid, $FeCl_3$, generated **6d** in 65% yield (Kockhar, 1983). Using this iodide reagent, the pro-drug, DIDOX-f, was formed via a simple nucleophilic substitution over the course of 72 hours.

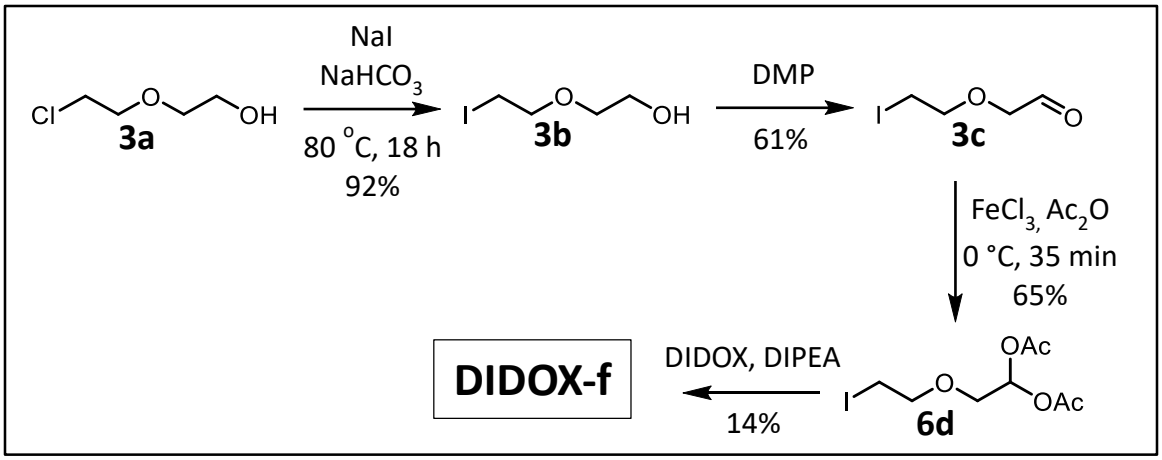

Scheme 2.10 Synthesis of DIDOX-f. The aldehyde, **3c**, was obtained via previously described methods. Iron (III) chloride and acetic anhydride reacted with **3c** for 45 minutes, while chilled on ice, to produce **6d**. The iodide, **6d**, was stirred with DIDOX for 72 hours at room temperature to generate DIDOX-f.

While the synthesis of DIDOX-f was successful, purification proved problematic as silica gel chromatography resulted in rapid decomposition. Unfortunately, if the silica was neutralized by treatment with triethylamine, the product and all of the impurities eluted together. Furthermore, attempts to obtain pure product using reverse-phase silica were not successful. Ultimately, a series of purifications were required to obtain a pure analog. The initial purification involved slowly eluting using $CHCl_3$/IPA and collecting semi-pure fractions. Next, a second column using $CHCl_3$/MeOH was performed and the exposure to silica gel was minimized to prevent serious degradation. The inefficient purification provided the analog in only 14% yield, after converting to a TFA salt, however, with a purity of greater than 90%. Given that the LC chromatogram demonstrated the crude product consisted of roughly 50% DIDOX-f, further optimization of purification techniques will improve this abysmal result.

2.2.6 *In Vitro* Cytotoxicity Results of DIDOX Analogs

To evaluate the anticancer activity of the DIDOX analogs, several different cell lines were employed in cytotoxicity assays. Specifically, all the analogs, DIDOX, and

DOX were subjected to a series of resazurin reduction assays—results of which are shown in **Table 2.1**—to compare antiproliferative activity (Mallory, 2015). This assay followed the reduction of non-fluorescent blue resazurin to fluorescent pink resorufin, which only occurs in healthy and metabolically active cells. The cell lines used include DOX-resistant MES-SA/MX2 uterine sarcoma and non-resistant MES-SA uterine sarcoma, SW-872 liposarcoma, RDCCL136 rhabdomyosarcoma, HT1080 and HT1080-luc2 fibrosarcoma, and CT-26 mouse colon carcinoma. As expected, the data clearly demonstrates that conversion of DOX to DIDOX reduces efficacy across all cancer lines—typically by orders-of-magnitude—and, for the most part, functionalization of the 3'-amine generally returns potency back to similar levels displayed by DOX. These cytotoxicity results provide an initial opportunity to draw conclusions regarding the structural features that are important for anticancer activity.

Table 2.1 *In vitro* activity of DOX, DIDOX, and DIDOX-analogs against sarcoma and carcinoma cell lines.[a]

Cell Line and Tumor Type	IC_{50} (μM)							
	DOX	DIDOX	DIDOX-a	DIDOX-b	DIDOX-c	DIDOX-d	DIDOX-e	DIDOX-f
MES-SA - Uterine sarcoma	0.58 ± 0.17	10.6 ± 1.00	0.76 ± 0.16	85 ± 17	0.68 ± 0.04	0.28 ± 0.04	45.5 ± 14.1	0.15 ± 0.03
MES-SA/MX2 - Uterine sarcoma	13.3 ± 1.68	17.8 ± 0.52	0.73 ± 0.04	119 ± 46	0.66 ± 0.23	0.44 ± 0.10	19.1 ± 6.7	0.32 ± 0.08
SW-872 - Liposarcoma	0.31 ± 0.09	7.38 ±0.45	0.57 ± 0.23	IP	0.32 ± 0.01	0.37 ± 0.09	63.24 ± 9.21	*0.133
RDCCL136 - Rhabdomyosarcoma	0.19 ± 0.06	11.9 ± 3.99	0.44 ± 0.13	IP	0.41 ± 0.11	0.46 ± 0.15	67.13 ± 10.21	IP
HT1080 - Fibrosarcoma	0.46 ± 0.06	47.6 ± 15.5	3.87 ± 0.50	32 ± 8.4	0.82 ± 0.27	0.53 ± 0.06	*9.36	*0.313
HT1080-luc2 - Fibrosarcoma	0.51 ± 0.01	3.32 ± 0.59	3.51 ± 1.79	61 ± 15	0.80 ± 0.19	0.69 ± 0.10	*8.75	*0.267
CT-26 - Colon Carcinoma	3.3 ± 0.65	160 ± 17	1.3 ± 0.21	56 ± 8.5	1.5 ± 0.13	*0.41	*31.3	1.8 ± 0.14

[a]The IC_{50} values were obtained and shown as the mean (±SEM) of at least n = 3, unless marked with an asterisk, indicating preliminary values (n < 3). IP = in progress. Cytotoxicity data was collected by Phil Moon, LJ McKenzie, and Tyler Smith.

While most DIDOX analogs increased cytotoxicity, the results showed that DIDOX-b produced IC_{50} values ranging from 55 µM to 84.8 µM, considerably less potent than the parent DIDOX. The lack of reactivity is presumably due to the morpholino ring requiring biotransformation from hepatic oxidases in order to become active (Lau, 1989). Such enzymatic activation would likely occur by hydroxylation of either nitrogen α-carbons on the morpholino ring that would offer analogous cytotoxic properties as the cyanomorpholino substituent. As such, these *in vitro* experiments may not suitably represent whole animal systems.

When comparing DIDOX-d and DIDOX-e, the only difference is that, respectively, one forms a five-membered ring and the other a six-membered ring after enzymatic activation. At first glance, the addition of one carbon may seem insignificant, but the results, so far, clearly show that the five-membered ring is consistently orders-of-magnitude more cytotoxic. For instance, DIDOX-d has an IC_{50} of 0.37 µM for SW-872 liposarcoma, while DIDOX-e, having an IC_{50} of 63.24 µM, is more than 150 times less potent. Although it is not entirely known why, the drastic change in potency may be attributed to the increase in steric hindrance a six-membered ring contains. This explanation becomes more reasonable when realizing that a five-membered ring is nearly planar, whereas, a six-membered ring forms a bulky chair conformation. It's quite possible that this expanded structure forces the iminium carbon further from DNA base pairs, reducing its ability to covalently bind (Nagy, 1996).

Although the six-membered ring of DIDOX-e hinders its cytotoxic ability, the six membered rings of DIDOX-c and DIDOX-f analogs are vastly more potent. Preliminary results show that DIDOX-c and DIDOX-f are comparably cytotoxic with IC_{50} values as

low as 0.32 μM and 0.15 μM, respectively. The difference stems from these two analogs containing an oxygen at the 4-position, which produces less steric hindrance compared to the methylene of DIDOX-e. Also, hydrogen bonding from this oxygen may be important in bringing this moiety into close proximity or correct orientation to facilitate DNA binding.

The only analog with an inherently reactive site is DIDOX-a, the other DIDOX analogs require some form of activation. The importance behind this observation can be realized when comparing DIDOX-a to its pro-drug DIDOX-d. So far, the cytotoxicity of the protected form is up to six times more potent than the continuously active pyrrolino, however this data is preliminary and warrants further investigation. Due to the fact that DIDOX-a does not require enzymatic activation, it is potentially available to react with surrounding proteins instead of the DNA target, thus decreasing its cytotoxicity.

Additional benefits from functionalization of the 3'-amine appears to include lower susceptibility to MDR and PGP-mediated efflux. Against the MES-SA cell lines, DOX and DIDOX had IC_{50} values of 0.69 μM and 10.6 μM, respectively. Against the resistant MES-SA/MX2 cell lines, the IC_{50} values were up to 20-fold greater. However, as expected, the 3'-amine substituted DIDOX analogs displayed similar activity against the set of resistant and non-resistant cell lines.

2.3 Conclusion

Six analogs of DIDOX were synthesized by functionalization of the 3'-amine to improve the ability to form DNA interstrand cross-links and were evaluated for cytotoxic improvement, as well as for the susceptibility of MDR. Three of the analogs were developed in an already active form and three were isolated as protected latent aldehydes

to improve stability. The synthesis of DIDOX-a,b,d,e analogs used reaction schemes that had been reported to successfully prepare comparable DOX derivatives. However, new synthetic routes were required to isolate DIDOX-c and DIDOX-f. To acquire DIDOX-c, a novel reagent, 2-iodo-3-(2-iodoethoxy)propanenitrile, was prepared and used to alkylate DIDOX through two subsequent nucleophilic substitutions (intermolecular then intramolecular) to form a cyanomorpholino ring in yields greater than 60%. Furthermore, DIDOX-f was produced by single nucleophilic substitution using the newly synthesized reagent, 2-(2-iodoethoxy)ethylidene diacetate.

Results from the resazurin reduction assay determined that most of the modifications allowed DIDOX to regain potency back to comparable levels seen with DOX. This was demonstrated with only a few exceptions, such as in the MES-SA cell line when comparing DIDOX with DIDOX-b, which can be attributed to the absence of oxidases required for morpholino biotransformation. In addition, DIDOX-e consistently performed inadequately compared to other analogs due to its activated form being a more sterically hindered six-membered piperidono ring. From these results, it can be determined that the modification of the 3'-amine appears to produce more cytotoxic anticancer agents, particularly when the modifications include a reactive Schiff base or masked aldehyde. As expected, these modifications appear, at least initially, to overcome MDR as a result of encumbering the free basic amine, which is essential for PGP-mediated drug efflux. Future work will focus on improving the yields of the DIDOX analogs by trying different reaction conditions (i.e. solvents, reagents, temperature, concentration, etc.) and optimization of the purification process. Notably, optimization of purification would drastically benefit the synthesis of DIDOX-f, since HPLC analysis suggested it was produced in high yield prior

to purification, but degradation during silica gel chromatography allowed for only 14% yield. In conclusion, the cytotoxicity data, so far, supports the premise that these modifications do in fact produce potent DIDOX analogs that can overcome MDR that will potentially remain non-cardiotoxic.

2.4 Materials and Methods

2.4.1 Materials and Reagents

DIDOX was supplied by Gem Pharmaceuticals, LLC. Doxorubicin hydrochloride was purchased from Advanced ChemBlocks, Inc. Ethylene glycol mono-2-chloroethyl ether and 4-chlorobuteraldehyde dimethyl acetal were purchased from TCI. Sodium iodide and indium(III) chloride came from Strem Chemicals Inc. Both sodium bicarbonate and hydrochloric acid were supplied from VWR Analytical. Chemicals purchased from Oakwood Chemical include Dess-Martin periodinane, 1,1,1,3,3,3-hexafluoro-2-propanol, and ruthenium chloride. Sodium cyanide, DIPEA, trifluoroacetic acid, and sodium thiosulfate were purchased from Alfa Aesar. Methane sulfonyl chloride, acetic anhydride, and sodium triacetoxyborohydride were obtained from Acros Chemical. 5-Hexene-1-ol, sodium metaperiodate, and 4-pentene-1-ol were purchased from Beantown Chemical. Acetic acid was purchased from EMD. Triethylamine and all solvents were purchased from Fisher Scientific unless otherwise specified.

For cytotoxicity assays, DOX, DIDOX, and DIDOX analogs were all diluted to 30 mM stock solutions in anhydrous DMSO (obtained from Sigma-Aldrich) and stored at -80 °C. All media and components of media were obtained from Thermo Fisher Scientific if not stated otherwise.

2.4.2 Equipment

NMR data was acquired using either 600MHz Bruker Avance III 600 coupled with Bruker Ultrashield 600 Plus or 300MHz Bruker Ultrashield 300 coupled with Bruker Avance III 300. HPLC chromatography was performed using Agilent 1100 series equipped with 50x4.6 mm Hypersil Gold Phenyl column having 5 µm pore size. Coupled with the HPLC was a Bruker Daltonics HCT ultra ETD II ion trap mass spectrometer. A Bruker Daltonics maXis quadrupole time-of-flight was used for high resolution mass spectrometry analysis during DIDOX analog characterization.

2.4.3 Cell Cultures

The following cell lines were purchased from American Type Culture Collection: HT1080, RDCCL, SW-872, MES-SA, and MES-SA/MX2. HT1080-luc2 was ordered from Perkin Elmer. Cells were incubated at 37 °C in a humidified atmosphere containing 5% CO_2. Dulbecco's Modified Eagle Medium—supplemented with 10% (v/v) fetal bovine serum and 1% penicillin/streptomycin—was used to culture RDCCL136, SW-872, MES-SA, and MES-SA/MX2. MES-SA/MX2 was grown under 1 µM DOX stress. Minimum Essential Medium—with 10% fetal bovine serum and 1% penicillin/streptomycin—was used to culture both HT1080 and HT1080-luc2.

2.4.4 *In Vitro* Assays

A resazurin reduction assay was used to determine the cytotoxicity of DOX, DIDOX, and DIDOX analogs against an array of cancer lines (Mallory, 2015). Cells were washed with 1x PBS three times and suspended in trypsin-EDTA while incubating at 37 °C for five minutes. After suspension was achieved, the cells were placed into a centrifuge at 1200 x g for five minutes to form a small pellet. The supernatant was discarded and the

cells were resuspended into their respective media to produce a concentration between 25,000-40,000 cells/mL. These cells were then seeded in a 96-well plate where each well contained between 5,000-8,000 cells. The 96-well plate was then allowed to incubate in a humidified 5% CO_2 atmosphere at 37 °C overnight. After incubating, the media was removed from the wells and discarded. The wells were replenished with 180 μL fresh media and 20 μL drug at the appropriate concentration. The cell-drug combination was allowed to incubate for 48 hours and then 20 μL 0.1% (w/v) resazurin was added to each well and incubated for an additional 24 hours. Fluorescent data was then collected using a BioTek Synergy HT Multi-detection microplate reader and graphed using GraphPad Prism as percent viability versus drug concentration.

2.4.5 Experimental

4-Iodobuteraldehyde dimethyl acetal (**1b**)

4-Chlorobuteraldehyde dimethyl acetal (2.5 ml, 17.0 mmol) was made to be 0.25 M in dry acetone. NaI (5.1070 g, 34.0 mmol, 2 eq) and $NaHCO_3$ (0.4285 g, 5.1mmol, 0.3 eq) were then added and reaction was placed under nitrogen. It was allowed to reflux at 80 ºC for 24 h before removing from heat and allowing solution to cool to RT. The acetone was then removed *in vacuo* and 35 mL Et_2O was added and stirred for 10 min. The precipitates were removed via filtration and discarded. The solvent was then evaporated leaving 3.6611 g clear oil (88% yield). The NMR spectral data matched that previously reported (Wu, 1994).

4-Iodobutanal (**1c**)

4-Iodobuteraldehyde dimethyl acetal (3.6611 g, 15.0 mmol) was dissolved in 150 mL THF before adding 500 mL H_2O/HCl (20:1, v/v). The reaction was monitored by TLC using hexanes/Et_2O (9:1, v/v) and potassium permanganate staining. When reaction was

completed, it was added to a separatory funnel and crude product extracted using 100mL DCM x3. This was then dried using sodium sulfate, filtered, and solvent evaporated. The crude oil was purified on silica gel using hexanes/Et_2O (3:1, v/v). All fractions containing product (R_f = 0.17) were combined, yielding 1.9176 g of pale yellow oil (65% yield). The NMR spectral data matched that previously reported (Studenovsky, 2011)

Bis(2-Iodoethyl) ether (**2b**)

Bis(2-iodoethyl) ether (1.3171 g, 9.21 mmol) was made to be 0.2 M in dry acetone before NaI (5.5219 g, 36.8 mmol, 4 eq) and $NaHCO_3$ (0.4642 g, 5.53 mmol, 0.6 eq) were added. This was allowed to react under reflux at 80 ºC for 24 h under a nitrogen atmosphere before removing from heat. After cooling to RT, 40 mL of Et_2O was added and mixed for 10 min before precipitates were removed by filtration. Solution was then dried *in vacuo* and 50 mL Et_2O was added and mixed for 10 minutes and the additional precipitates were removed by filtration. After drying, the final production was obtained as a yellow oil (3.0017 g) in 77% yield. ^{1}H NMR ($CDCl_3$ with 0.03% v/v TMS, 300 MHz) δ: 3.77 (t, 4H, J = 6.8 Hz), 3.27 (t, 4H, J = 6.8 Hz)

2-(2-Iodoethoxy)ethanol (**3b**)

Ethylene glycol mono-2-chloroethyl ether (0.500 mL, 4.74 mmol) was dissolved in 24 mL dry acetone before NaI (1.5589 g, 10.4 mmol, 2.2 eq) and $NaHCO_3$ (0.1193 g, 1.42 mmol, 0.3 eq) were added to the solution. It was allowed to reflux at 85 °C for 24 h and then diluted to 0.05 M using EtOAc and washed five times using 15 mL water. The organic solution was dried using sodium sulfate, followed by filtration. The solvent was evaporated *in vacuo* to deliver 0.9420 g pure product (92% yield) as a colorless oil. NMR spectral data matches that previously reported (Phillips, 2008)

2-(2-Iodoethoxy)acetaldehyde (**3c**)

2-(2-Iodoethoxy)ethanol (3.0675 g, 14.2 mmol,) was dissolved in 40 mL DCM and then Dess-Martin (9.0342 g, 21.3 mmol, 1.5 eq) was added. The solution was developed in EtOAc/Hexanes (3:2, v/v) on TLC. Following chromatography, the plate was stained using potassium permanganate to resolve a bright yellow spot with R_f = 0.35 for SM and R_f = 0.53 for product. Once SM was no longer present on TLC (3.5 h), the reaction was quenched using 100 mL 15% $Na_2S_2O_3$/5% $NaHCO_3$. Crude product was then extracted using 50 ml DCM x3, dried using sodium sulfate, and filtered. After evaporation of solvent, the crude oil was applied to silica gel and eluted using EtOAc/Hexanes (1:1, v/v). Fractions containing product – determined using TLC – were combined and condensed, providing 1.8401 g of pure colorless oil (61% yield). ^{1}H NMR ($CDCl_3$ with 0.03% v/v TMS, 300 MHz) δ: 9.72 (s, 1H), 4.17 (s, 2H), 3.84 (t, 2H, J = 6.7 Hz), 3.31 (t, 2H, J = 6.7)

2-hydroxy-3-(2-iodoethoxy)propanenitrile (**3d**)

2-(2-Iodoethoxy)acetaldehyde (1.2028 g, 5.62 mmol) was made to be 2.9 M in AcOH (1.9 mL) and NaCN (0.8264 g, 16.9 mmol, 3 eq) was made to be 0.9 M in water (19 mL). Both solutions were allowed to chill to ~0 ºC before the NaCN solution was added to the aldehyde via cannula and allowed to react overnight (16 h) at 5 ºC. It was quench by adding to 150 mL saturated aqueous $NaHCO_3$ and extracting crude product using 50 mL DCM x4. The organic solution was then dried using sodium sulfate, filtered, and solvent evaporated *in vacuo*. The desired product had an R_f of 0.60 on TLC using EtOAc/Hexanes (3:2, v/v) and required staining using potassium permanganate. The crude oil was applied to silica gel and eluted using Hexanes/EtOAc (2:1, v/v) resulting in 1.1005 g clear oil (81% yield). ^{1}H NMR ($CDCl_3$ with 0.03% v/v TMS, 300 MHz) δ: 4.61 (dt, 1H, J = 8.3 Hz, 4.1 Hz),

3.96-3.77 (m, 4H), 3.31 (t, 2H, J = 6.4 Hz), 3.10 (dd, 1H, J = 30.2 Hz, 8.3 Hz). ^{13}C NMR ($CDCl_3$ with 0.03% v/v TMS, 600 MHz) δ:117.8, 72.1, 71.2, 60.8, 2.1.

3-(2-iodoethoxy)-2-(methylsulfonyl)propanenitrile (**3e**)

2-hydroxy-3-(2-iodoethoxy)propanenitrile (1.0851 g, 4.50 mmol) was dissolved in 3 mL anhydrous DCM while methane sulfonyl chloride (418 μL, 5.40 mmol, 1.2 eq) was dissolved in 27 mL anhydrous DCM, both chilled to 0 ºC. The sulfonyl chloride solution was added to the cyanohydrin followed by triethylamine (1.25 mL, 9.00 mmol, 2 eq) and reacted for 30 min at 0 ºC and then allowed to warm to RT. The reaction was monitored via TLC using EtOAC/Hexanes (3:2, v/v) and stained with potassium permanganate. Product had R_f = 0.64. When SM had disappeared – shown by TLC – it was added to 150 mL water and crude product extracted using 50 mL DCM x3, then dried using sodium sulfate, and filtered. Solvent was removed *in vacuo* and crude oil was applied to silica gel. Purification using EtOAc/Hexanes (1:1, v/v) yielded 1.4138 g of clear oil (99% yield). ^{1}H NMR ($CDCl_3$ with 0.03% v/v TMS, 600 MHz) δ: 5.33 (dd, 1H, J = 6.2 Hz, 4.8 Hz), 3.97-3.83 (m, 4H), 3.27 (t, 2H, J = 6.6 Hz), 3.23 (s, 3H, CH_3). ^{13}C NMR ($CDCl_3$ with 0.03% v/v TMS, 600 MHz) δ: 113.9, 72.6, 69.6, 65.4, 39.2, 1.1.

2-iodo-3-(2-iodoethoxy)propanenitrile (**3f**)

3-(2-iodoethoxy)-2-(methylsulfonyl)propanenitrile (1.2892 g, 4.04 mmol) was dissolved in 16 mL anhydrous acetone. NaI (1.2111 g, 8.08 mmol, 2 eq) and $NaHCO_3$ (0.1017 g, 1.21 mmol, 0.3 eq) were then added and reaction was refluxed at 80 ºC for 18 h. This was monitored via TLC using EtOAc/Hexanes (3:2, v/v) and staining with potassium permanganate, product R_f = 0.70. After SM had all been used, the solution was cooled to RT and the 5 mL of Et_2O was added and precipitates were removed by filtration and washed

with 10 mL Et_2O x5. Excess solvent was evaporated and crude product was added to 150 mL water and extract using 50 mL DCM x4. It was then dried using sodium sulfate, filtered, and solvent removed. It was then applied to silica gel and purified using EtOAc/Hexanes (1:1, v/v). Fractions containing product were combined and solvent evaporated. 1.2548 g of clear oil was obtained (89% yield) with a density of 1.8 g/mL. ^{1}H NMR ($CDCl_3$ with 0.03% v/v TMS, 300 MHz) δ: 4.33 (dd, 1H, J = 7.7 Hz, 6.8 Hz), 3.93-3.83 (m, 4H), 3.28 (dt, 2H, J = 6.8 Hz, 0.9 Hz). ^{13}C NMR ($CDCl_3$ with 0.03% v/v TMS, 600 MHz) δ: 117.7, 72.9, 72.3, 1.3, -6.2.

5-Hexene-1,1-Diacetate (**5c**)

5-Hexene-1-ol (1.20 mL, 10 mmol) was dissolved in 30 mL DCM and chilled to between 0-5 ºC on ice. Dess-Martin periodinane (5.0897 g, 12.0 mmol, 1.2 eq) was then added and stirred on ice for 5 min. It was then allowed to warm to RT. Reaction progress was monitored by TLC using hexanes/Et_2O (1:1, v/v) followed by potassium permanganate staining. When starting material had completely reacted, 100 mL aqueous 15% sodium thiosulfate/5% sodium bicarbonate was added and allowed to stir for 10 min to quench. Crude product was then extracted using 30 mL DCM x3, dried using sodium sulfate, and filtered. The solvent was then evaporated to produce crude 5-hexene-1-al. This was then diluted with 30 mL ice-cold DCM and $InCl_3$ (0.1106 g, 0.5 mmol, 0.05 eq) was added and allowed to thoroughly mix for 5 minutes before Ac_2O (1.42 mL, 15.0 mmol, 1.5 eq) was added. This was monitored by TLC using hexanes/Et_2O (8:1, v/v) followed by potassium permanganate staining. Reaction was complete after 48 h and quenched using 20 mL aqueous 25% sodium acetate and then added to 70 mL brine. Product was extracted using 25 mL DCM x4, then dried using sodium sulfate, and filtered. After solvent was

evaporated, it was loaded onto silica gel and purified using hexanes/Et_2O (2:1, v/v). All fractions containing product (R_f of 0.14) were combined to give 0.8655 g (43% yield) clear oil. The NMR spectral data matched that previously reported (Cherif, 1992)

4-Pentene-1,1-diacetate (**4c**)

Product obtained using same procedures as 5-Hexene-1,1-Diacetate. Final product R_f was found to be 0.26. Yield was 89% over first two steps. The NMR spectral data matched that previously reported (Cherif, 1992)

5-Oxopentane-1,1-diacetate (**5d**)

5-Hexene-1,1-diacetate (0.7117 g, 3.55 mmol) and $RuCl_3$ (25.8 mg, 0.124 mmol, 0.035 eq) were made to be 0.1 M in ACN/H_2O (6:1, v/v) and mixed for 3-4 min. Sodium periodate (1.5186 g, 7.10 mmol, 2 eq) was then slowly added over 5 minutes. This was monitored by TLC using EtOAc/hexanes (3:2, v/v) stained with potassium permanganate. Reaction was complete, shown by TLC, after 3 h. It was then added to a separatory funnel along with 40 mL saturated aqueous sodium thiosulfate and vigorously shaken. The top organic layer was removed and set aside. Product was extracted from the aqueous layer using 25 mL EtOAc x3. All the organic layers were then combined and washed with 40 mL H_2O followed by an additional wash using 40 mL brine. It was then dried using sodium sulfate, filtered, and solvent removed *in vacuo*. The crude oil was loaded onto silica gel and purified using EtOAc/hexanes (1:1, v/v). All fractions containing product (R_f of 0.12) were combined, yielding 0.3189 g (45% yield) clear oil. The NMR spectral data matched that previously reported (Cherif, 1992)

4-Oxobutane-1,1-diacetate (**4d**)

Product obtained using same procedures as 5-Oxopentane-1,1-diacetate. Final product R_f was found to be 0.49. Yield was 47%. The NMR spectral data matched that previously reported (Cherif, 1992)

2-(2-Iodoethoxy) ethylidene diacetate (**6d**)

2-(2-Iodoethoxy)acetaldehyde (1.3704 g, 6.40 mmol) was chilled to 0 ºC and dissolved in 2.1 mL ice-cold acetic anhydride. This was allowed to react on ice for 15 min and then $FeCl_3$ (31.2 mg, 0.192 mmol, 0.03 eq) was added and reaction proceeded an additional 20 min while still on ice. It was then added directly onto silica gel for purification using Hexanes/Et_2O (2:1, v/v). TLC was performed using Hexanes/Et_2O (8:3, v/v) followed by potassium permanganate staining. Product R_f was 0.19. All pure fractions were collected and combined to give 1.3094 g clear oil (65% yield). ^{1}H NMR ($CDCl_3$ with 0.03% v/v TMS, 600 MHz) δ: 6.91 (t, 1H, J = 4.9 Hz), 3.79 (t, 2H, J = 6.8 Hz), 3.69 (d, 2H, J = 4.9 Hz), 3.24 (t, 2H, J = 6.8 Hz), 2.11 (s, 6H). ^{13}C NMR ($CDCl_3$ with 0.03% v/v TMS, 600 MHz) δ: 168.8, 87.5, 72.3, 69.7, 20.8, 2.1

DIDOX-a

DIDOX HCl (93.5 mg, 0.165 mmol) was made to be 0.1 M DMF and 4-iodobutanal (0.9830 g, 4.96 mmol, 30 eq) was made to be 0.06 M in DCM containing DIPEA (172 μL, 0.990 mmol, 6 eq). DCM solution was added to the dissolved DIDOX over 5 min. Reaction was monitored via LC-MS. The reaction was complete after 5 h and 3 mL 5% TFA in MeOH was added. The solution was then condensed to 5 mL and recrystallized using 25 mL Et_2O/hexanes (4:1, v/v). The purple precipitate was then loaded onto silica gel (treated with 0.5% triethylamine) and purified using $CHCl_3$/MeOH (10:1, v/v). Fractions

containing product were combined and 3 mL 10% TFA in MeOH was added and solution condensed to 5 mL. It was then recrystallized using 20 mL Et_2O/hexanes (4:1, v/v). The solid was then placed under high vacuum for one h (<150 mTorr). The final product was obtained in 80% yield (91.6 mg) as a purple TFA salt with purity of >90%. Molecular ion ($M+H^+$) calculated for $C_{31}H_{37}N_2O_9^+$: 581.2494 amu; found m/z = 581.2489 amu, error = -0.86 ppm.

DIDOX-b

DIDOX HCl (43.0 mg, 0.0761 mmol) was dissolved in 2.0 mL DMF and then bis(2-iodoethyl) ether (495.1 mg, 1.52 mmol, 20 eq) was added and stirred for 5 min before DIPEA (79.5 µL, 0.457 mmol, 6 eq) was added. The reaction progress was monitored by HPLC. Starting DIDOX had completely reacted after two days prompting the addition of 18 mL Et_2O/hexanes (2:1, v/v) to recrystallize crude product. The purple solid was purified using silica gel packed into a 1 X 15 cm column using 200 mL 20:1 $CHCl_3$/MeOH then 200 mL 10:1 $CHCl_3$/MeOH. Fractions containing product were collected and solvent was removed. The solid was collected and placed under high vacuum for 45 min (<150 mTorr). Final product was obtained as a purple solid (42.7 mg) in 93.6% yield and 96% purity. Molecular ion ($M+H^+$) calculated for $C_{31}H_{39}N_2O_{10}^+$: 599.2600 amu; found m/z = 599.2619 amu, error = 3.17 ppm.

DIDOX-c

DIDOX HCl salt (48.6 mg, 0.0860 mmol) was made to be 0.08 M in DMF that already contained 2-iodo-3-(2-iodoethoxy)propanenitrile (754.5 mg, 2.15 mmol, 25 eq) followed by the addition of DIPEA (90 µL, 0.516 mmol, 6 eq). The reaction completed after 50 h as determined via LC-MS. At this point 25 mL Et_2O/Hexanes (4:1, v/v) was added and

precipitate was collected. It was then dissolved in 2 mL 1:1 MeOH/DCM (v/v) and recrystallized a second time using 25 mL Et_2O/Hexanes (4:1, v/v). The crude solid was then purified on a column (3 X 15 cm) packed with silica gel. The mobile phase consisted of $CHCl_3$/MeOH (10:1, v/v). Fractions containing product were collected and solvent removed *in vacuo*. The pure product was then placed under high-vacuum for 60 min (<150 mTorr). A purple DIDOX-c solid (32.9 mg) was obtained in free base form with a yield of 61% and purity of 92%. A 10.9 mg sample of free base DIDOX-c was dissolved in 1 mL of 1:1 MeOH/DCM (v/v) containing 5% TFA and mixed for 5 min before 12 mL Et_2O/Hexanes (4:1, v/v) was added. The precipitate was collected and dried under high-vacuum ((<150 mTorr) for 45 min. 12.9 mg of the final purple solid was obtained as a TFA salt in 100% yield with a purity of 90%. Molecular ion ($M+H^+$) calculated for $C_{32}H_{38}N_3O_{10}^+$: 624.2552 amu; found m/z = 624.2596 amu, error = 7.05 ppm.

DIDOX-d

DIDOX HCl (46.6 mg, 0.0825 mmol) was made to be 0.02 M in 1,1,1,3,3,3-hexafluoro-2-propanol containing 4-oxobutane-1,1-diacetate (0.1242 g, 0.660 mmol, 8 eq) and then DIPEA (86 μL, 0.495 mmol, 6 eq) was added. This was allowed to stir for 3 min before sodium triacetoxyborohydride was added and reacted for 10 min. It was then directly loaded onto a column (2 X 15 cm) packed with silica gel. It was purified using 300 mL $CHCl_3$/MeOH (20:1, v/v), followed by 250 mL $CHCl_3$/MeOH (10:1, v/v), and finally with 200 mL $CHCl_3$/MeOH (4:1, v/v). Fractions containing product (determined by LC-MS) were combined and evaporated to dryness. The purple solid was then dissolved in 1 mL 3% TFA in MeOH and stirred for 5 min before recrystallizing using 15 mL Et_2O/hexanes (5:1, v/v). The solid was then placed under high vacuum for one h (<150 mTorr). The final

product was obtained in 45% yield (30.0 mg) as a purple TFA salt with purity of >95%. Molecular ion ($M+H^+$) calculated for $C_{35}H_{45}N_2O_{13}^+$: 701.2917 amu; found m/z = 701.3009 amu, error = 13.1 ppm.

DIDOX-e

DIDOX HCl (44.6 mg, 0.0789 mmol) was made to be 0.03 M in 1,1,1,3,3,3-hexafluoro-2-propanol containing 5-oxopentane-1,1-diacetate (0.1594 g, 0.789 mmol, 10 eq) followed by the addition of DIPEA (82 μL, 0.473 mmol, 6 eq) and allowed to stir for 2 min. Sodium triacetoxyborohydride (25.0 mg, .0118 mmol, 1.5 eq) was added and reacted for 10 min before being loaded directly onto a column (2 X 15 cm) packed with silica gel. It was purified using 300 mL $CHCl_3$/MeOH (20:1, v/v), followed by 250 mL $CHCl_3$/MeOH (10:1, v/v), and finally with 200 mL $CHCl_3$/MeOH (4:1, v/v). Fractions containing product (determined by LC-MS) were combined and evaporated to dryness. The purple solid was then dissolved in 1 mL 3% TFA in MeOH and stirred for 5 min before recrystallizing using 15 mL Et_2O/hexanes (5:1, v/v). The solid was then placed under high vacuum for one h (<150 mTorr). The final product was obtained in 50% yield (32.8 mg) as a purple TFA salt with purity of >95%. Molecular ion ($M+H^+$) calculated for $C_{36}H_{47}N_2O_{13}^+$: 715.3073 amu; found m/z = 715.3059 amu, error = -1.96 ppm.

DIDOX-f

DIDOX HCl (20.9 mg, 0.0370 mmol) was dissolved in 2 mL DMF containing 2-(2-iodoethoxy) ethylidene diacetate (0.2339 g, 0.740 mmol, 20 eq) and DIPEA (39 μL, 0.222 mmol, 6 eq) was added via syringe. Reaction was monitored via LC-MS. After 72 h, the solution was added to 150 mL H_2O and extracted using 25 mL DCM x4. It was then dried using sodium sulfate, filtered, and solvent evaporated. The purple solid was then dissolved

in 1 mL DCM/MeOH (1:1, v/v) and recrystallized using 20 mL Et_2O/hexanes (3:1, v/v). The solid precipitate was loaded onto silica gel and purified using $CHCl_3$/IPA (2:1, v/v). Fractions containing product were collected and solvent evaporated. Product at this point was less than 90% pure so an additional purification was performed on silica gel using $CHCl_3$/MeOH (4:1, v/v). Fractions containing product were combined and solvent removed *in vacuo.* The purple solid was then dissolved in 2 mL 5% TFA in MeOH and stirred for 5 min before being recrystallized using 20 ml Et_2O/hexanes (3:1, v/v). The solid was then placed under high vacuum for one h (<150 mTorr). The final product was obtained in 14% yield (4.3 mg) as a purple TFA salt with purity of >90%. Molecular ion ($M+H^+$) calculated for $C_{35}H_{45}N_2O_{14}^+$: 717.2866 amu; found m/z = 717.2929 amu, error = 8.78 ppm.

2.5 References

Acton, E. M., & Tong, G. L. (1981). Synthesis and preliminary antitumor evaluation of 5-iminodoxorubicin. *Journal of Medicinal Chemistry*, *24*(6), 669-673.

Bao, L., Haque, A., Jackson, K., Hazari, S., Moroz, K., Jetly, R., & Dash, S. (2011). Increased expression of P-glycoprotein is associated with doxorubicin chemoresistance in the metastatic 4T1 breast cancer model. *The American Journal of Pathology*, *178*(2), 838-852.

Batist, G., Ramakrishnan, G., Rao, C. S., Chandrasekharan, A., Gutheil, J., Guthrie, T., & Tkaczuk, K. (2001). Reduced cardiotoxicity and preserved antitumor efficacy of liposome-encapsulated doxorubicin and cyclophosphamide compared with conventional doxorubicin and cyclophosphamide in a randomized, multicenter trial of metastatic breast cancer. *Journal of Clinical Oncology*, *19*(5), 1444-1454.

Boucek, R. J. (1997). Mechanisms for anthracycline-induced cardiomyopathy: clinical and laboratory correlations. *Progress in Pediatric Cardiology*, *8*(2), 59-70.

Burton, K. P., McCord, J. M., & Ghai, G. E. E. T. H. A. (1984). Myocardial alterations due to free-radical generation. *American Journal of Physiology-Heart and Circulatory Physiology*, *246*(6), H776-H783.

Capranico, G., Kohn, K. W., & Pommier, Y. (1990). Local sequence requirements for DNA cleavage by mammalian topoisomerase II in the presence of doxorubicin. *Nucleic Acids Research*, *18*(22), 6611-6619.

Cherif, A., & Farquhar, D. (1992). N-(5, 5-diacetoxypent-1-yl) doxorubicin: a new intensely potent doxorubicin analog. *Journal of Medicinal Chemistry*, *35*(17), 3208-3214.

Cullinane, C., & Phillips, D. R. (1993). Thermal stability of DNA adducts induced by cyanomorpholinoadriamycin in vitro. *Nucleic Acids Research*, *21*(8), 1857-1862.

Cummings, J., Willmott, N., Hoey, B. M., Marley, E. S., & SMyth, J. F. (1992). The consequences of doxorubicin quinone reduction in vivo in tumour tissue. *Biochemical Pharmacology*, *44*(11), 2165-2174.

Cusack, B. J., Mushlin, P. S., Voulelis, L. D., Li, X. D., Boucek, R. J., & Olson, R. D. (1993). Daunorubicin-induced cardiac injury in the rabbit: a role for daunorubicinol?. *Toxicology and Applied Pharmacology*, *118*(2), 177-185.

Cutts, S. M., Swift, L. P., Rephaeli, A., Nudelman, A., & Phillips, D. R. (2003). Sequence specificity of adriamycin-DNA adducts in human tumor cells1. *Molecular Cancer Therapeutics*, *2*(7), 661-670.

Danesi, R., Fogli, S., Gennari, A., Conte, P., & Del Tacca, M. (2002). Pharmacokinetic-pharmacodynamic relationships of the anthracycline anticancer drugs. *Clinical Pharmacokinetics*, *41*(6), 431-444.

Farquhar, D., Cherif, A., Bakina, E., & Nelson, J. A. (1998). Intensely potent doxorubicin analogues: structure− activity relationship. *Journal of Medicinal Chemistry*, *41*(6), 965-972.

Frank, N. E., Cusack, B. J., Talley, T. T., Walsh, G. M., & Olson, R. D. (2016). Comparative effects of doxorubicin and a doxorubicin analog, 13-deoxy, 5-

iminodoxorubicin (GPX-150), on human topoisomerase IIβ activity and cardiac function in a chronic rabbit model. *Investigational New Drugs*, *34*(6), 693-700.

Frézard, F., Pereira-Maia, E., Quidu, P., Priebe, W., & Garnier-Suillerot, A. (2001). P-Glycoprotein preferentially effluxes anthracyclines containing free basic versus charged amine. *The FEBS Journal*, *268*(6), 1561-1567.

Govindan, S. V., McBride, W. J., Sathyanarayan, N., Mazza-Ferreira, C., & Goldenberg, D. M. (2014). *U.S. Patent No. 8,877,202*. Washington, DC: U.S. Patent and Trademark Office.

Grant, C. E., Valdimarsson, G., Hipfner, D. R., Almquist, K. C., Cole, S. P., & Deeley, R. G. (1994). Overexpression of multidrug resistance-associated protein (MRP) increases resistance to natural product drugs. *Cancer Research*, *54*(2), 357-361.

Gruber, B. M., Anuszewska, E. L., & Priebe, W. (2004). The effect of new anthracycline derivatives on the induction of apoptotic processes in human neoplastic cells. *Folia Histochemica et Cytobiologica*, *42*(2), 127-130.

Hohl, R. J., Vestal, R. E., Holstein, S. A., Olson, R. D., Parrott, K., & Walsh, G. M. (2013). Phase I dose-escalation clinical trial with 5-imino-13-deoxydoxorubicin in cancer patients.

Holstein, S. A., Bigelow, J. C., Olson, R. D., Vestal, R. E., Walsh, G. M., & Hohl, R. J. (2015). Phase I and pharmacokinetic study of the novel anthracycline derivative 5-imino-13-deoxydoxorubicin (GPX-150) in patients with advanced solid tumors. *Investigational New Drugs*, *33*(3), 594-602.

Kassner, N., Huse, K., Martin, H. J., Gödtel-Armbrust, U., Metzger, A., Meineke, I., & Wojnowski, L. (2008). Carbonyl reductase 1 is a predominant doxorubicin reductase in the human liver. *Drug Metabolism and Disposition*, *36*(10), 2113-2120.

Kochhar, K. S., Bal, B. S., Deshpande, R. P., Rajadhyaksha, S. N., & Pinnick, H. W. (1983). Protecting groups in organic synthesis. Part 8. Conversion of aldehydes into geminal diacetates. *The Journal of Organic Chemistry*, *48*(10), 1765-1767.

Kumar, D., Kirshenbaum, L. A., Li, T., Danelisen, I., & Singal, P. K. (2001). Apoptosis in adriamycin cardiomyopathy and its modulation by probucol. *Antioxidants and Redox Signaling*, *3*(1), 135-145.

Lau, D. H., Lewis, A. D., & Sikic, B. I. (1989). Association of DNA cross-linking with potentiation of the morpholino derivative of doxorubicin by human liver microsomes. *JNCI: Journal of the National Cancer Institute*, *81*(13), 1034-1038.

Lefrak, E. A., Piťha, J., Rosenheim, S., & Gottlieb, J. A. (1973). A clinicopathologic analysis of adriamycin cardiotoxicity. *Cancer*, *32*(2), 302-314.

Loe, D. W., Deeley, R. G., & Cole, S. P. C. (1996). Biology of the multidrug resistance-associated protein, MRP. *European Journal of Cancer*, *32*(6), 945-957.

Mallory, C. M., Carfi, R. P., Moon, S., Cornell, K. A., & Warner, D. L. (2015). Modification of cellular DNA by synthetic aziridinomitosenes. *Bioorganic & Medicinal Chemistry*, *23*(23), 7378-7385.

Nagy, A., Armatis, P., & Schally, A. V. (1996). High yield conversion of doxorubicin to 2-pyrrolinodoxorubicin, an analog 500-1000 times more potent: structure-activity relationship of daunosamine-modified derivatives of doxorubicin. *Proceedings of the National Academy of Sciences*, *93*(6), 2464-2469.

O'brien, M. E. R., Wigler, N., Inbar, M. C. B. C. S. G., Rosso, R., Grischke, E., Santoro, A., & Orlandi, F. (2004). Reduced cardiotoxicity and comparable efficacy in a phase III trial of pegylated liposomal doxorubicin HCl (CAELYX™/Doxil®) versus conventional doxorubicin for first-line treatment of metastatic breast cancer. *Annals of Oncology*, *15*(3), 440-449.

Olson, R. D., Mushlin, P. S., Brenner, D. E., Fleischer, S., Cusack, B. J., Chang, B. K., & Boucek, R. J. (1988). Doxorubicin cardiotoxicity may be caused by its metabolite, doxorubicinol. *Proceedings of the National Academy of Sciences*, *85*(10), 3585-3589.

Olson, R. D., Headley, M. B., Hodzic, A., Walsh, G. M., & Wingett, D. G. (2007). In vitro and in vivo immunosuppressive activity of a novel anthracycline, 13-deoxy, 5-iminodoxorubicin. *International Immunopharmacology*, *7*(6), 734-743.

Phillips, R. L., Kim, I. B., Carson, B. E., Tidbeck, B., Bai, Y., Lowary, T. L., & Bunz, U. H. (2008). Sugar-substituted poly (p-phenyleneethynylene) s: sensitivity enhancement toward lectins and bacteria. *Macromolecules*, *41*(20), 7316-7320.

Priebe, W., Van, N. T., Burke, T. G., & Perez-Soler, R. (1993). Removal of the basic center from doxorubicin partially overcomes multidrug resistance and decreases cardiotoxicity. *Anti-cancer drugs*, *4*(1), 37-48.

Robert Jr, J., Olson, R. D., Brenner, D. E., Ogunbunmi, E. M., Inui, M., & Fleischer, S. (1987). The major metabolite of doxorubicin is a potent inhibitor of membrane-associated ion pumps. *Journal of Biological Chemistry*, *262*(33), 15851-15856.

Sawyer, D. B., Fukazawa, R., Arstall, M. A., & Kelly, R. A. (1999). Daunorubicin-induced apoptosis in rat cardiac myocytes is inhibited by dexrazoxane. *Circulation Research*, *84*(3), 257-265.

Shen, A. L., Sem, D. S., & Kasper, C. B. (1999). Mechanistic studies on the reductive half-reaction of NADPH-cytochrome P450 oxidoreductase. *Journal of Biological Chemistry*, *274*(9), 5391-5398.

Siveski-Iliskovic, N., Hill, M., Chow, D. A., & Singal, P. K. (1995). Probucol protects against adriamycin cardiomyopathy without interfering with its antitumor effect. *Circulation*, *91*(1), 10-15.

Smith, T. H., Fujiwara, A. N., & Henry, D. W. (January 01, 1978). Adriamycin analogues. 2. Synthesis of 13-deoxyanthracyclines. *Journal of Medicinal Chemistry*, *21*, 3, 280-3.

Streeter, D. G., Johl, J. S., Gordon, G. R., & Peters, J. H. (1986). Uptake and retention of morpholinyl anthracyclines by adriamycin-sensitive and-resistant P388 cells. *Cancer Chemotherapy and Pharmacology*, *16*(3), 247-252.

Studenovsky, M., Ulbrich, K., Ibrahimova, M., & Rihova, B. (2011). Polymer conjugates of the highly potent cytostatic drug 2-pyrrolinodoxorubicin. *European Journal of Pharmaceutical Sciences*, *42*(1), 156-163.

Swain, S. M., Whaley, F. S., & Ewer, M. S. (2003). Congestive heart failure in patients treated with doxorubicin. *Cancer*, *97*(11), 2869-2879.

Taatjes, D. J., Fenick, D. J., & Koch, T. H. (1998). Epidoxoform: A hydrolytically more stable anthracycline− formaldehyde conjugate toxic to resistant tumor cells. *Journal of Medicinal Chemistry*, *41*(8), 1306-1314.

Takahashi, Y., Kinoshita, M., Masuda, T., Tatsuta, K., Takeuchi, T., & Umezawa, H. (1982). 3'-deamino-3'-morpholino derivatives of daunomycin, adriamycin and carminomycin. *The Journal of Antibiotics*, *35*(1), 117-118.

Tehrani, K. A., D'hooghe, M., & De Kimpe, N. (2003). Novel synthesis of indolizidines and quinolizidines. *Tetrahedron*, *59*(17), 3099-3108.

Tewey, K. M., Rowe, T. C., Yang, L., Halligan, B. D., & Liu, L. F. (1984). Adriamycin-induced DNA damage mediated by mammalian DNA topoisomerase II. *Science*, *226*(4673), 466-468.

Vásquez-Vivar, J., Martasek, P., Hogg, N., Masters, B. S. S., Pritchard, K. A., & Kalyanaraman, B. (1997). Endothelial nitric oxide synthase-dependent superoxide generation from adriamycin. *Biochemistry*, *36*(38), 11293-11297.

Verweij, J., Lee, S. M., Ruka, W., Buesa, J., Coleman, R., van Hoessel, R., & Judson, I. R. (2000). Randomized phase II study of docetaxel versus doxorubicin in first-and second-line chemotherapy for locally advanced or metastatic soft tissue sarcomas in adults: a study of the European Organization for Research and Treatment of Cancer Soft Tissue and Bone Sarcoma Group. *Journal of Clinical Oncology*, *18*(10), 2081-2086.

Weiss, R. B. (1992, December). The anthracyclines: will we ever find a better doxorubicin?. In *Seminars in Oncology* (Vol. 19, No. 6, pp. 670-686).

Yang, D., & Zhang, C. (2001). Ruthenium-catalyzed oxidative cleavage of olefins to aldehydes. *The Journal of Organic Chemistry*, *66*(14), 4814-4818.

CHAPTER THREE: HYDRAZONE REDUCTIONS FOR IMPROVEMENT OF DIDOX YIELD

3.1 Introduction

The anthracycline doxorubicin (DOX) is an extensively used anticancer agent (**Figure 3.1**). However, it is plagued by dose-dependent cardiotoxicity stemming from two structural moieties: the C-13 carbonyl and the quinone (Boucek, 1997; Cusack, 1993). Enzymatic reduction of DOX's carbonyl, mediated by carbonyl reductase, forms an alcohol metabolite that accumulates in cardiac tissue and disrupts function by inhibiting ion pumps (Robert Jr, 1987). In addition, DOX's quinone catalyzes the production of reactive oxygen species that disproportionately damages cardiac myocytes (Cummings, 1992).

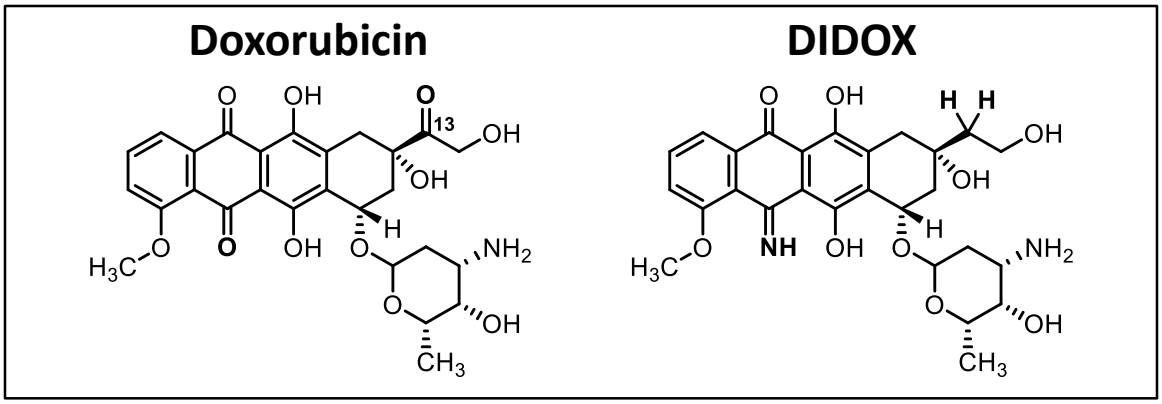

Figure 3.1 Structure of Doxorubicin and the non-cardiotoxic DIDOX analog. Both the C-13 carbonyl and quinone of doxorubicin produce cardiotoxicity. The carbonyl is reduced by carbonyl reductase to form a cardiotoxic C-13 alcohol and the quinone catalyzes the formation of reactive oxygen species. The structure of DIDOX is analogous to DOX except the carbonyl is completely reduced to a methylene and the quinone has been altered to an iminoquinone.

Previous work has been successful at alleviating this terrible side effect by reducing the carbonyl to a methylene and converting the quinone to an iminoquinone, producing 5-

imino-13-deoxydoxorubicin (DIDOX). However, conversion of doxorubicin to DIDOX has been hindered by a poor method for the reduction of the C-13 carbonyl to generate the intermediate 13-deoxydoxorubicin (DeoxyDOX). The current method employs a Wolff-Kishner style reduction comprised of an initial condensation of benzene sulfonylhydrazide onto DOX's carbonyl to afford BSHDOX, followed by treatment with $NaBH_3CN$ and pyridinium p-toluenesulfonate (PPTS) (**Scheme 3.1**) (Walsh, 2007; Zhang, 1999). The reduced anthracycline, after these two steps, is generally produced in very low yields that range from 5-35% (Smith, 1978).

It was hypothesized that using a different hydrazone during the reduction could potentially help improve overall yield. In these experiments, six different hydrazones were formed and each reduced under similar conditions. The deoxygenated products were not able to be purified and isolated as it required expensive and non-available preparative HPLC. In light of this, the yield of each reaction is reported as a relative abundance (RA), determined by analytical HPLC, in order to compare the hydrazone reductions. It was found that the current hydrazone used for the reduction produced only 43% RA, whereas four alternate hydrazones produced up to 59% RA. This data suggests that the current method to synthesize DeoxyDOX could be improved by a simple adaptation to a different hydrazone.

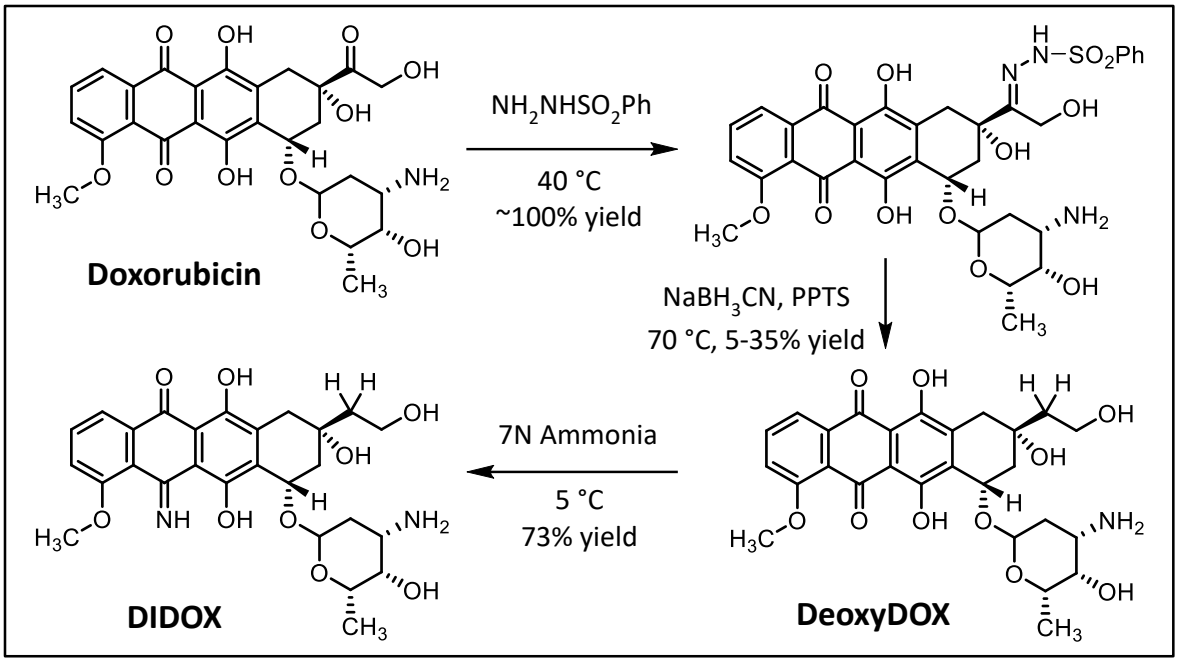

Scheme 3.1 DIDOX Synthesis. Condensation of DOX and NH_2NHSO_2Ph affords BSHDOX. It then follows a Wolff-Kishner style reduction to produce DeoxyDOX in 5-35% yield. Lastly, the quinone is converted to an iminoquinone using concentrated ammonia.

3.2 Results and Discussion

In this work, a series of six different hydrazone formation/reductions were performed to optimize the relative formation of DeoxyDOX, as determined by HPLC. Four of the hydrazone reductions attempted appeared to outperform the conventional commercial method. It was found that more electron-withdrawing hydrazones were able to undergo reduction at a much faster rate. Nevertheless, a temperature of 70 °C was required in order for the reduction reactions to go to completion.

In order to test the impact of the aromatic ring on the reduction step, it was determined that six different hydrazones of varying electronic characteristics needed to be evaluated. Three of the precursor hydrazides were commercially available and the remaining three required a simple, one step preparation. The syntheses of 4-fluorobenzenesulfonohydrazide (FSH), 4-(trifluoromethyl) benzenesulfonohydrazide

(TFSH) & pyridine 3-sulfonylhydrazide (PSH), shown in **Figure 3.2**, were performed using identical methods, which involved chilling to -30 °C in THF and substituting their respective chlorides using hydrazine (Myers, 1997). Purification of these hydrazides was accomplished by simple extraction and recrystallization. The hydrazide, PSH, was difficult to obtain in high yields using this method, possibly due to increased solubility in water and loss of material during workup and preliminary extraction steps. While it was not attempted in this work, a back extraction in the future may be able to improve the yield.

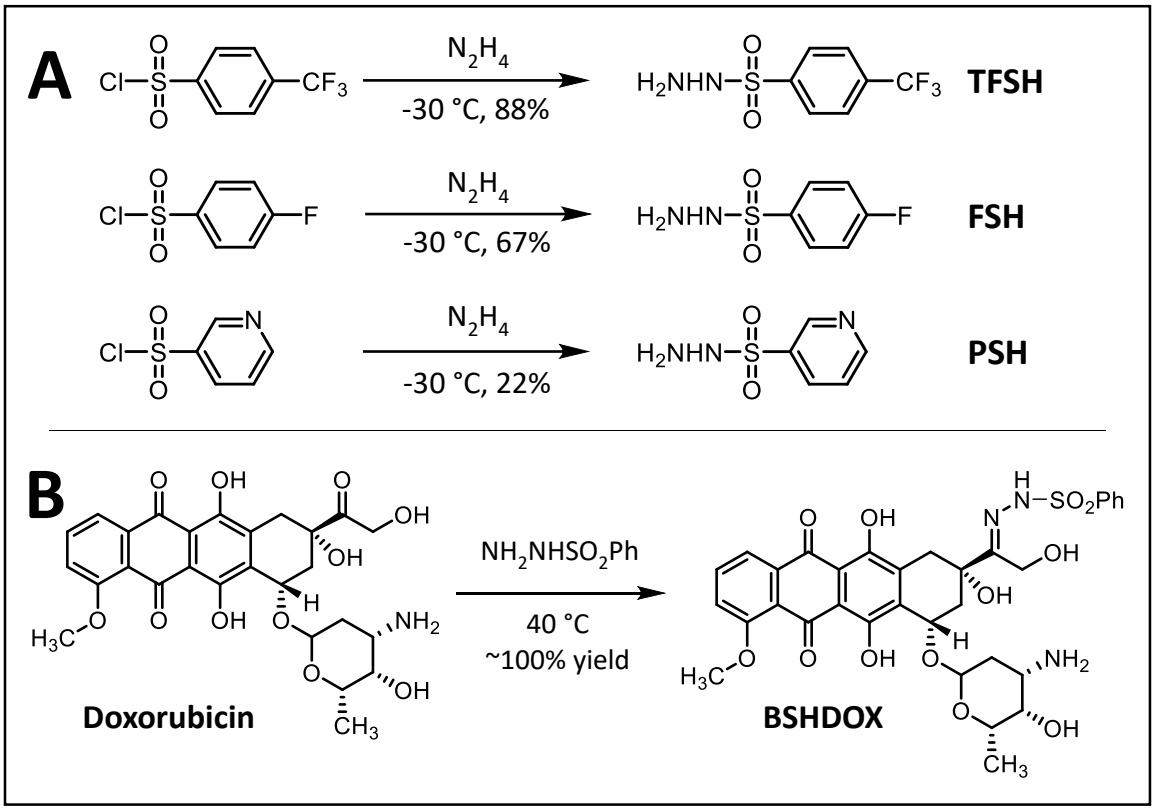

Figure 3.2 Synthesis of hydrazides and DOX-hydrazone. (A) Hydrazine is used to displace chlorine during the formation of hydrazides. **(B)** Shown is the attachment of BSH onto DOX through condensation. The formation of the five other DOX-hydrazones were all isolated using analogous conditions and in similar yields.

The other three hydrazides—benzenesulfonylhydrazide (BSH), tosylhydrazide (TSH), and 4-nitrobenzenesulfonohydrazide (NSH)—were purchased from commercial sources.

Attachment of the six hydrazides used the same reaction conditions (**Figure 3.2**). First, DOX was dissolved in MeOH and then the corresponding hydrazide was added and allowed to react at 40 °C overnight under nitrogen. After recrystallization, the DOX-hydrazones were isolated in nearly 100% yield. The hydrazones FSH, TFSH, NSH, and PSH were thought to be more electron-withdrawing than BSH and thus might possibly be easier to reduce. To obtain a broader representation, TSH was also considered because of its slight electron-donating ability.

The six distinct DOX-hydrazones were then reduced to DeoxyDOX using $NaBH_3CN$ and PPTS at 70 °C (**Figure 3.3**). The reaction progress was monitored using LC-MS to determine the required time for all of the starting hydrazone to no longer be present. Only BSHDOX required more than 60 minutes to be completely consumed. In fact, it took nearly three times as long as the next slowest hydrazone reduction. Interestingly, this is the hydrazone currently used to prepare DIDOX (Walsh, 2007). One apparent trend seen with this data is that more electron-withdrawing hydrazones produced less DeoxyDOX and more of the main side product. For example, all starting NSHDOX was consumed after only 30 minutes under reductive condition, but produced significantly less DeoxyDOX than the reduction of TSHDOX, which required twice the time.

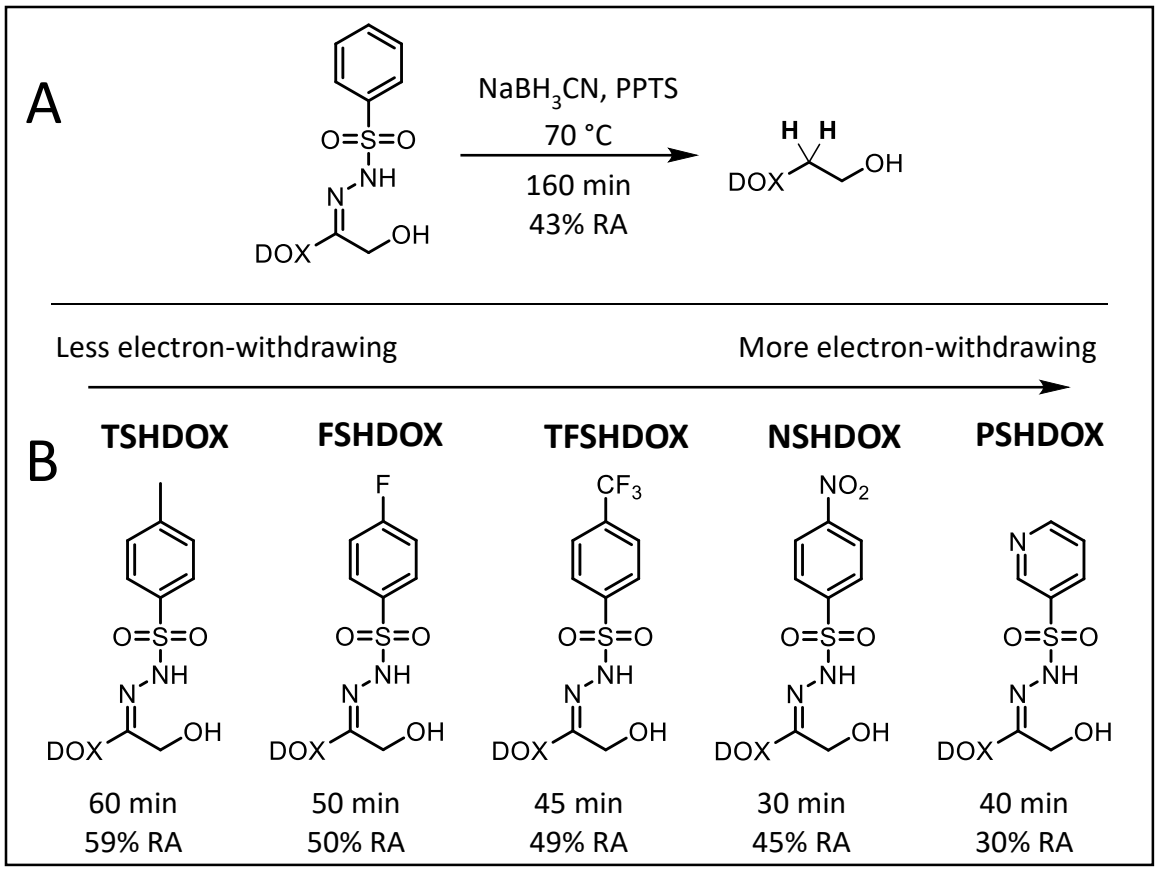

Figure 3.3 DOX-Hydrazone reductions. (**A**) Shown is the Wolff-Kishner reduction of BSHDOX to DeoxyDOX using $NaBH_3CN$ and PPTS, at 70 °C. The time required for complete reduction was found to be 160 minutes and there was 43% RA of DeoxyDOX formed. (**B**) These five hydrazones were reduced using similar methods as shown for BSHDOX and are ordered by decreasing percent RA DeoxyDOX. Interestingly, as the hydrazones become more electron-withdrawing, the **RA** of DeoxyDOX formed becomes smaller.

The relative abundance (RA) for DeoxyDOX formation was determined immediately following reduction completion. It was found that only one DOX-hydrazone, PSHDOX, produced less relative DeoxyDOX than the currently used BSHDOX. The RA of DeoxyDOX formed using BSHDOX was 43%, while it increased to 59% when using TSHDOX. This was slightly surprising, as the only difference between BSH and TSH is a methyl group at the para-position. Nonetheless, TSH outperformed the other, more electron-withdrawing hydrazones. The lower abundance of DeoxyDOX formation from the BSHDOX reduction can be explained by the lengthy 160 minutes in these reaction

conditions, which allows for the formation of numerous side products not observed with any other hydrazones (**Figure 3.4**). Along with lower abundance, these impurities could potentially make purification using BSH much more difficult than the other hydrazones.

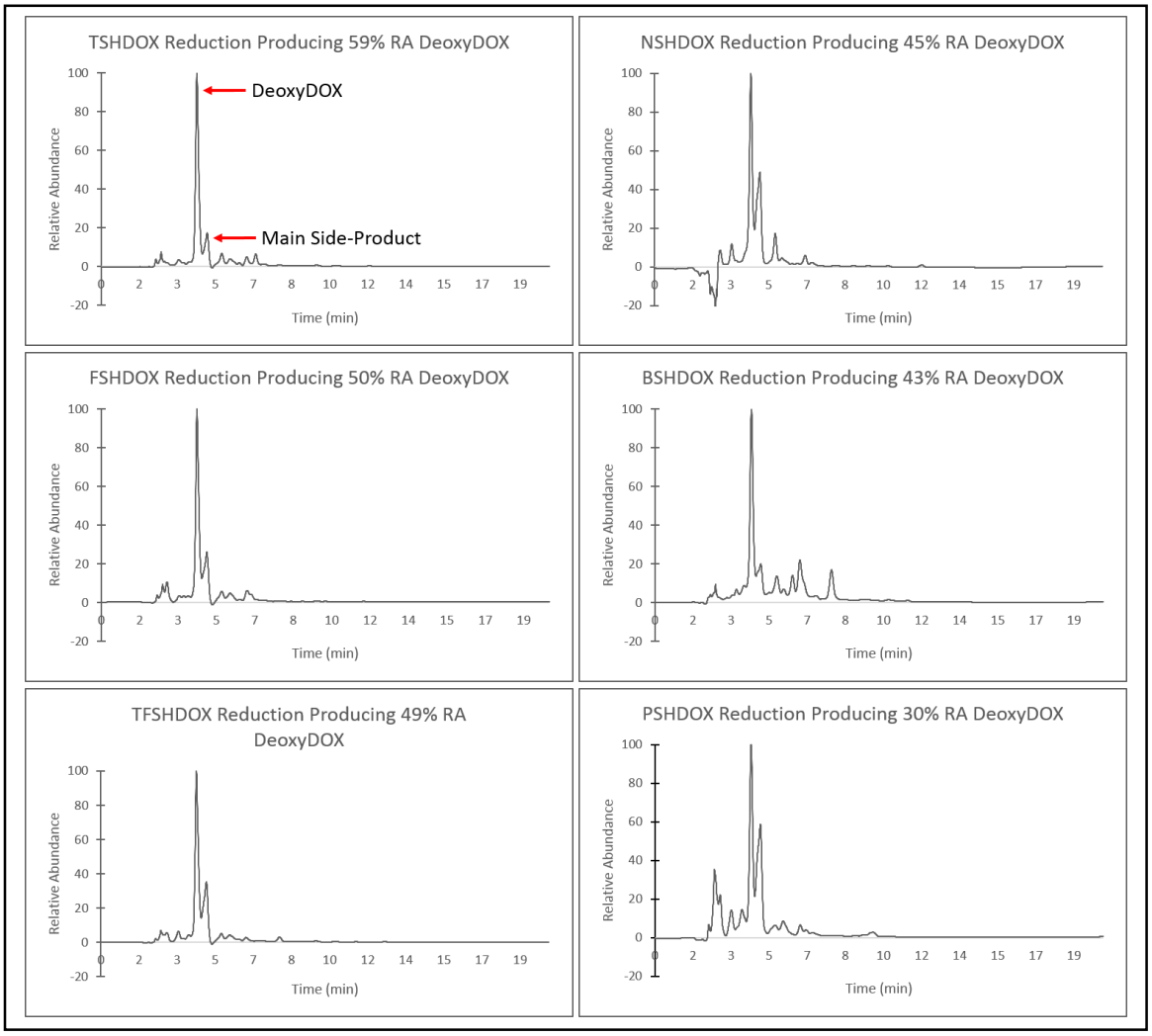

Figure 3.4 HPLC chromatograms of DOX-hydrazone reductions. The above chromatograms were obtained using HPLC at a wavelength 480 nm and ordered by RA of DeoxyDOX formed after reduction. DeoxyDOX is shown with a red arrow and elutes just after 4 minutes as the main product in all chromatograms. The main side product elutes just after DeoxyDOX and increases as the RA of DeoxyDOX decreases, BSHDOX being the exception.

Reduction of these DOX-hydrazones all exhibited the formation of a distinct and prominent side product that elutes between 4.5-5.0 minutes on HPLC, just after the elution of DeoxyDOX. It has not yet been structurally characterized, but it appears to be the main

side product formed and the quantity produced varies greatly depending on which hydrazone was used. Interestingly, the observed m/z for this side product, 599.16 amu, is the same regardless of the hydrazone used, suggesting an analogous impurity. Also, it appears that more of this side product forms as the electron-withdrawing effects increase. Initially, it was thought that the impurity was an intermediate that had not yet been fully reduced, however, prolonging the reduction following complete consumption of the starting hydrazone proved insufficient to decrease the side product. Future work will need to focus on characterizing and identifying the root source of this side product to better optimize the reaction.

An understanding of the reduction mechanism may allow for explanation of the accelerated reaction time seen with the electron-withdrawing hydrazones, as shown in **Scheme 3.2** (Kosower, 1992; Miller, 1989). Initially, treatment with an acid produces the iminium, which is then reduced by $NaBH_3CN$. Next, elimination of the sulfonyl group (SG) produces a diazene, which is readily deprotonated to form a diazenyl anion. Finally, this anion decomposes to N_2 and a carbanion, followed by protonation to form the reduced methylene. The rate of this initial step has been monitored using LC-MS and has shown that formation of the hydrazine-DOX occurs at similar rates for all the hydrazones. However, it is thought that elimination of more electron-withdrawing SG's occur much faster than that of TSH and BSH, allowing for quicker decomposition to the methylene. On the other hand, while these increased reduction rates may be appealing, they are hampered by an increased production of the main side product.

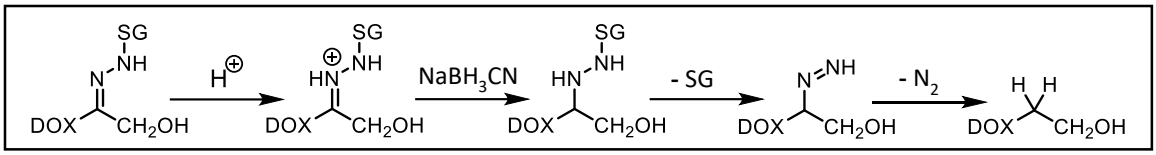

Scheme 3.2 Mechanism of hydrazone reduction. The mechanism for reduction follows this route. It is initiated by the formation of an iminium, followed by $NaBH_3CN$ reduction. At this point, the SG is eliminated and decomposition produces the reduced methylene.

3.3 Conclusion

The traditional BSHDOX used during the synthesis of DeoxyDOX has been shown in these experiments to be the suboptimal choice. All but one DOX-hydrazone appeared to yield higher quantities of DeoxyDOX than the commercially employed BSHDOX, which was determined by comparing RA. One straightforward possibility as to why this occurred could simply be attributed to the fact that the necessary time in order for a full reduction of BSHDOX was significantly longer than that for all other hydrazones. A longer reaction time could potentially facilitate the production of more side products, such as the removal of the daunosamine sugar moiety through acid-catalyzed hydrolysis. Conversely, the more rapid reductions from electron-withdrawing sulfonyls produced a significant quantity of undesired side products as well. From these results, it was determined that an inverse relation existed between the strength of electron-withdrawing hydrazones and relative DeoxyDOX formed. The exception to this being BSH, due to the prolonged reaction time, which creates additional impurities.

In the future, alternative methods for carbonyl reduction will be investigated to further improve the synthesis of DIDOX. Two potential options would be the implemention of a Clemmensen reduction or Lewis acid ionic hydrogenation (Goddard-Borger, 2007; Kursanov, 1974; Luchetti, 1991). The general mechanism of the Clemmensen reduction involves replacement of the carbonyl with a methylene through radical rearrangements

using zinc (**Scheme 3.3**). Specifically, both zinc and the carbonyl donate a single electron to form a zinc-oxygen bond, which displaces a radical onto the tertiary carbon. Next, that radical and an electron from a second zinc combine, then an additional two-electron donation removes zinc oxide from the compound. The newly formed zinc carbenoid is then removed after the addition of acid. In contrast, Lewis acid (LA) coordination during ionic hydrogenation enhances carbonyl electrophilicity, which allows for reduction using a hydride source. Implementation of these methods may improve the yield of DeoxyDOX over the currently used Wolff-Kishner approach. However, there are several potential issues with these two methods. One problem would be the inadvertent acid-catalyzed hydrolysis of the daunosamaine glycosidic bond during the Clemmensen reduction. Over-reduction may also be an issue with the LA, since reduction of the quinone carbonyl or various hydroxyl moieties of DOX may occur. As such, further investigation will be required to determine the optimal method toward producing the methylene present in DeoxyDOX.

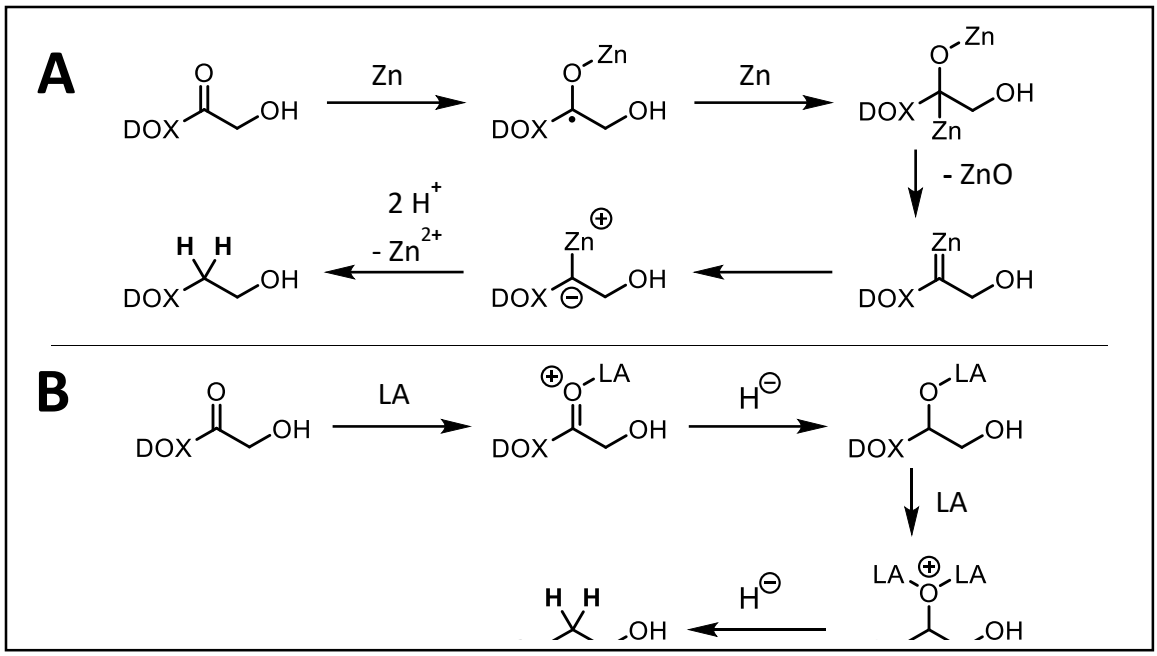

Scheme 3.3 Alternative carbonyl reductions to produce DeoxyDOX. (**A**) During the Clemmensen reduction, both the carbonyl and zinc donate a single electron to form a zinc-oxygen bond which forces the other carbonyl electron onto the tertiary carbon. Next, this carbon radical and an electron from a second zinc come together to form a zinc-carbon bond. Ensuing radical rearrangement, ZnO is removed by forming a zinc carbenoid that readily reduced using an available acid, such as HCl. (**B**) Dehydrogenation using a Lewis acid, such as $AlCl_3$, begins by coordinating with the carbonyl, making the attached carbon significantly more electrophilic and available for hydride reduction. After the first reduction, another Lewis acid will coordinate with the oxygen and allow for a second hydride reduction to occur.

3.4 Materials and Methods

3.4.1 Materials and Reagents

Doxorubicin hydrochloride was purchased from Advanced ChemBlocks, Inc. Pyridinium p-toluenesulfonate (PPTS), sodium cyanoborohydride, and tosylhydrazide were purchased from Aldrich chemicals. Benzenesulfonylhydrazide and 4-fluorobenzenesulfonyl chloride were supplied by TCI. 4-(Trifluoromethyl) benzenesulfonyl chloride and pyridine-3-sulfonyl chloride were purchased from Matrix Scientific. Hydrazine monohydrate was acquired from Beantown Chemical. 4-

Nitrobenzenesulfonohydrazide came from Combi-Blocks. All solvents were purchased from Fisher Scientific unless otherwise specified.

3.4.2 Equipment

NMR data was acquired using either 600 MHz Bruker Avance III 600 coupled with Bruker Ultrashield 600 Plus or 300 MHz Bruker Ultrashield 300 coupled with Bruker Avance III 300. HPLC chromatography was performed using Agilent 1100 series equipped with 50x4.6 mm Hypersil Gold Phenyl column having 5µm pore size. A Bruker HCTultra ETD II Ion Trap was used for mass spectrometry.

3.4.3 Experimental

4-fluorobenzenesulfonohydrazide

4-fluorobenzenesulfonyl chloride (514.2mg, 2.64mmol) was made to be 0.5M in THF (5.3mL) and allowed chilled to -30°C. Hydrazine (208mL, 6.61mmol, 2.5eq) was then added via syringe. This was allowed to react at -30°C and monitored by TLC using EtOAc/Hexanes (2:1, v/v). Starting material had all reacted after 30 minutes. Solution was then diluted with 10mL EtOAc and washed with 10 mL ice-cold 10% NaCl aqueous solution x5. It was then dried using sodium sulfate and filtered. The solution was then slowly added over 5 minutes to 30mL hexanes and allowed to stir for 15 minutes. The precipitate was then collected by vacuum filtration and washed with 15mL hexanes x3. The final product, 4-fluorobenzenesulfonohydrazide, was collected as a white powder and placed under high vacuum (>150mTorr) for 90 minutes (338.5mg, 67.4% yield). ^{1}H NMR ($CDCl_3$ with 0.03% v/v TMS, 600 MHz) δ: 7.98-7.94 (m, 2H), 7.25 (t, 2H, J = 8.6 Hz), 5.59 (s, 1H), 3.63 (s, 2H)

4-(Trifluoromethyl) benzenesulfonohydrazide

Synthesis followed procedures analogous as stated above for 4-fluorobenzenesulfonohydrazide. Final product was obtained in 88% yield as a white powder. ^{1}H NMR (C_2D_6OS with 0.03% v/v TMS, 300 MHz) δ: 8.65 (s, 1H), 8.00 (s, 4H), 4.29 (s, 2H).

Pyridine 3-sulfonylhydrazide

Synthesis followed procedures analogous as stated above for 4-fluorobenzenesulfonohydrazide. Final product was obtained as a white powder in in 22% yield. ^{1}H NMR (C_2D_6OS with 0.03% v/v TMS, 300 MHz) δ: 8.93 (dd, 1H, J = 2.4 Hz, 0.8 Hz), 8.82 (dd, 1H, J = 4.8 Hz, 1.6 Hz), 8.61 (br, 1H), 8.16 (ddd, 1H, J = 8.0 Hz, 2.4 Hz, 1.6 Hz), 7.65 (ddd, 1H, J = 8.0 Hz, 4.8 Hz, 0.8 Hz), 4.311 (br, 2H).

Tosylhydrazone DOX HCl

DOX HCl (40.0mg, 0.0709mmol) was made to be 0.02M in MeOH (3.5mL) before tosyl hydrazide (29.1mg, 0.156mmol, 2.2 eq) was added. This was allowed to react at 50 °C overnight. When starting material had completely reacted (determine by LC-MS) it was removed from heat and allowed to cool to RT. The product was then recrystallized by slowly adding 15mL MTBE/hexanes (4:1, v/v) and allowed to stir for 15 minutes at RT. The solid was then isolated by centrifuge (1800 rpm, 10 minutes, 4 °C) and placed under high vacuum (>150mTorr) for 60 minutes. Hydrazone DOX was collected as a red solid in greater than 95% purity and ~100% yield.

Synthesis of Additional DOX-Hydrazones

The other 5 hydrazones, BSHDOX, FSHDOX, TFSHDOX, NSHDOX, and PSHDOX were formed using similar procedures and in similar yields as tosylhydrazone DOX HCl.

Hydrazone Reductions

Tosylhydrazone DOX HCl (47.2mg, 0.0631mmol) was dissolved in 1mL MeOH. PPTS (95.1mg, 0.379mmol, 6eq) and $NaBH_3CN$ (39.7mg, 0.631mmol, 10eq) were combined and dissolved in 2.2mL MeOH (DOX was made to be 0.02M in MeOH overall) before being added to DOX. This was allowed to react at 70 °C until starting hydrazone had been completely reduced (60 minutes). Monitored via LC-MS. No purification was attempted, however a RA of DeoxyDOX formation was obtained through HPLC analysis.

All hydrazone reductions followed these procedures (with varying times to obtain full reduction).

3.5 References

Boucek, R. J. (1997). Mechanisms for anthracycline-induced cardiomyopathy: clinical and laboratory correlations. *Progress in Pediatric Cardiology*, *8*(2), 59-70.

Cummings, J., Willmott, N., Hoey, B. M., Marley, E. S., & SMyth, J. F. (1992). The consequences of doxorubicin quinone reduction in vivo in tumour tissue. *Biochemical Pharmacology*, *44*(11), 2165-2174.

Cusack, B. J., Mushlin, P. S., Voulelis, L. D., Li, X. D., Boucek, R. J., & Olson, R. D. (1993). Daunorubicin-induced cardiac injury in the rabbit: a role for daunorubicinol?. *Toxicology and Applied Pharmacology*, *118*(2), 177-185.

Goddard-Borger, E. D., Ghisalberti, E. L., & Stick, R. V. (2007). Synthesis of the germination stimulant 3-methyl-2H-furo [2, 3-c] pyran-2-one and analogous compounds from carbohydrates. *European Journal of Organic Chemistry*, *2007*(23), 3925-3934.

Kosower, E. M., & Tsuji, T. (1971). Diazenes. VI. Alkyldiazenes. *Journal of the American Chemical Society*, *93*(8), 1992-1999.

Kursanov, D. N., Parnes, Z. N., & Loim, N. M. (1974). Applications of ionic hydrogenation to organic synthesis. *Synthesis*, *1974*(09), 633-651.

Luchetti, L., & Rosnati, V. (1991). Zinc-promoted reactions. 2. Ionic and nonionic pathways in the reduction of acetophenone and 2, 2-dimethyl-1-phenylpropan-1-one. *The Journal of Organic Chemistry*, *56*(24), 6836-6839.

Miller, V. P., Yang, D. Y., Weigel, T. M., Han, O., & Liu, H. W. (1989). Studies of the mechanistic diversity of sodium cyanoborohydride reduction of tosylhydrazones. *The Journal of Organic Chemistry*, *54*(17), 4175-4188.

Myers, A. G., Zheng, B., & Movassaghi, M. (1997). Preparation of the reagent o-nitrobenzenesulfonylhydrazide. *The Journal of Organic Chemistry*, *62*(21), 7507-7507.

Robert Jr, J., Olson, R. D., Brenner, D. E., Ogunbunmi, E. M., Inui, M., & Fleischer, S. (1987). The major metabolite of doxorubicin is a potent inhibitor of membrane-associated ion pumps. *Journal of Biological Chemistry*, *262*(33), 15851-15856.

Smith, T. H., Fujiwara, A. N., & Henry, D. W. (January 01, 1978). Adriamycin analogues. 2. Synthesis of 13-deoxyanthracyclines. *Journal of Medicinal Chemistry*, *21*, 3, 280-3.

Walsh, G. M., & Olson, R. D. (2007). *U.S. Patent No. 7,244,829*. Washington, DC: U.S. Patent and Trademark Office.

Zhang, X., & Olson, R. D. (1999). *U.S. Patent No. 5,942,605*. Washington, DC: U.S. Patent and Trademark Office.

APPENDIX A: ^{1}H NMR SPECTRA

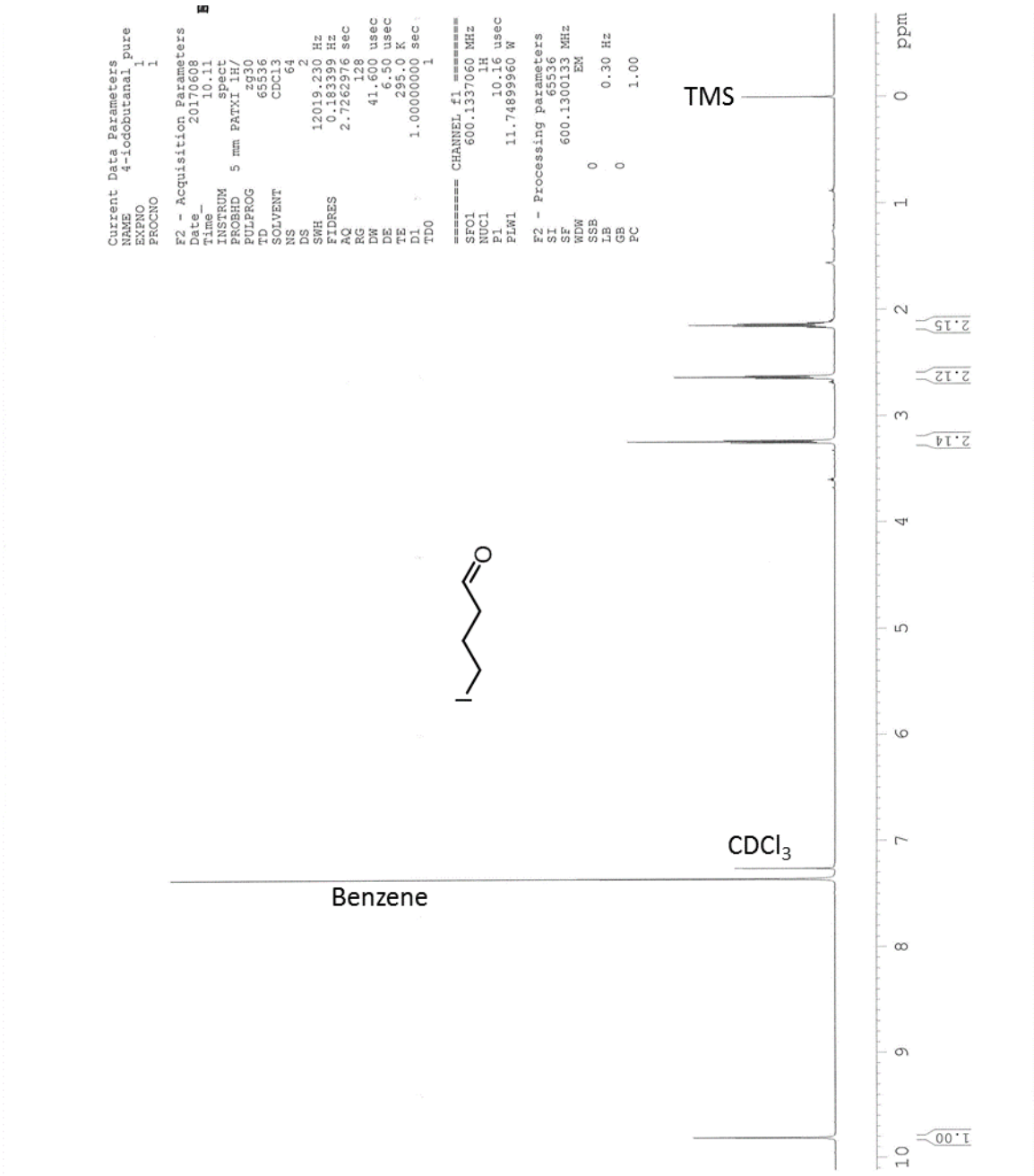

^{1}H NMR ($CDCl_3$ with 0.03% v/v TMS, 600 MHz)

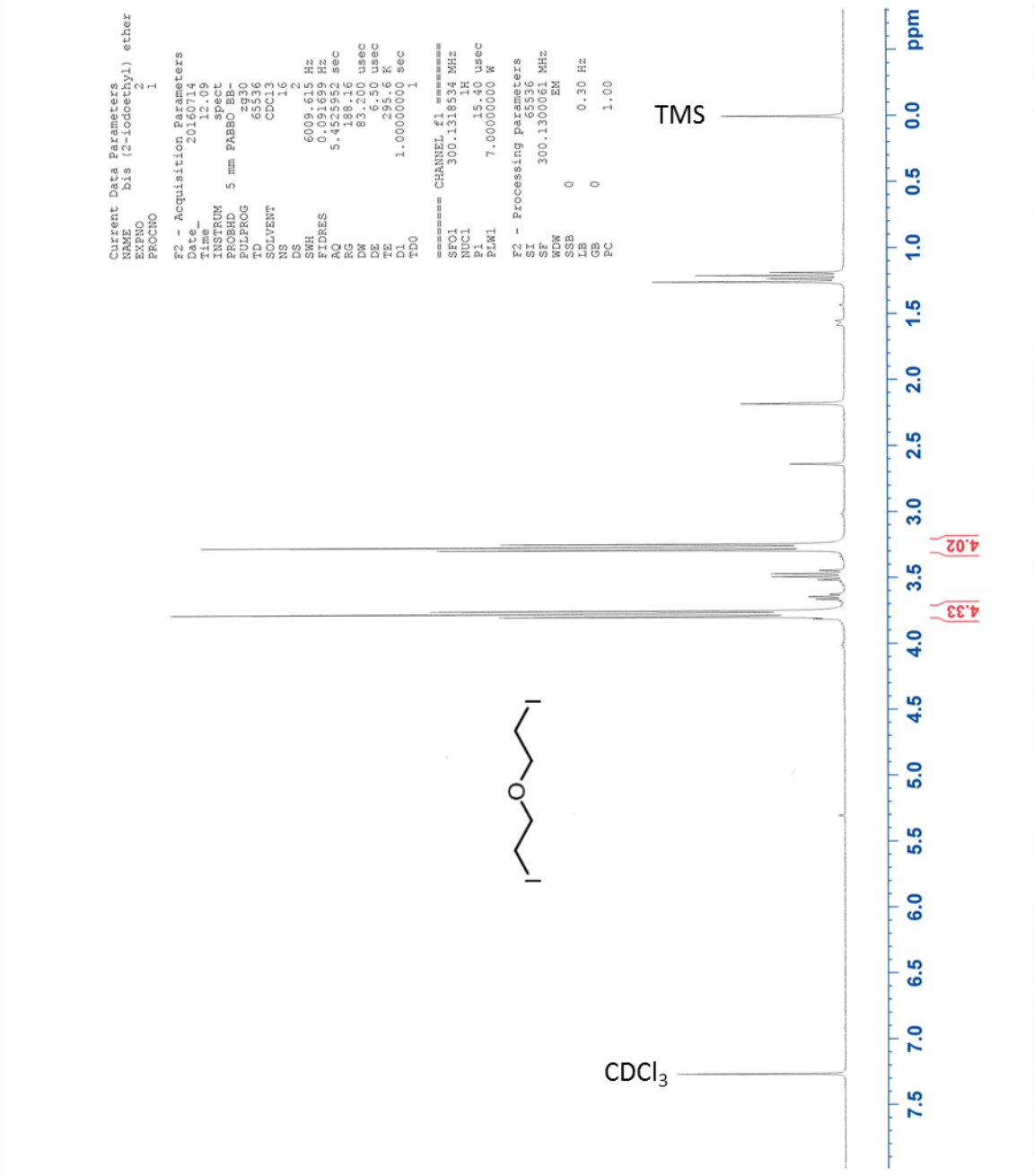

^{1}H NMR ($CDCl_3$ with 0.03% v/v TMS, 300 MHz)

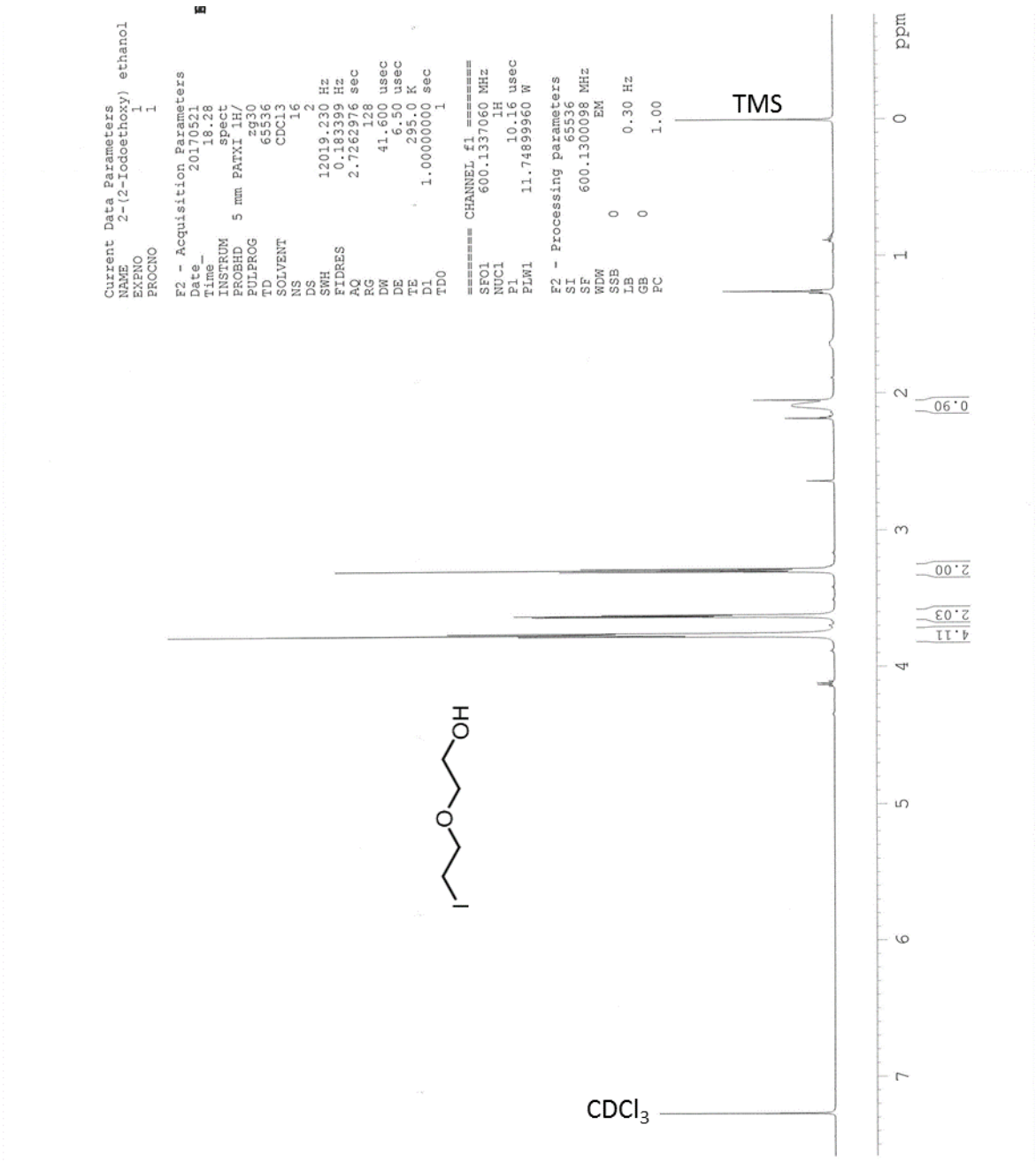

^{1}H NMR ($CDCl_3$ with 0.03% v/v TMS, 600 MHz)

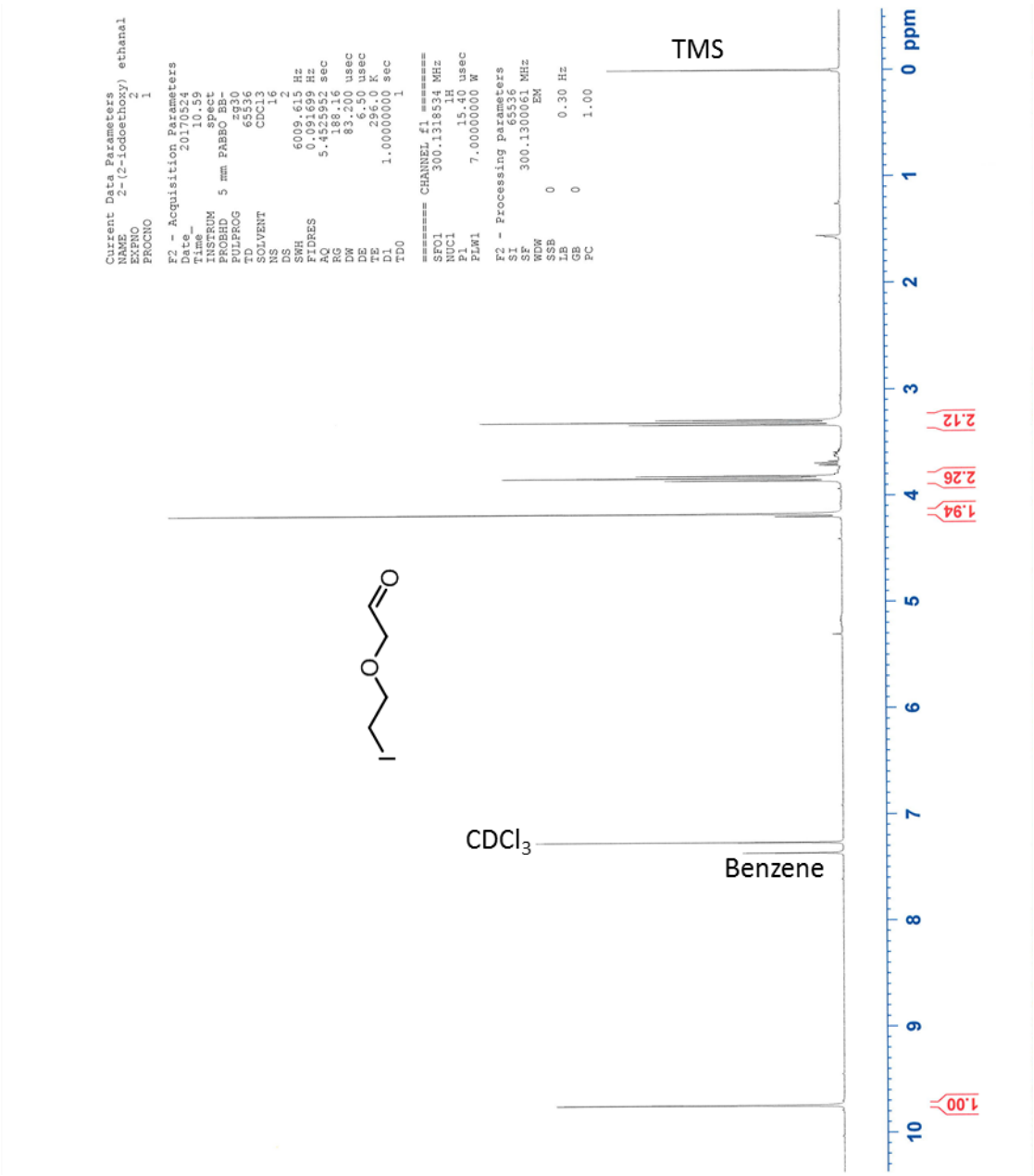

^{1}H NMR ($CDCl_3$ with 0.03% v/v TMS, 300 MHz)

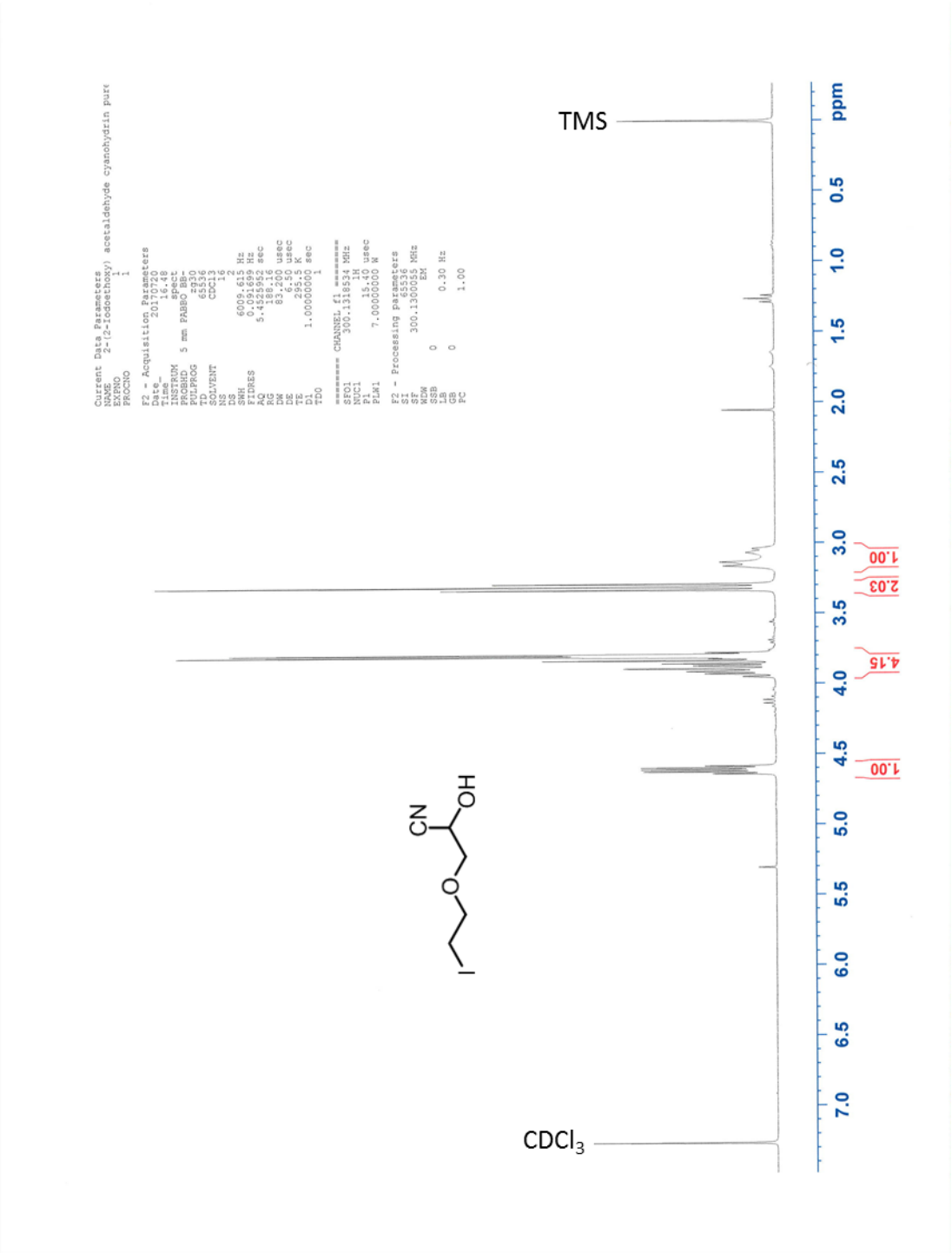

^{1}H NMR ($CDCl_3$ with 0.03% v/v TMS, 300 MHz)

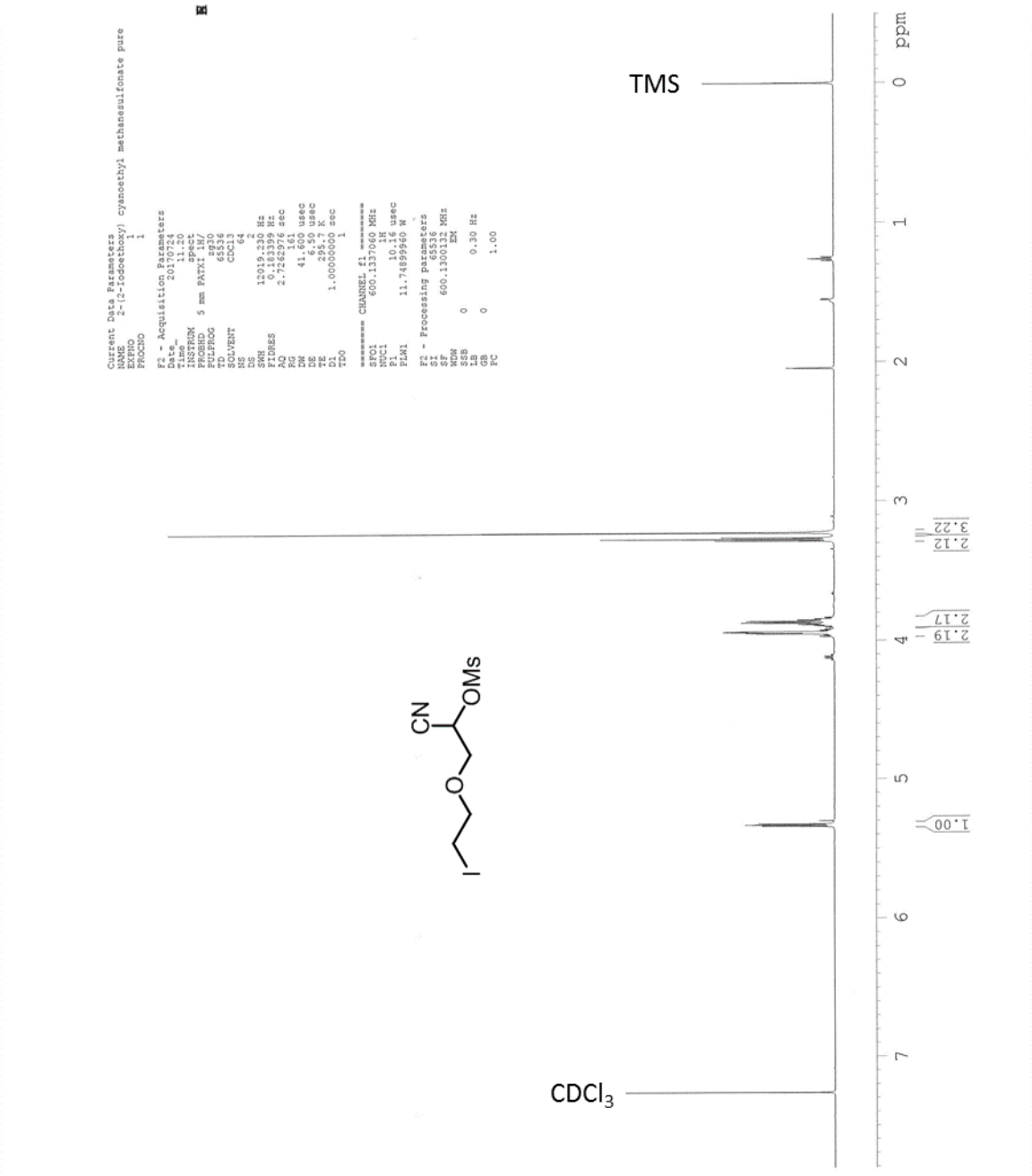

^{1}H NMR ($CDCl_3$ with 0.03% v/v TMS, 600 MHz)

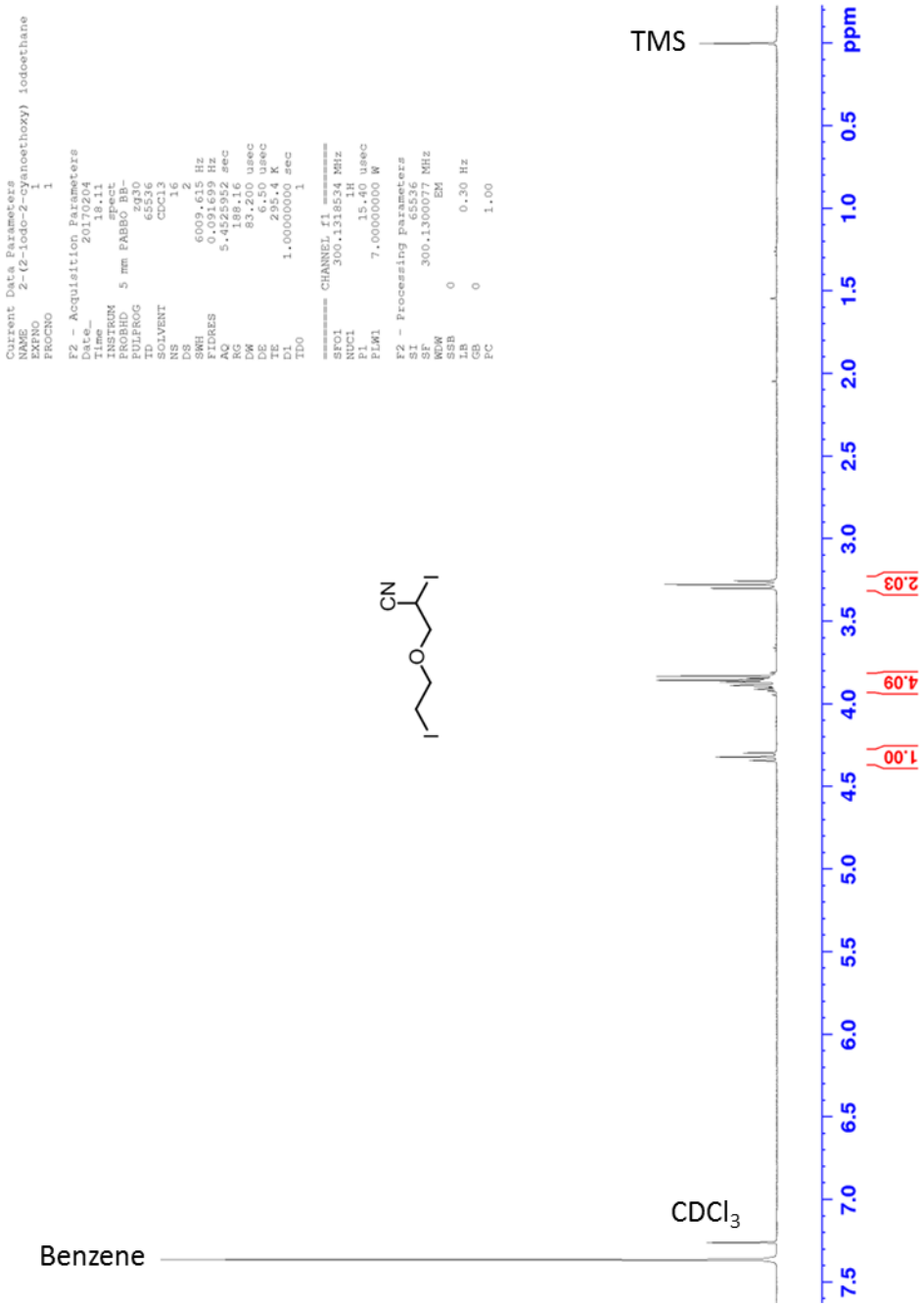

^{1}H NMR ($CDCl_3$ with 0.03% v/v TMS, 300 MHz)

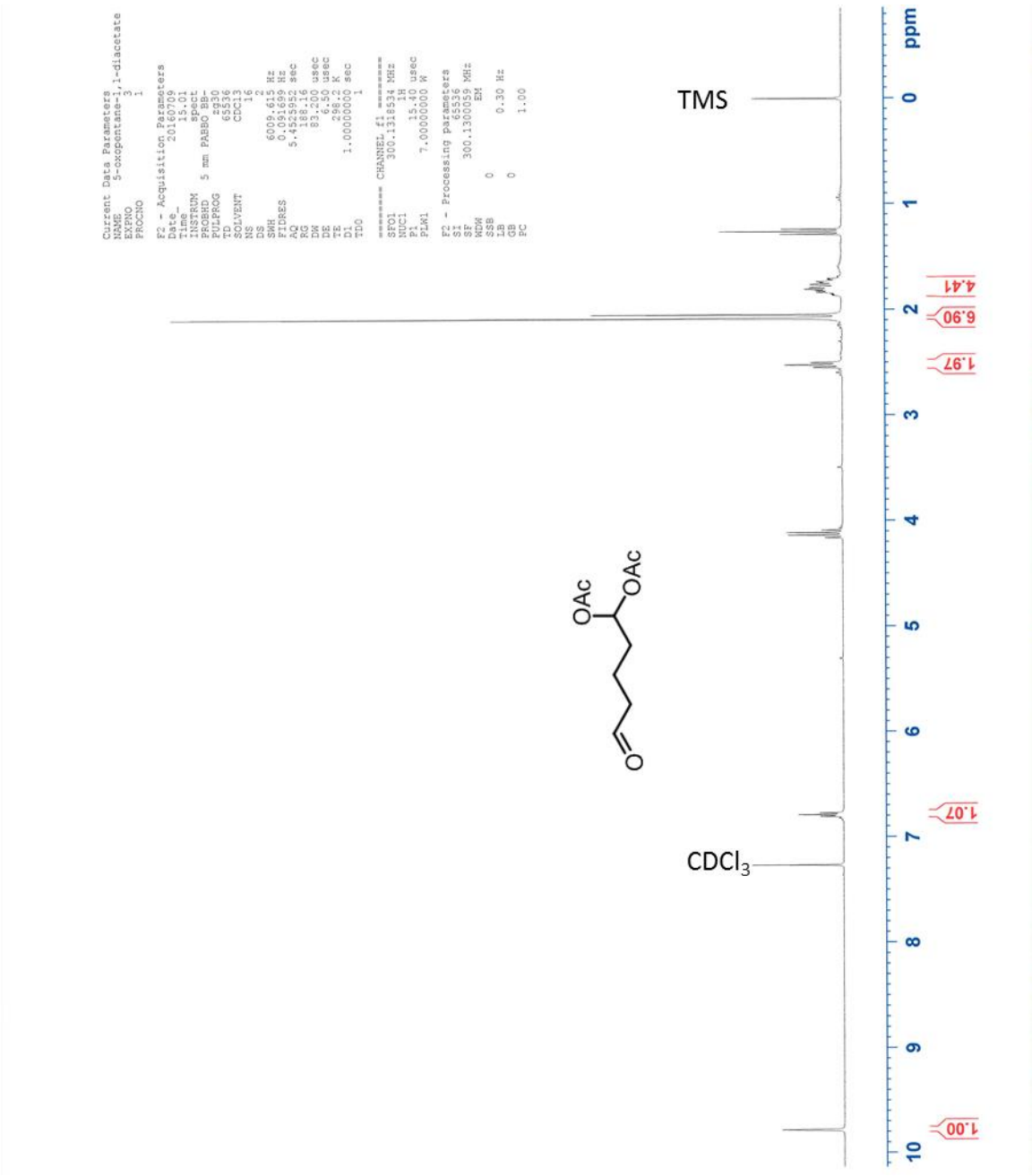

^{1}H NMR ($CDCl_3$ with 0.03% v/v TMS, 300 MHz)

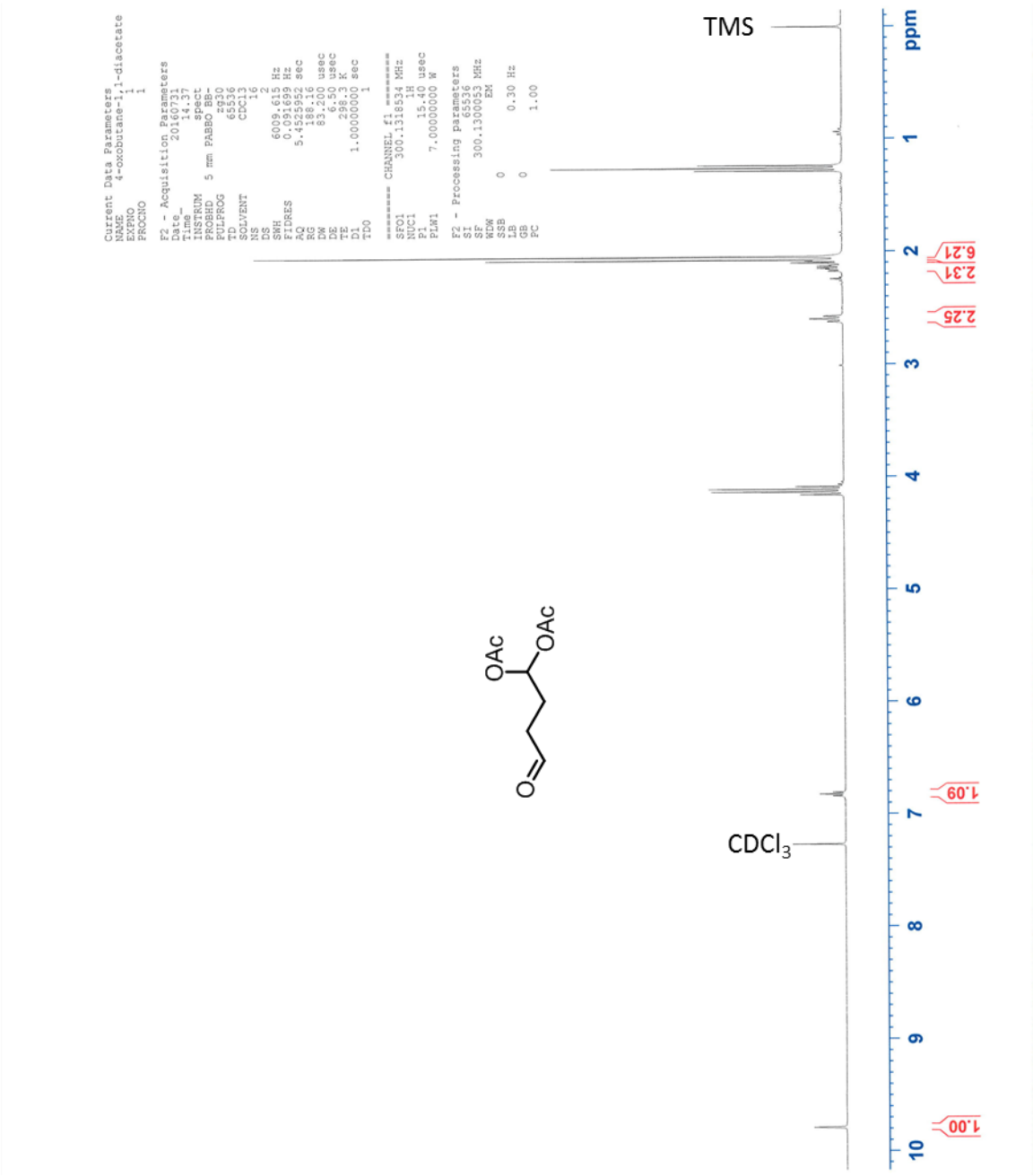

^{1}H NMR ($CDCl_3$ with 0.03% v/v TMS, 300 MHz)

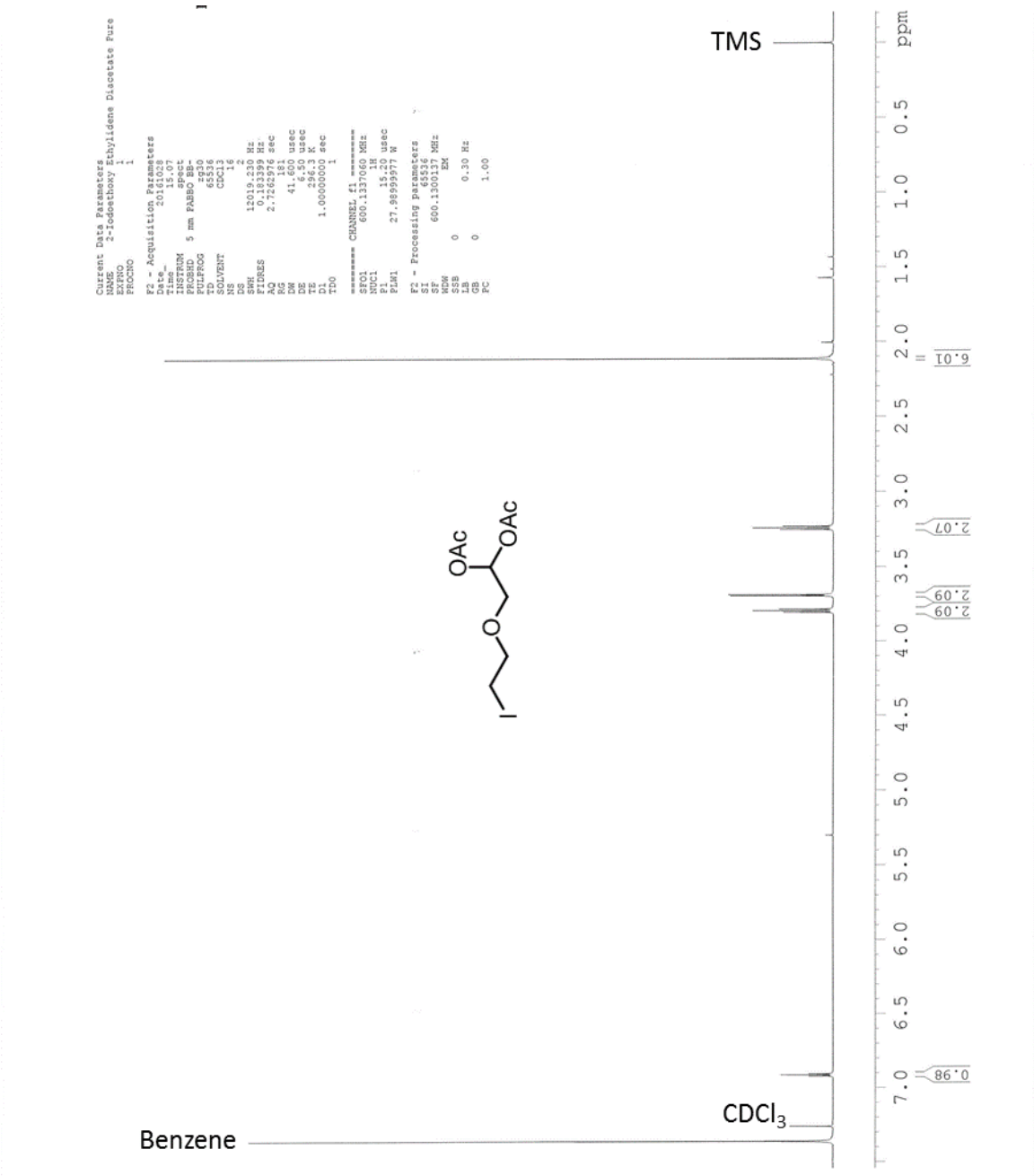

^{1}H NMR ($CDCl_3$ with 0.03% v/v TMS, 600 MHz)

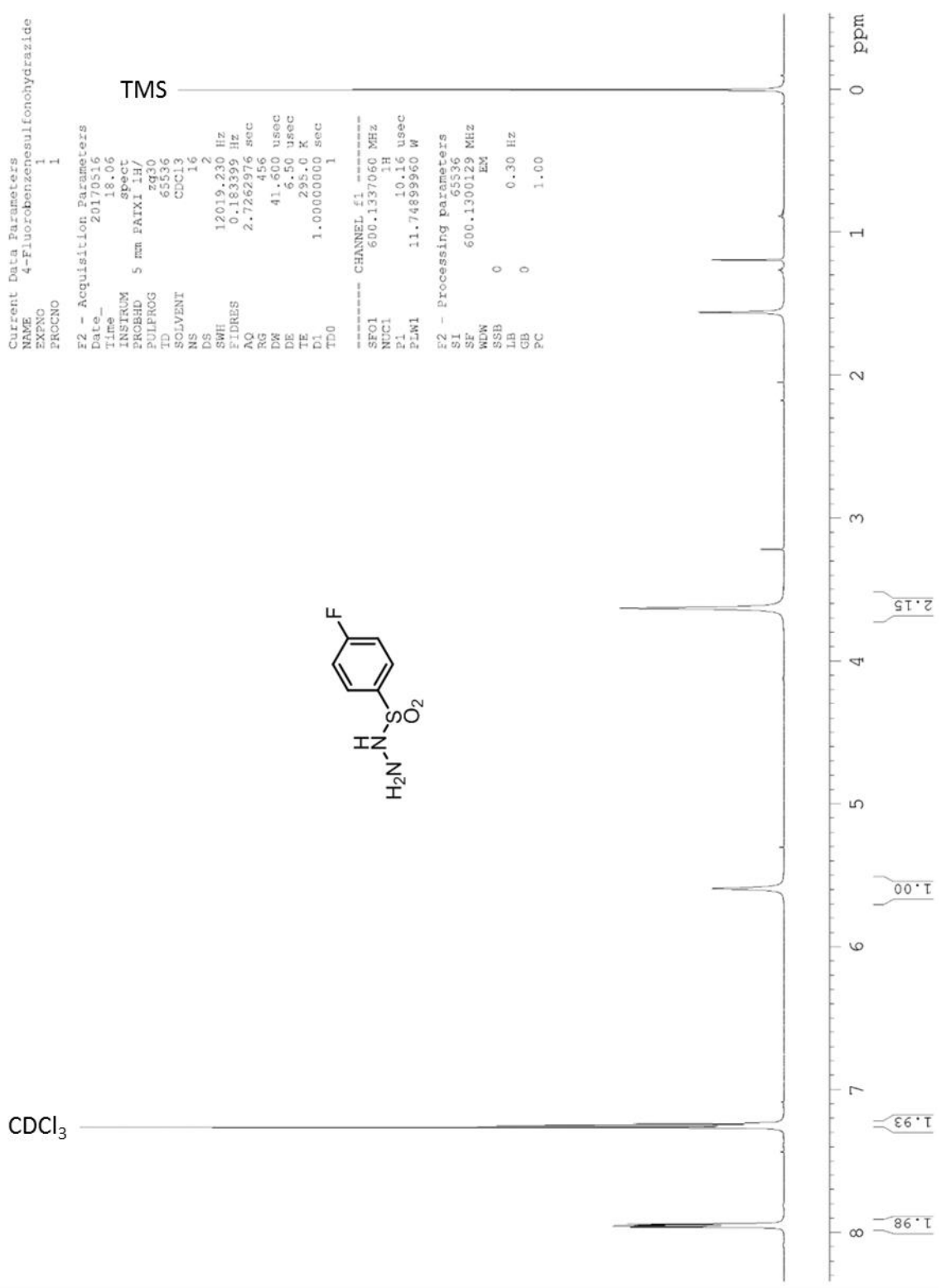

^{13}C NMR ($CDCl_3$ with 0.03% v/v TMS, 600 MHz)

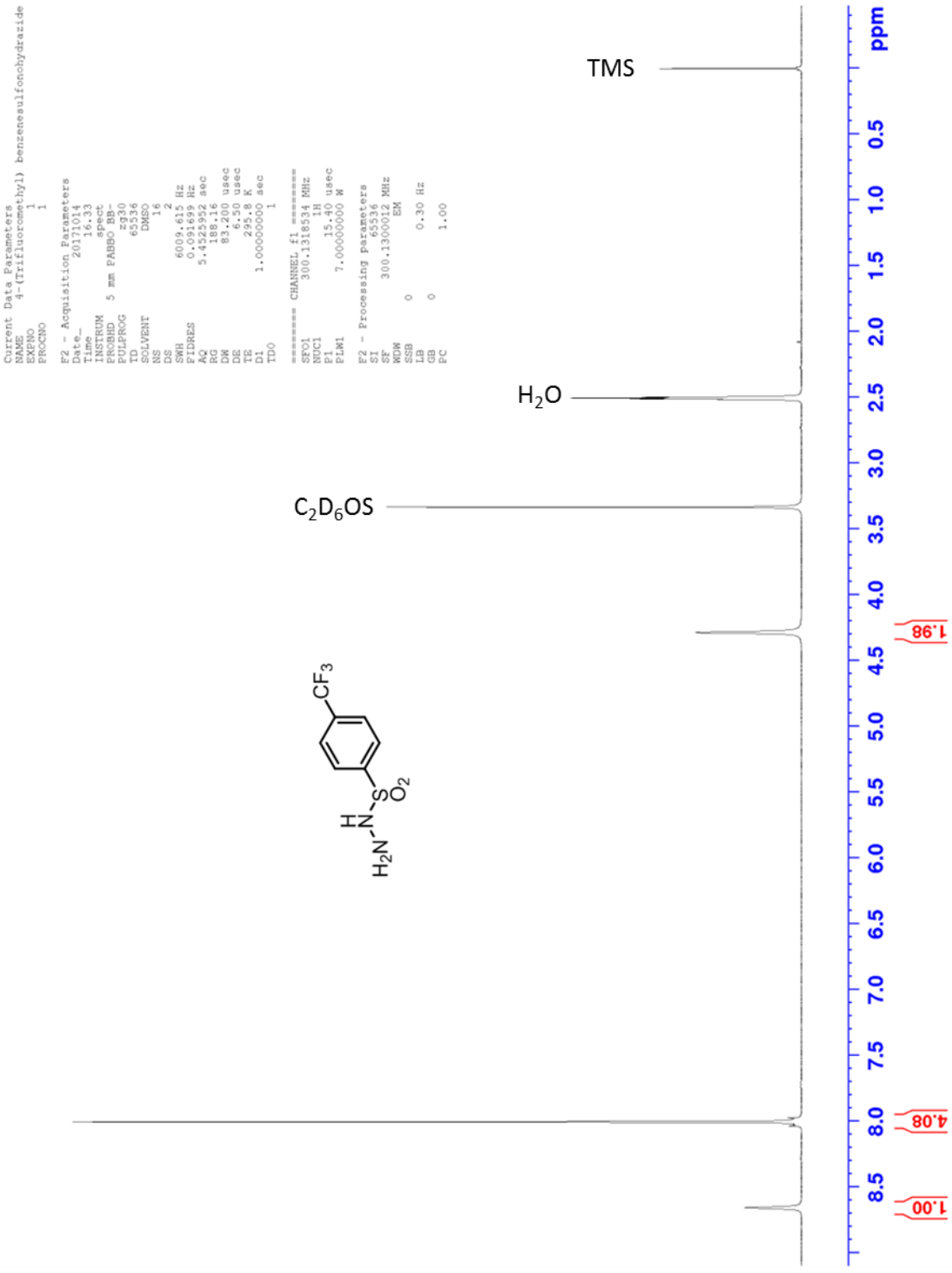

^{1}H NMR (C_2D_6OS with 0.03% v/v TMS, 300 MHz)

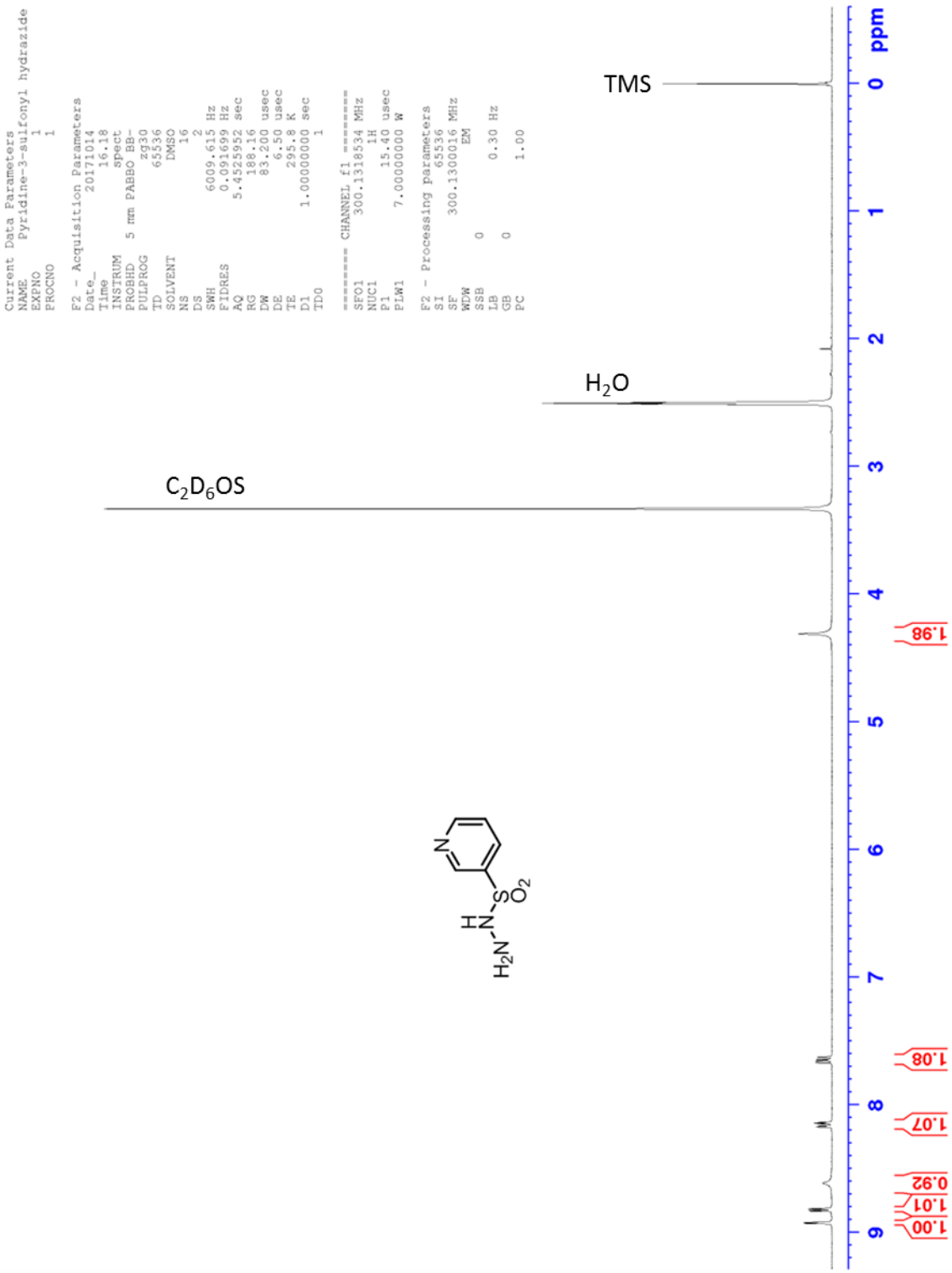

^{1}H NMR (C_2D_6OS with 0.03% v/v TMS, 300 MHz)

APPENDIX B: ^{13}C NMR SPECTRA

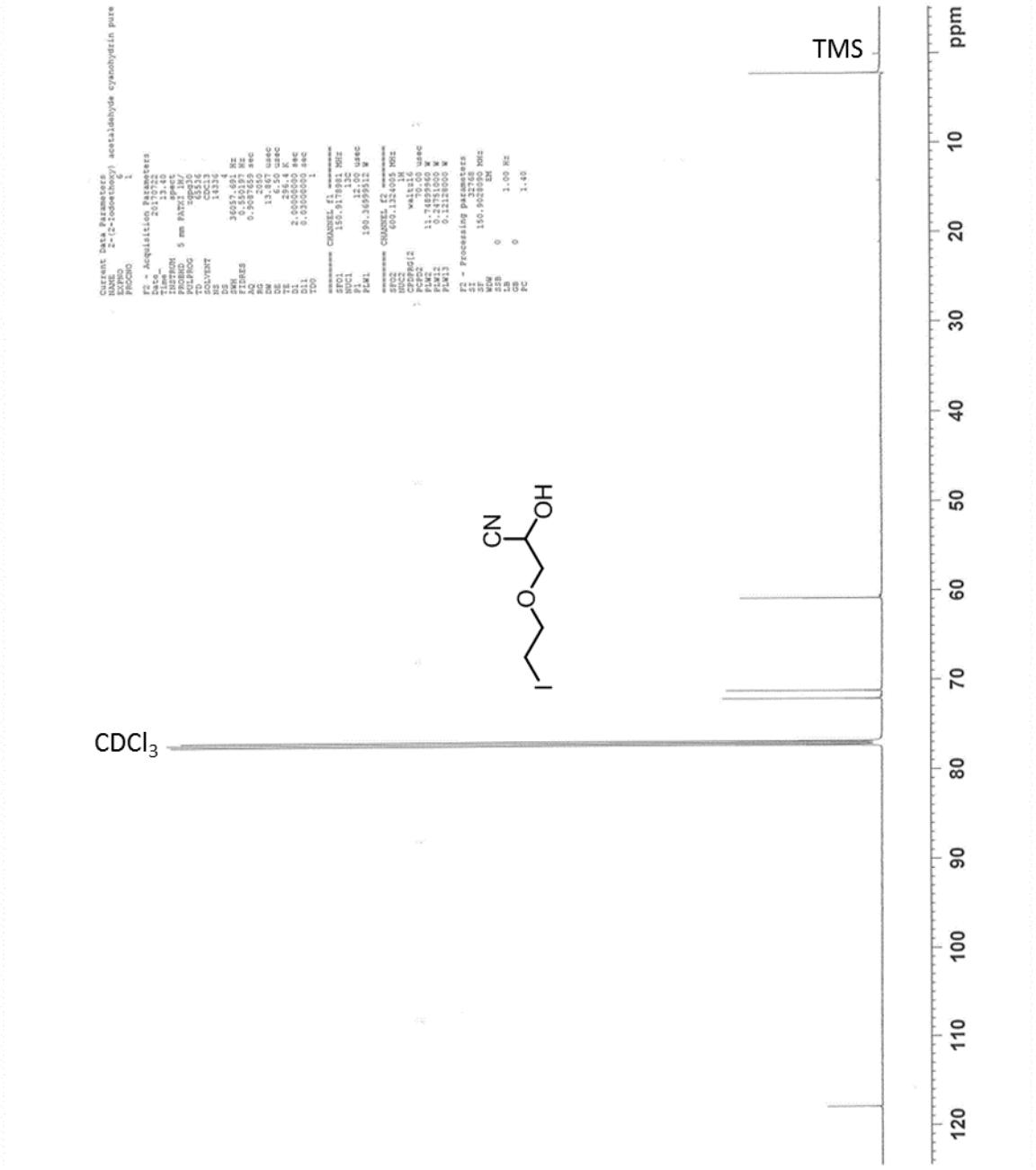

^{13}C NMR ($CDCl_3$ with 0.03% v/v TMS, 600 MHz)

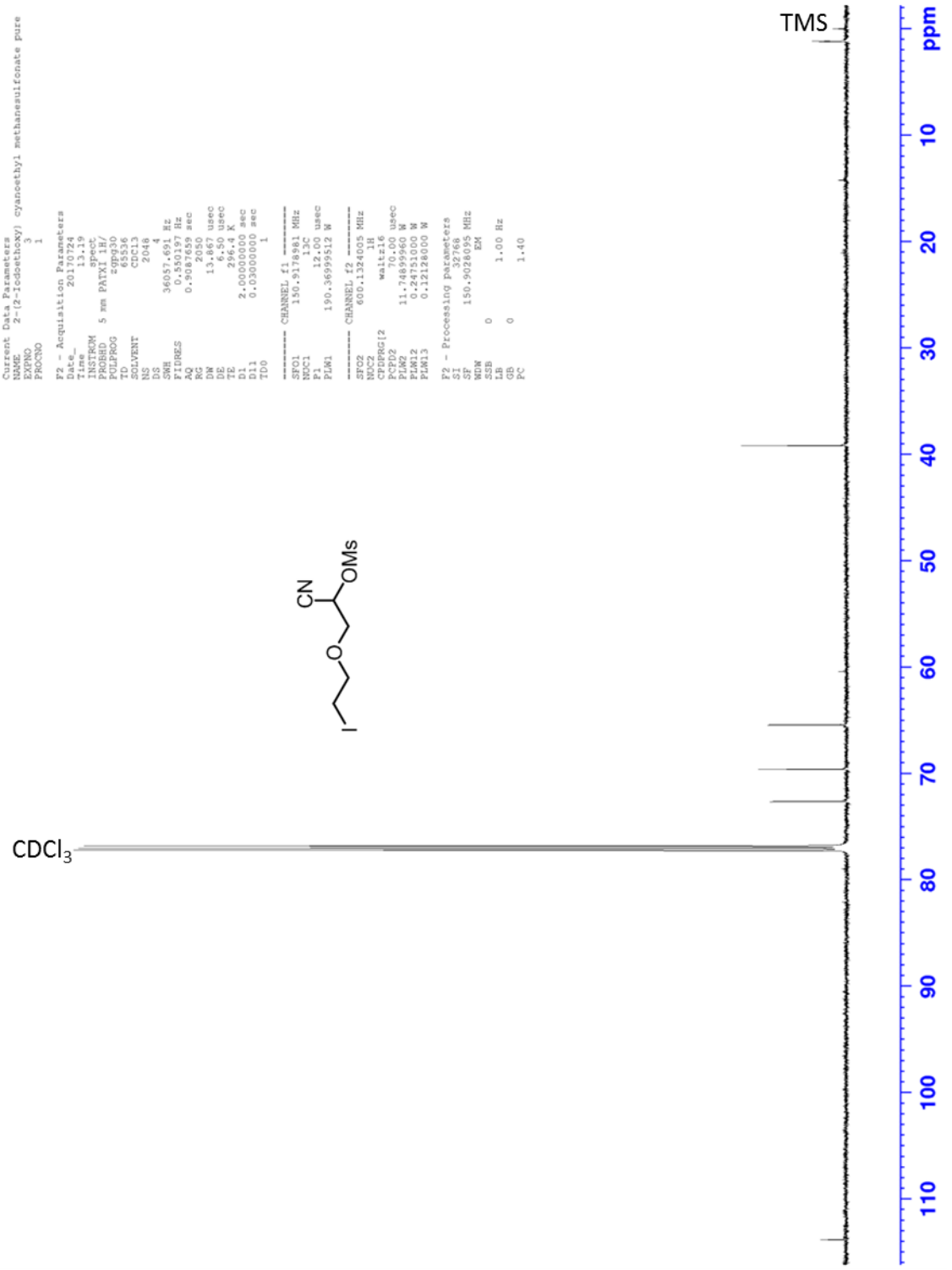

^{13}C NMR ($CDCl_3$ with 0.03% v/v TMS, 600 MHz)

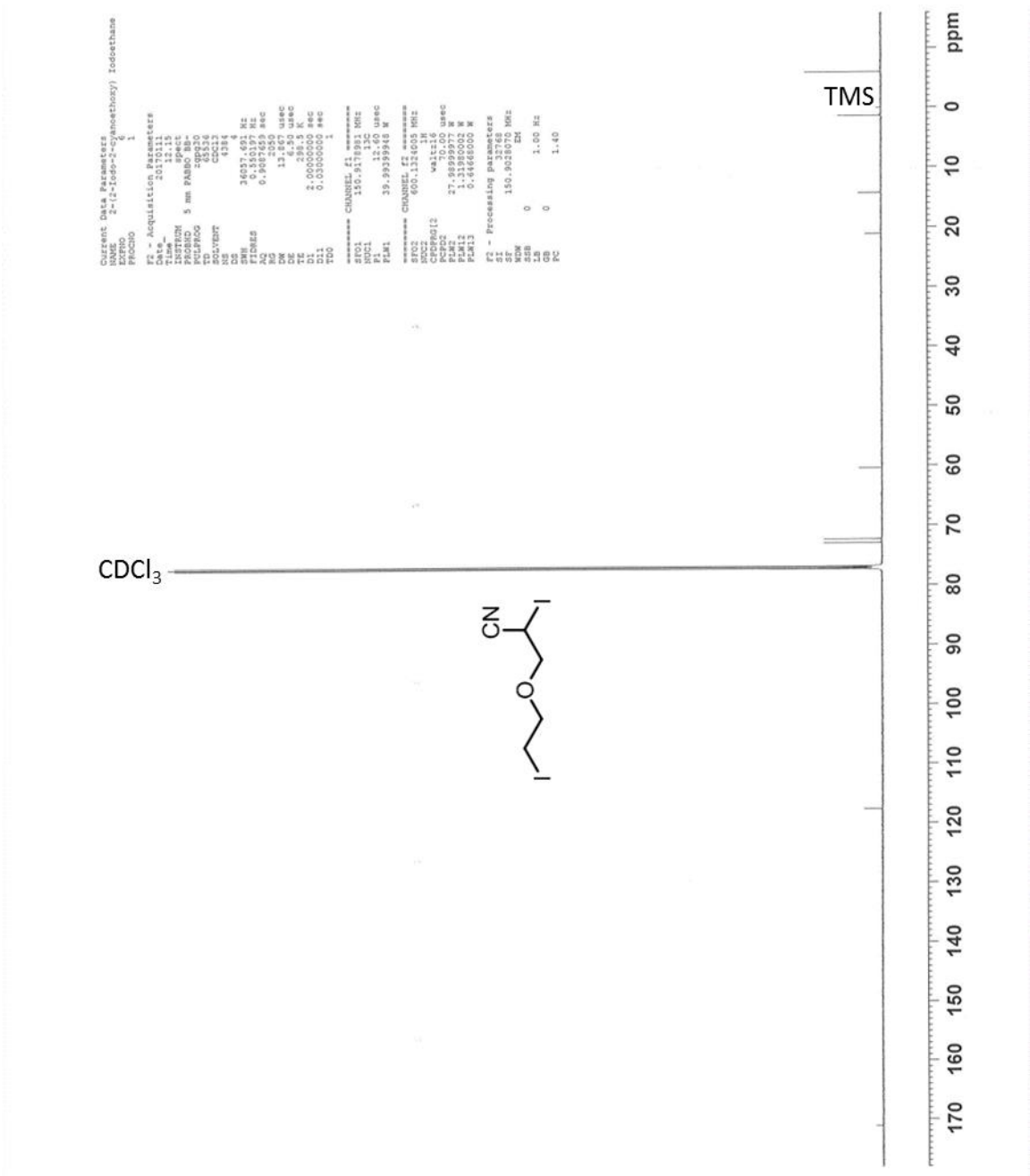

^{13}C NMR ($CDCl_3$ with 0.03% v/v TMS, 600 MHz)

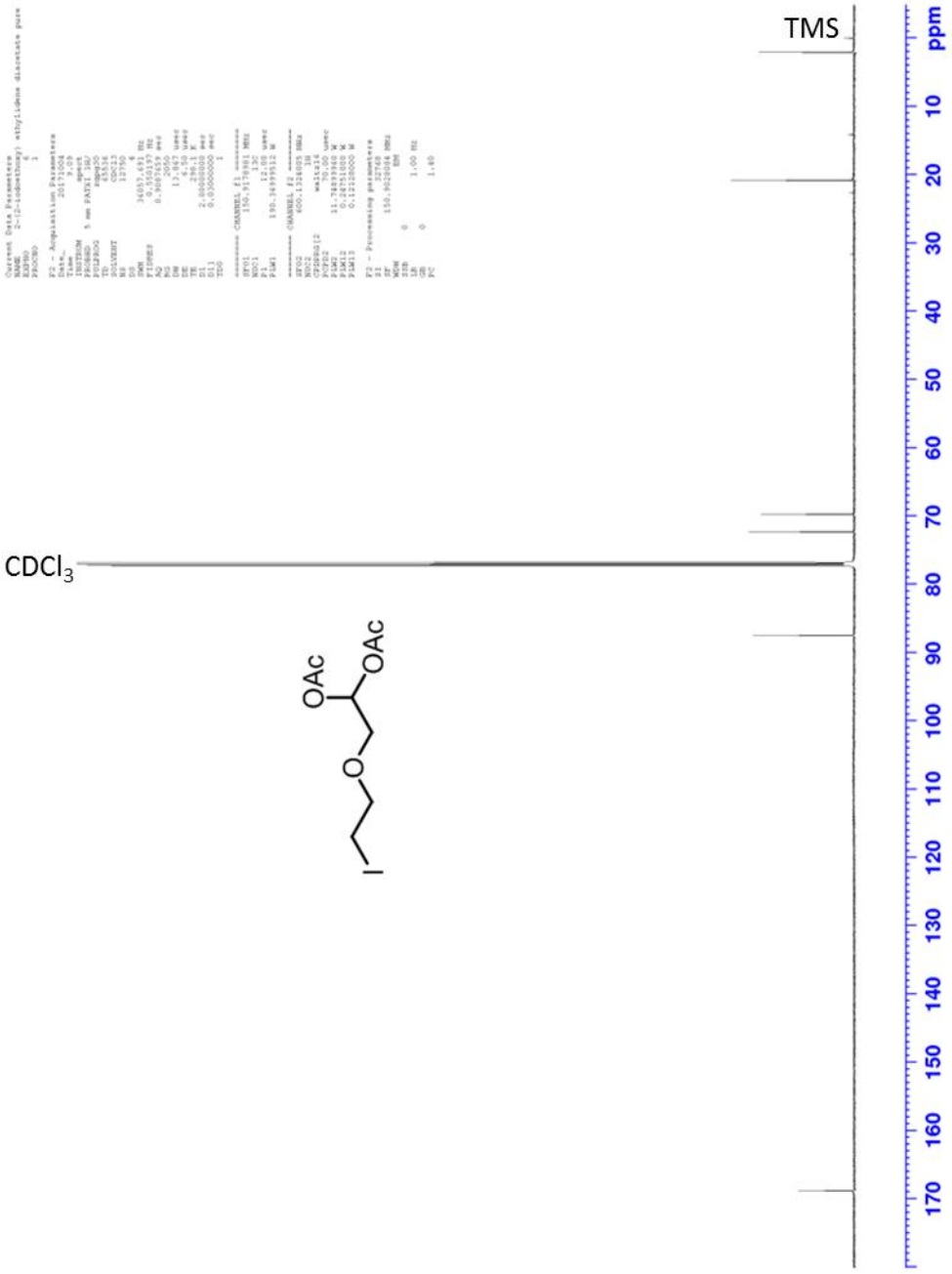

^{13}C NMR ($CDCl_3$ with 0.03% v/v TMS, 600 MHz)

APPENDIX C: MASS SPECTROMETRY

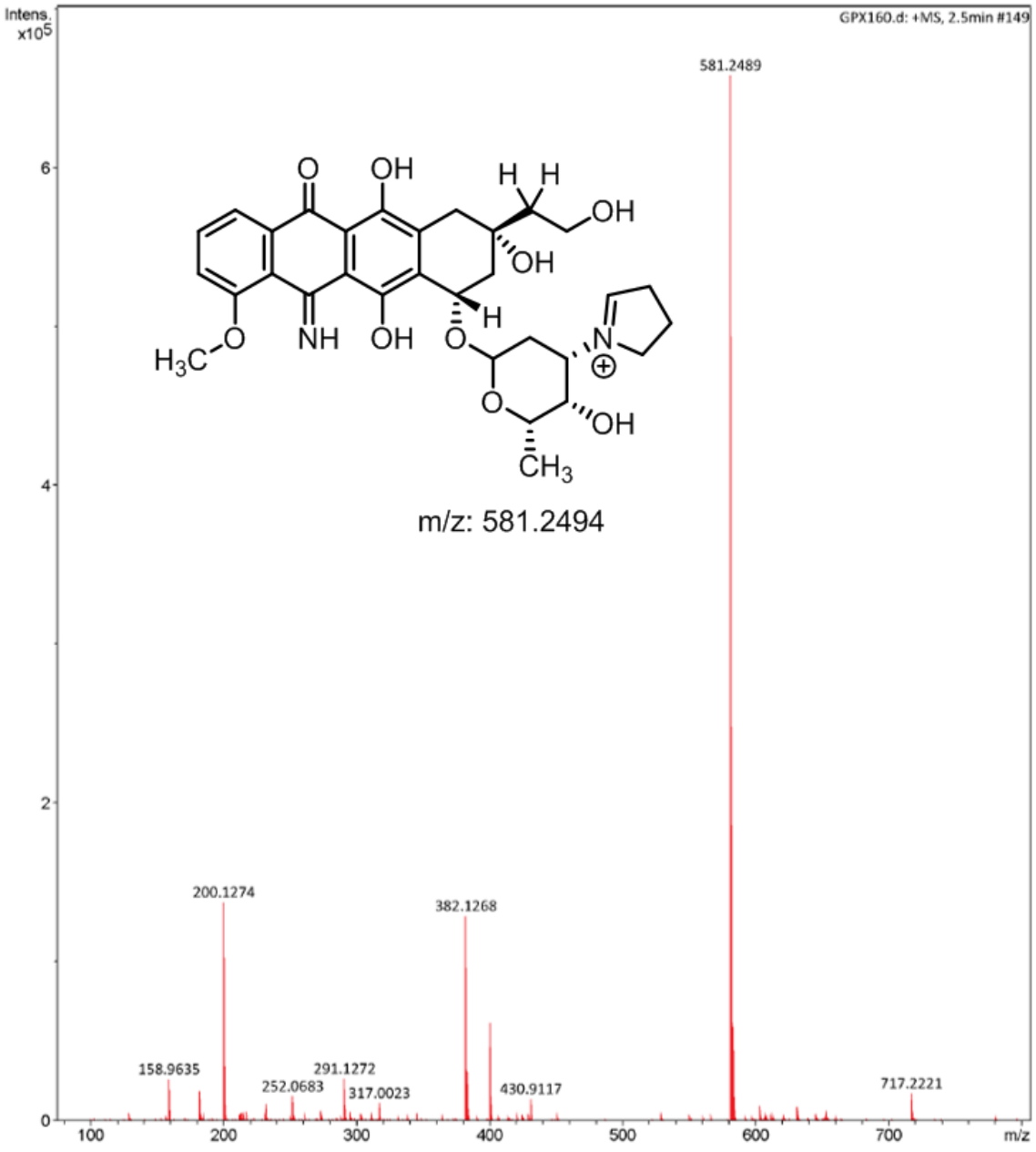
Intens.
x10^5
GPX160.d: +MS, 2.5min #149
581.2489
m/z: 581.2494
200.1274
382.1268
158.9635
291.1272
252.0683
317.0023
430.9117
717.2221
m/z

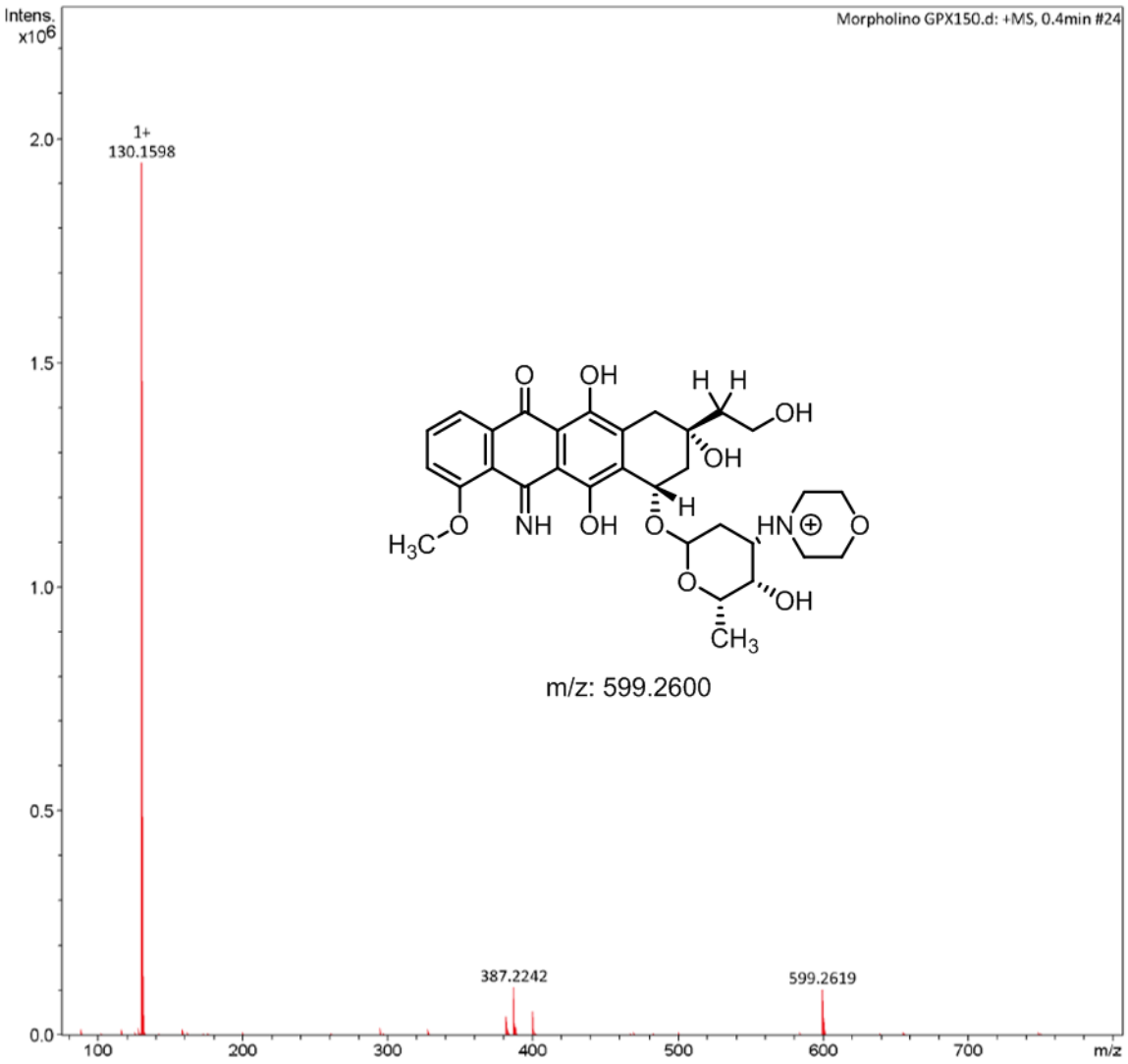
Intens.
x10^6
Morpholino GPX150.d: +MS, 0.4min #24
1+
130.1598
2.0
1.5
1.0
0.5
0.0
387.2242
599.2619
100
200
300
400
500
600
700
m/z
m/z: 599.2600

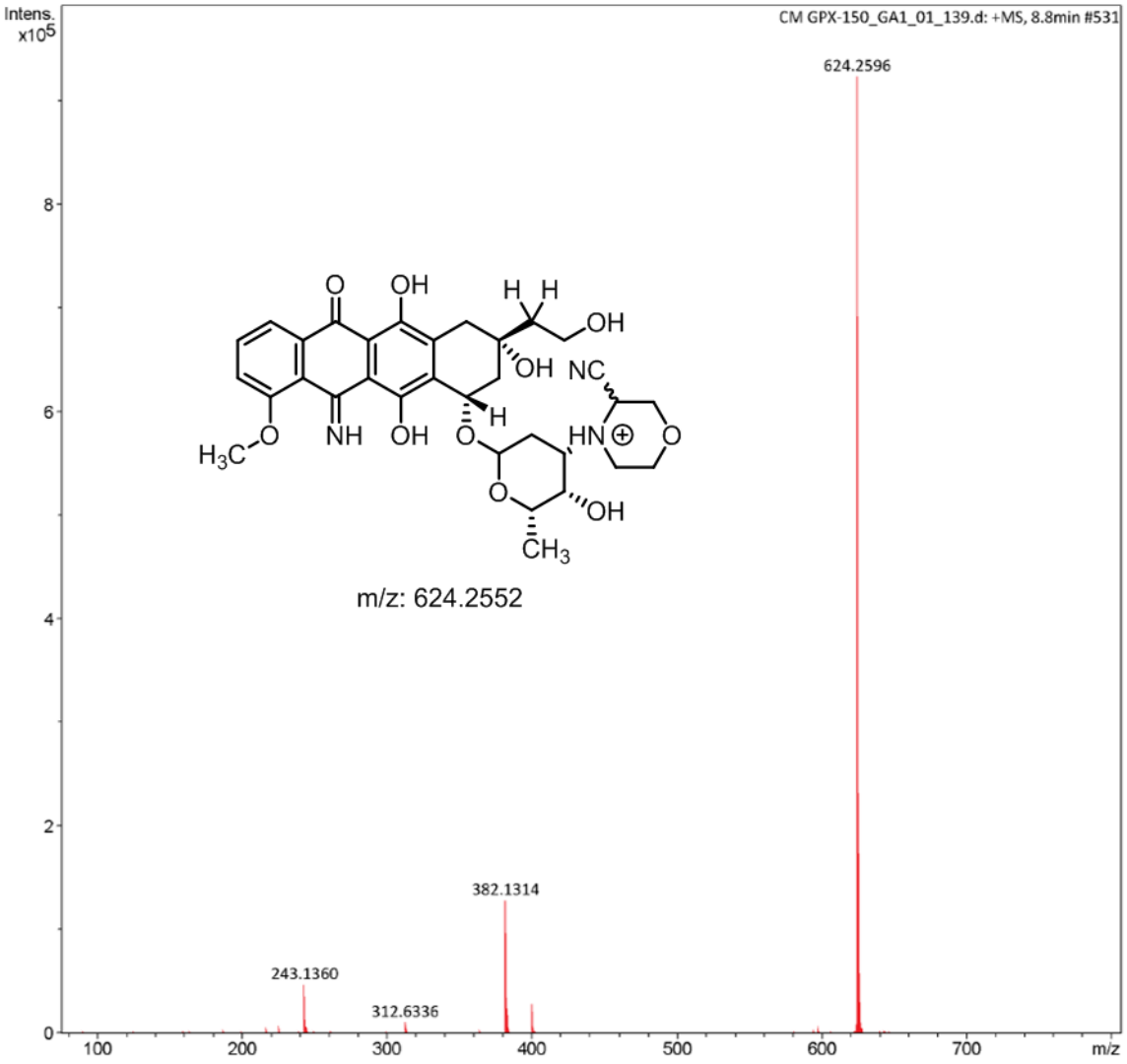
Intens.
x10^5
CM GPX-150_GA1_01_139.d: +MS, 8.8min #531
624.2596
382.1314
243.1360
312.6336
m/z: 624.2552
m/z

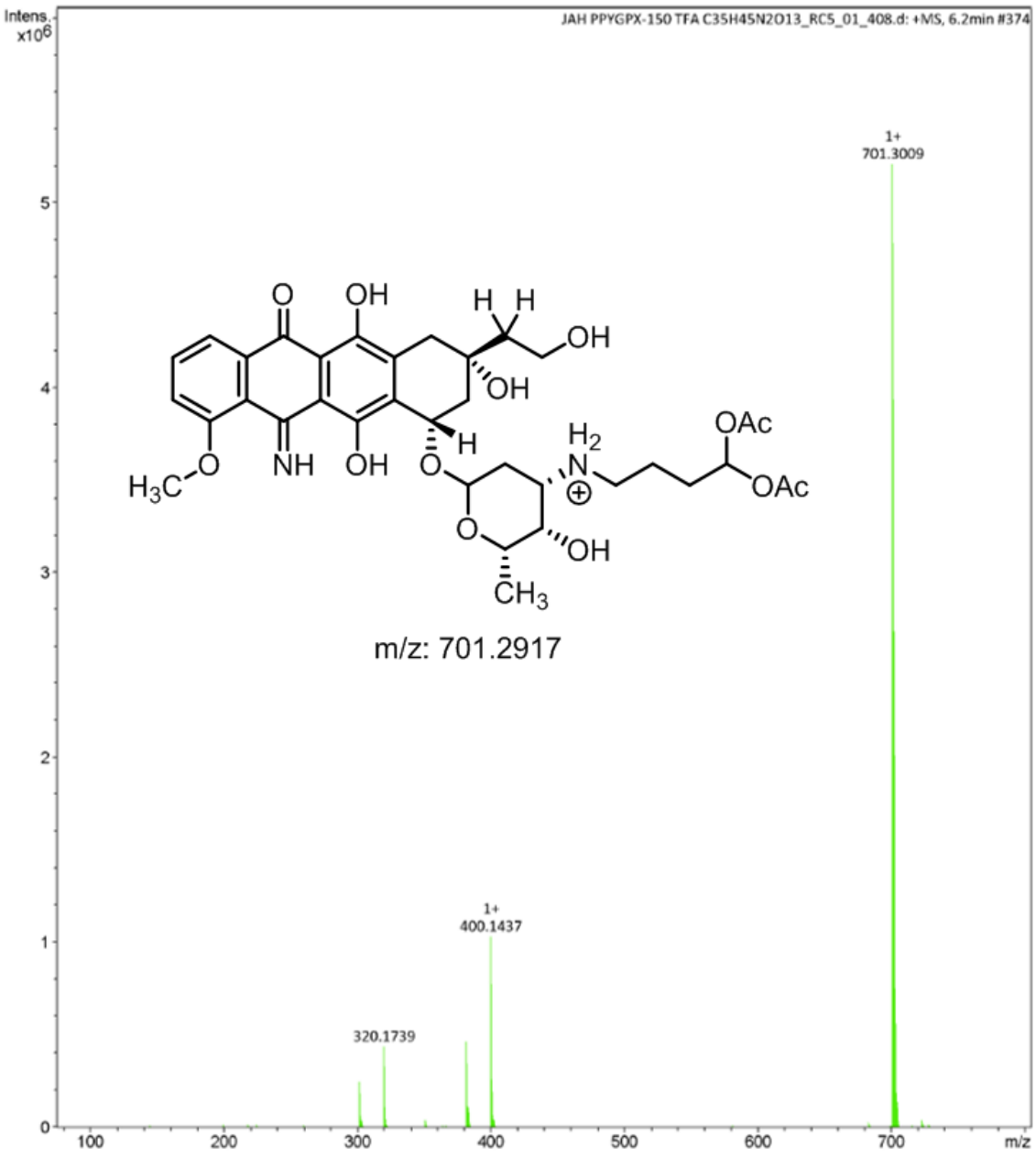
Intens.
x10^6
JAH PPYGPX-150 TFA C35H45N2O13_RC5_01_408.d: +MS, 6.2min #374
1+
701.3009
1+
400.1437
320.1739
m/z
m/z: 701.2917

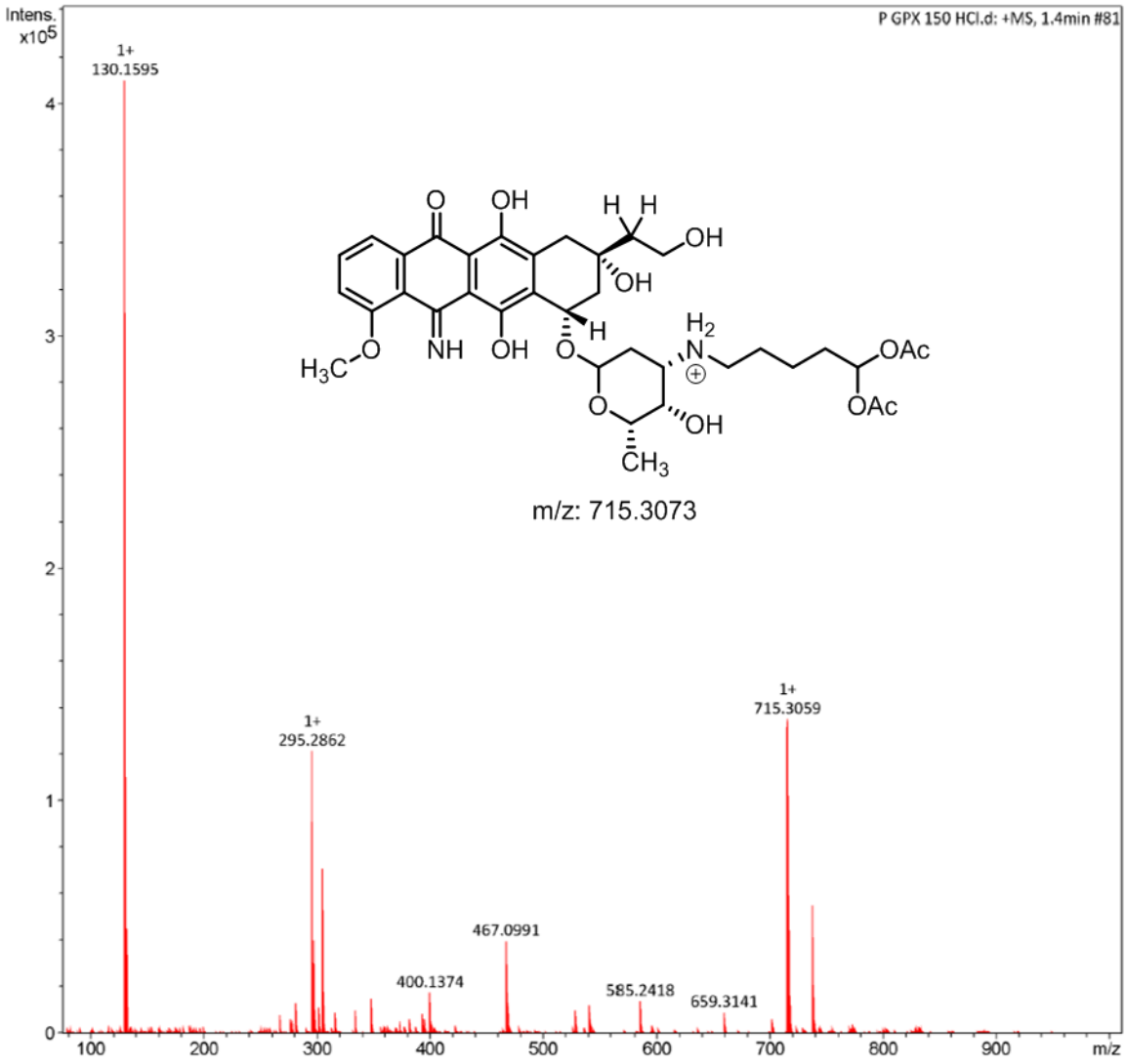
Intens.
x10^5
P GPX 150 HCl.d: +MS, 1.4min #81
1+
130.1595
1+
295.2862
1+
715.3059
467.0991
400.1374
585.2418
659.3141
m/z: 715.3073
m/z

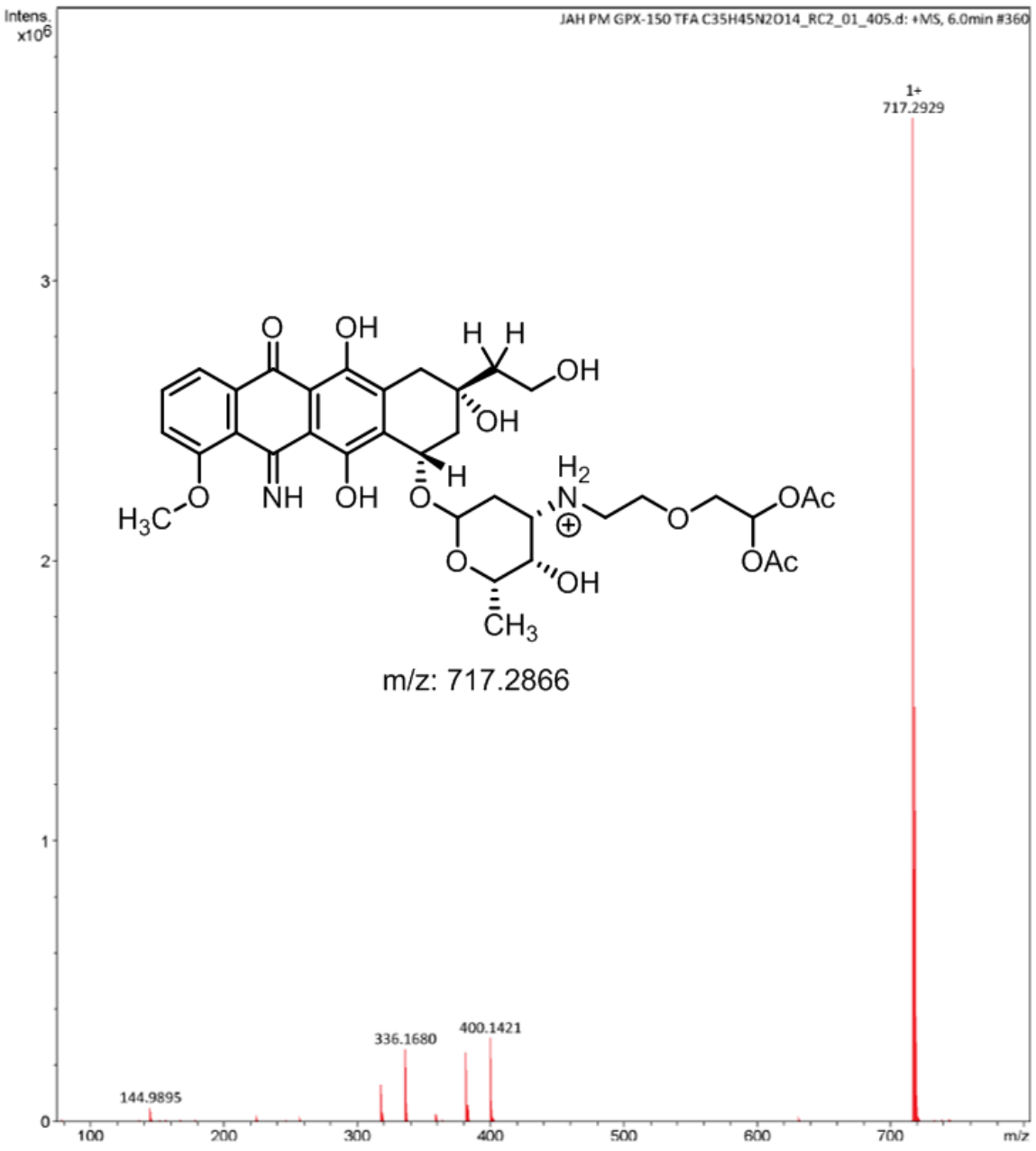
Intens.
x10^6
JAH PM GPX-150 TFA C35H45N2O14_RC2_01_405.d: +MS, 6.0min #360
1+
717.2929
3
2
1
0
O
OH
H H
OH
OH
H
H3C
O
NH
OH
O
H2
N
O
OAc
OAc
O
OH
CH3
m/z: 717.2866
144.9895
336.1680
400.1421
100
200
300
400
500
600
700
m/z

APPENDIX D: HPLC CHROMATOGRAMS

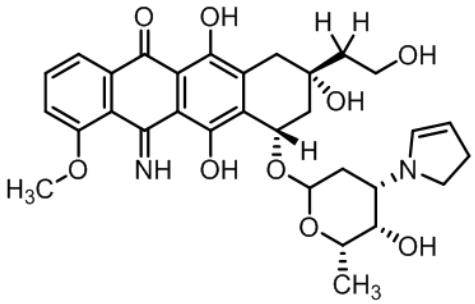
O
OH
H H
OH
OH
H
O
NH
OH
O
N
H3C
O
OH
CH3

m/z: 581.2494

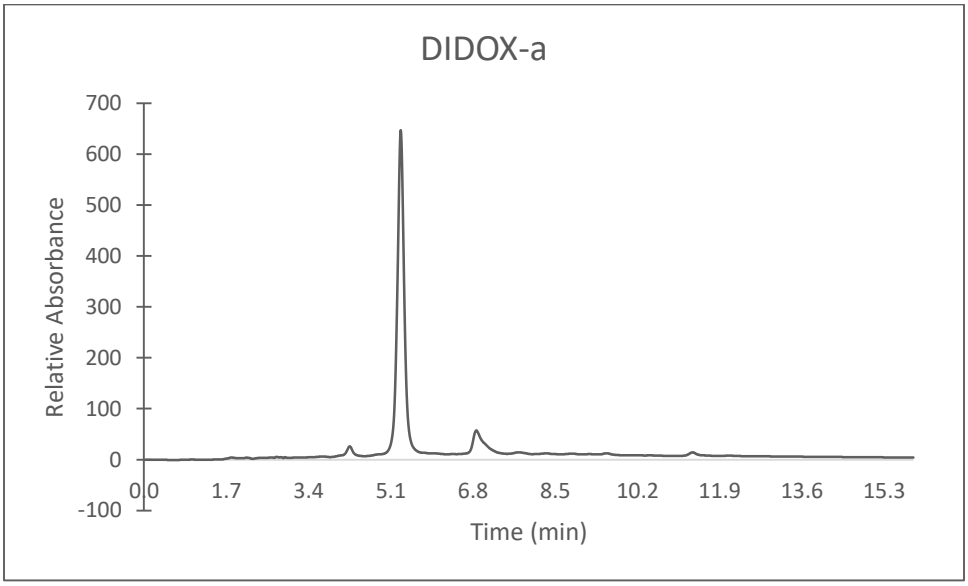
DIDOX-a
Relative Absorbance
700
600
500
400
300
200
100
0
-100
0.0
1.7
3.4
5.1
6.8
8.5
10.2
11.9
13.6
15.3
Time (min)

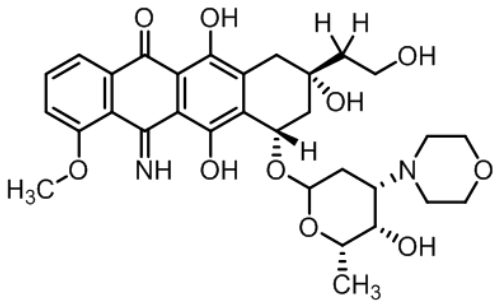
O
OH
H H
OH
OH
H
O
NH
OH
O
N
O
H3C
O
OH
CH3

m/z: 599.2600

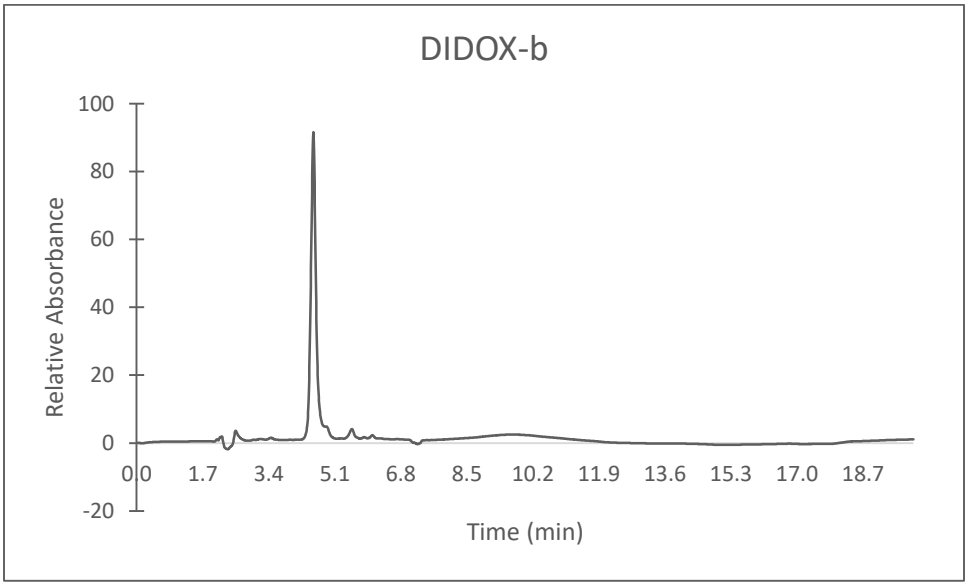
DIDOX-b
Relative Absorbance
100
80
60
40
20
0
-20
0.0
1.7
3.4
5.1
6.8
8.5
10.2
11.9
13.6
15.3
17.0
18.7
Time (min)

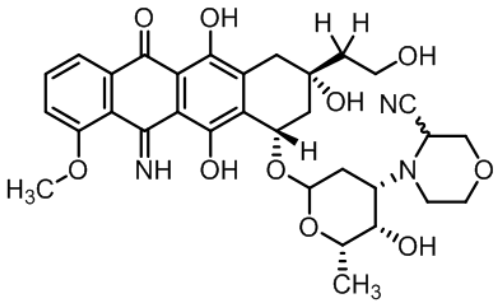
O
OH
H H
OH
OH
NC
H
O
NH
OH
O
N
O
H3C
O
OH
CH3

m/z: 624.2552

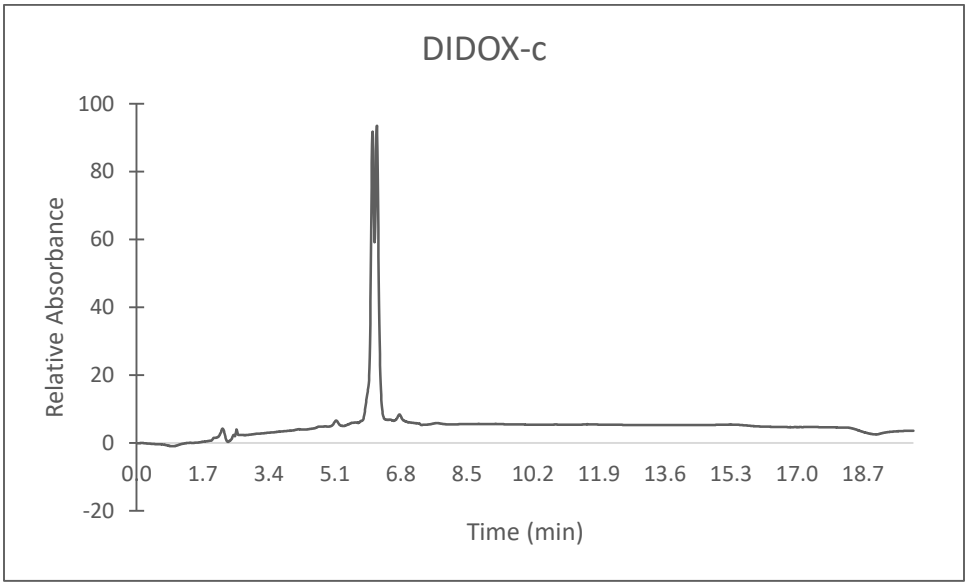
DIDOX-c
Relative Absorbance
100
80
60
40
20
0
-20
0.0
1.7
3.4
5.1
6.8
8.5
10.2
11.9
13.6
15.3
17.0
18.7
Time (min)

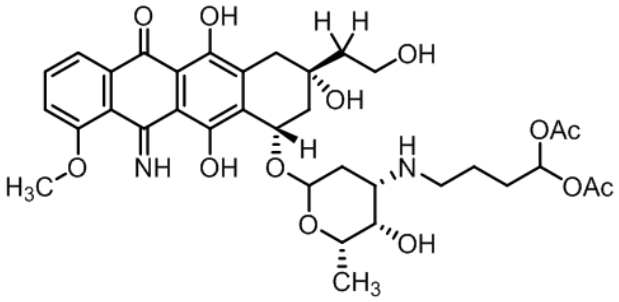
O
OH
H H
OH
OH
OAc
H
N
OAc
H3C
O
NH
OH
O
H
O
OH
CH3

m/z: 701.2917

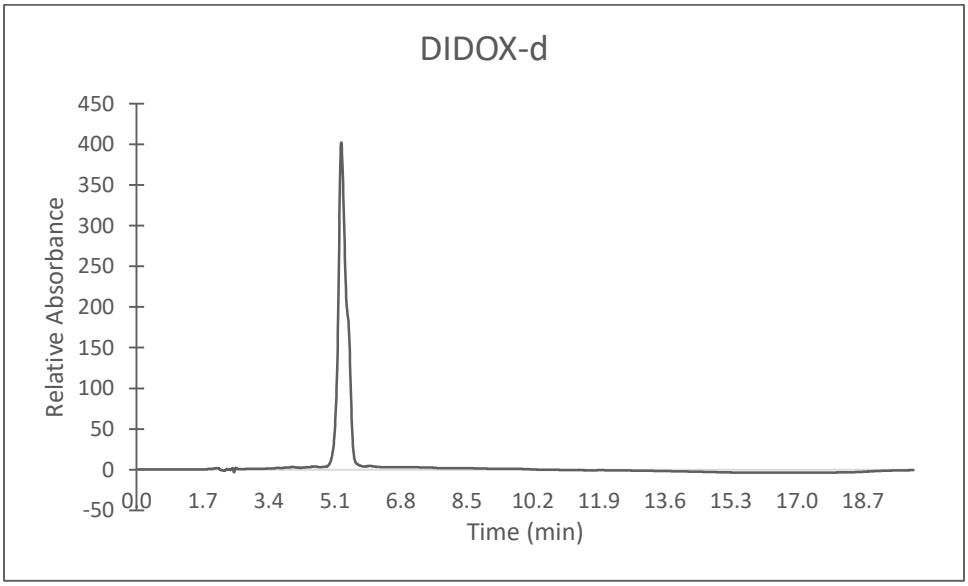
DIDOX-d
Relative Absorbance
450
400
350
300
250
200
150
100
50
0
-50
0.0
1.7
3.4
5.1
6.8
8.5
10.2
11.9
13.6
15.3
17.0
18.7
Time (min)

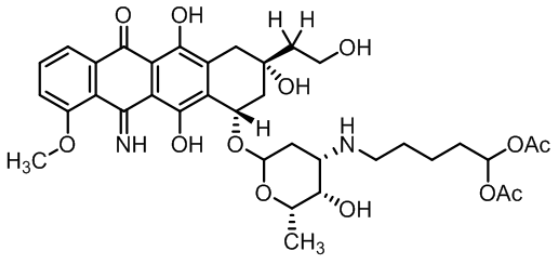
O
OH
H H
OH
OH
H
H3C
O
NH
OH
O
H
N
OAc
OAc
O
OH
CH3

m/z: 715.3073

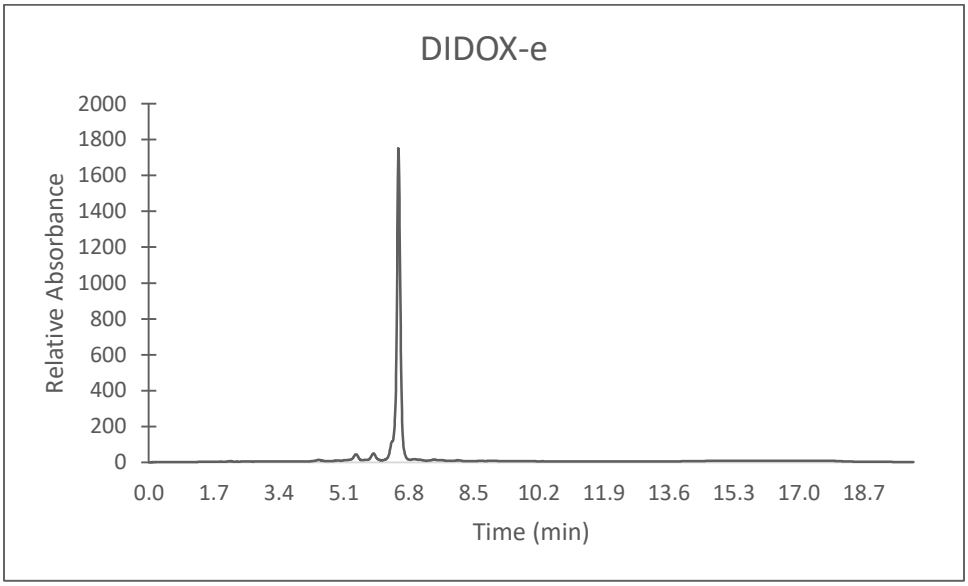
DIDOX-e
Relative Absorbance
2000
1800
1600
1400
1200
1000
800
600
400
200
0
0.0
1.7
3.4
5.1
6.8
8.5
10.2
11.9
13.6
15.3
17.0
18.7
Time (min)

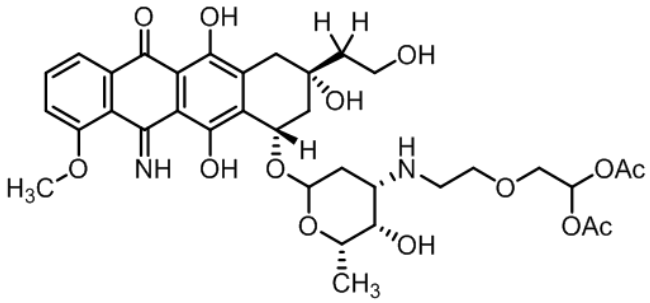
O
OH
H H
OH
OH
H
H
N
O
OAc
OAc
O
OH
CH3
H3C
O
NH
OH
O

m/z: 717.2866

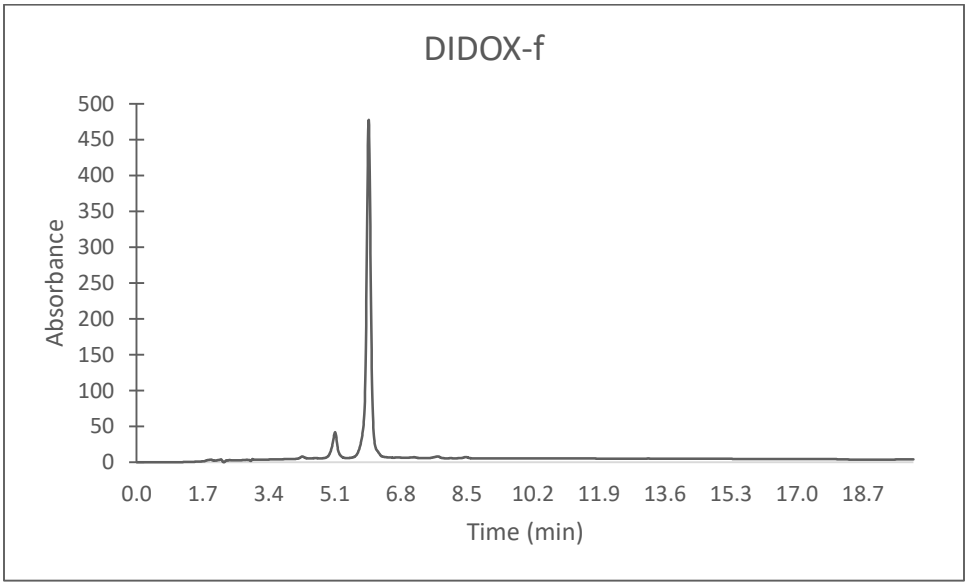
DIDOX-f
Absorbance
500
450
400
350
300
250
200
150
100
50
0
0.0
1.7
3.4
5.1
6.8
8.5
10.2
11.9
13.6
15.3
17.0
18.7
Time (min)